POLITECNICO di MILANO

Facolta di Ingegneria Industriale

Corso di Laurea Specialistica in Ingegneria Aeronautica

On the Atomization Behavior of Newtonian Fluids with an Impinging Jet Injector

Relatore: Prof. L.T. DE LUCA
Co-Relatore: Dr. H.K. CIEZKI

Tesi di Laurea di:
Giovanni BAILARDI
Matr. 711712

Anno Accademico 2009 - 2010

Abstract

The atomization characteristics of a large number of Newtonian fluids with an impinging jet injector under ambient and pressurized condition has been investigated. A distinct geometry configuration was chosen for all the experiment and the velocity of jet was varied up to $80m/s$. The properties of the selected liquids together with the variation of the jet velocity offered the possibility to conduct experiments in a wide range of dimensionless number, i.e. $10^1 < Re < 10^5$, $10^1 < We < 10^5$ and $0.0027 < Oh < 3.83$.
The ambient condition campaign has provided a characterization of atomization process in seven main spray patterns and a detailed investigations, comparing with the existent literature. First, a study on the pre-impingement length variation is taken in account, choosing a distance of $5mm$. Then the influence of Ohnesorge has been described in detail and the peculiarities of Glycerine mixture analyzed. Moreover the measurements of droplets has brought to a first correlation between the Re, Oh and Sauter Mean Diameter. The pressurized condition campaign has allowed to study the atomization behavior in high air density environment. A reduction of breakup length, an increase in droplets density and an anticipation of the spray pattern can be observed.

Key Words: impinging jet injector, Newtonian fluids, atomization behavior, Ohnesorge number, droplets, Sauter Mean Diameter, pressurized condition, glycerine mixture

Sommario

Nel presente laovoro sono state studiate sperimentalmente le caratteristiche di atomizzazione di una vasta gamma di fluidi Newtoniani mediante l'utilizzo di impinging jet injector, in condizioni standard ed in pressione. Mantenendo invariata la configurazione geometrica degli iniettori e con velocità d'iniezione fino a $80m/s$ sono stati investigati i processi di atomizzazione per una vasta gamma di fluidi Newtoniani. Il numero di liquidi e le velocità considerate hanno permesso di analizzare un ampio spettro di numeri adimensionali, $10^1 < Re < 10^5$, $10^1 < We < 10^5$ and $0.0027 < Oh < 3.83$.
Dai risultati in condizioni ambiente sono stati classificati 7 differenti processi di atomizzazione, comparati poi con la letteratura esistente, mentre dalle misurazioni sulle dropplets è stata stablilta una correlazione tra Re, Oh e il diametro medio di Sauter. In questa serie di esperimenti particolare attenzione è stata concessa allo studio dell'influenza del numero di Ohnesorge e alle peculiarità delle miscele Gliceriniche. In una seconda serie di prove a pressioni e densità elevate, sono stati osservati fenomeni di riduzione della breakup length, aumento della densità di droplets ed anticipo del tipo di atomizzazione secondo la caratterizzazione suggerita dai risultati a pressione ambiente.

Parole Chiave: impinging jet injector, fluidi Newtoniani, atomizzazione, numero di Ohnesorge, gocce, Diametro Medio di Sauter, ambiente pressurizzato, soluzioni di glicerina

Contents

List of Figures

List of Tables

Nomenclature

Roman Symbols

l_{pre}	=	Pre-impingement length [mm]
L	=	Internal nozzle length [mm]
D_0	=	Injection/orifice diameter [mm]
U_{jet}	=	Jet velocity [m/s]
h	=	Sheet half thickness [mm]
Re	=	Reynolds number [-]
We	=	Weber number [-]
Oh	=	Ohnesorge number [-]
P_c	=	Chamber pressure [bar]
T	=	Temperature [°C]
c_0	=	Universal speed limit [m/s]
n	=	Refractive index [-]
k_{GD}	=	Gladstone-Dale coefficient [cm^3/g]
d	=	Particle diameter [μm]
$D_{3,2}$	=	Sauter Mean Diameter [μm]
m	=	Slow correlation coefficient [μm]
q	=	Constant correlation coefficient [μm]
R^2	=	Goodness correlation coefficient [-]

Greek Symbols

λ	=	Wavelength [μm]
μ	=	Kinematic viscosity [Pa s]
ρ_l	=	Liquid density [kg/m^3]
ρ_g	=	Gas density [kg/m^3]
σ	=	Surface tension [N/m]
τ	=	shear stress [Pa s]
Ω	=	Growth rate [Pa s]
$\dot{\gamma}$	=	shear rate
θ	=	Impingement half angle

Abbreviation

LD	=	Like doublet injcector
UD	=	Un-like doublet injcector
NTO	=	Nitrogen Tetroxide
A-50	=	Aerozine 50
UDMH	=	Unsymmetrical dimethylhydrazine
LOx	=	Liquid oxygen
RP-1	=	Rocket propellant 1
ELD	=	Ensemble Laser Diffraction
KH	=	Kelvin Helmoltz
SMD	=	Sauter Mean Diameter
HBE	=	Extended Herschel-Bulkley

Chapter 1

Definition of the Work

1.1 Introduction

One of the most critical part of a rocket engine combustor is the injector. The injector system is comprised of injector elements that deliver propellant to the combustor and a manifold system that distributes the propellant to the injector elements. Because the design of the injector element, in conjunction with the injection pressure drop and the propellant properties, determines the propellant mass distribution and the spray drop size distribution, the injector determines the maximum achievable combustion efficiency, the heat transfer rates to the combustion chamber walls, and wether or not high frequency combustion instabilities will occur.

The choice of injector element type and its specific design is dependent on a number of factors: the propellant combination, the oxidizer-to-fuel mass ratio, the chamber pressure, the injection pressure drop, chamber diameter, the required performance level, and the engine manufacturer's own development experience. All these factors are usually determined long before the processes of design, analysis, and testing begin. The optimal injector design is one which meets the performance requirements of the propulsion system, is stable from combustion instabilities throughout its operating range, provides a compatible thermochemical environment around the chamber walls, and can be fabricated inexpensively and reliably.

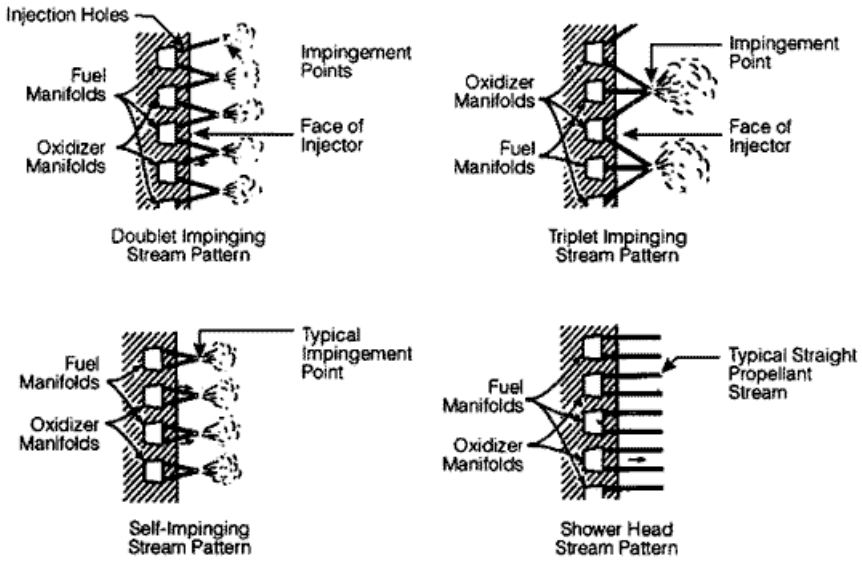

Figure 1.1: Representative of types of injector (Ref. [1])

In rocket engines that use liquid-liquid propellant combination (e.g. liquid oxygen-kerosene, nitromethane tetroxide-monomethyl hydrazine) or gelled propellants, impinging jets are usually used as the injector elements. The impingement of liquid jets is a very simple method that has a high efficiency and mixing because of its direct use of the propellant stream's dynamic head to disperse propellant.

A number of combinations of impinging jet elements have been used, including the like doublets where two streams of the same propellant impinge each other, unlike doublets with one stream of oxidizer that impinges on one stream of fuel, and triplets (two streams of one propellant impinge on one central stream of the opposite propellant). These three peculiar types are shown in Figure 1.1. The like doublet (LD) and unlike doublet (UD) are the most common type of impinging injector elements since both have the advantage that they are easy to manifold. The UD element promotes rapid mixing and combustion whereas the LD element provides a more distributed combustion zone along the combustor axis. For this reason the UD element is typically used more often in small thruster application, whereas the LD is used more often in large thruster where combustion instability can be a problem. The discussion in this work is focused specifically on the like dou-

blet element.
In Table 1.1 are given geometric and operating characteristics of a variety of impinging jet injectors used in production rocket engines. In all the engines both propellant enter the combustion chamber as a liquid.

Engine	Propellants	O/F	P_c $[MPa]$	Thrust $[MN]$	Number Elements	Orifice Diameter O/F$[mm]$
Gemini 1st stage	NTO/A-50	2	5.41	0.956	Ox:568 LD Fu:516 LD	3.05/2.03
Apollo LEMDE	NTO/A-50	1.60	1.03	0.047	165 F-O-F	1.96/1.24
Apollo LEMA	NTO/A-50	1.60	0.016	0.203	177 UD	0.05/0.040
Long March 3 FY-20	NTO/UDMH	2.21	7.38	0.697	Ox:607 LD Fu:605 LD	2.70/2.30
Ariane Viking V	NTO/UH25	1.85	5.35	0.680	Ox:216 LD Fu:216 LD	4.3/2.9
Space Shuttle OME	NTO/MMH	1.65	0.86	0.027	Ox:272 LD Fu:272 LD	0.81/0.71
Titan I Booster	LOX/RP-1	2.25	4.39	0.801	Ox:560 LD Fu:610 LD	3.02/2.08
Saturn 1B H-1	LOX/RP-1	2.23	4.86	0.910	Ox:365 LD Fu:612 LD	3.05/2.08
Saturn 1C F-1	LOX/RP-1	2.27	7.87	6.730	Ox:714 LD Fu:702 LD	6.15/7.14
Atlas MA-5 Booster	LOX/RP-1	2.28	4.03	1.469	Ox:335 LD Fu:582 LD	2.87/1.63
Atlas MA-5 Sustainer	LOX/RP-1	2.27	4.87	0.356	Ox:144 LD Fu:144 LD	3.05/2.39

Table 1.1: Engines using impinging jet injectors (see Ref. [3])

1.2 Research motivations

Impinging jet injector are often used for the atomization of storable liquid fuels in rocket engines due to their simplicity, low manufacturing costs, good atomization and mixing characteristics (Ref. [1]). Since the injector design process usually involves a trade-off between combustion efficiency, stability and thermal compatibility, the ability to obtain a stability margin and high performance simultaneously may depend on the ability to understand and control the atomization process, which depends generally on the jet Weber number, the ambient density and whether the jet is laminar or turbulent. Atomization, in fact, provides the initial conditions from subsequent combustion processes by its determinant effect on drop size and velocity. Moreover the periodic nature of primary atomization (ligament shedding) has pronounced similarities to combustion oscillations in rocket engines in terms of both frequency dependency on injector operational parameters (Ref. [2], [3]).
The investigations with Newtonian fluids are, as far as we know (in relation to open sources), in most cases dedicated to distinct liquids and also to ambient pressure conditions so that the breakup behavior in dependence on various parameters and dimensionless numbers is not completely presented up to now. Furthermore, gelled fuels show a weaker We-Re dependency, so that they cover a significantly broader (generalized) Reynolds number range e.g. in We-Re regime diagrams. For a more general comparison of the atomization behavior of Newtonian liquids and also for the realization of a base for the characterization non-Newtonian gelled fluids, a detailed characterization of the atomization behavior of various Newtonian liquids in dependence of e.g. Reynolds and Weber number and pressure is necessary.

1.3 Thesis Objectives

The aim of this work is to investigate and define the atomization behavior of several Newtonian fluids in regards of impinging injector system. In particular the influence of fluids properties such as surface tension, viscosity and density, will be studied both in ambient and pressurized conditions. With

these fluid candidates different Ohnesorge numbers can be realized so that e.g. the breakup behavior within a broad range of Reynolds and Weber numbers can be displayed. Thus a regime diagram could be presented whereas the spray pattern may identify breakup regions. The atomization behavior will be analyzed in detail through shadowgraph images and laser scattering of droplets in ambient pressure. A categorization of distinct breakup behavior and an attempt of correlation between dimensionless numbers and Sauter Mead Diameter will be performed.
The study in pressurized condition will allow to notice what kind of differences the high ambient density brings to the spray patterns in a wide range of operational condition, e.g. $3m/s < U_{jet} < 100m/s$, $1bar < P_c < 10bar$ and $0.003 < Oh < 3.8$.

1.4 Presentation Plan

Chapter 2
In the chapter 2 the state of the art regarding impinging jet injector is presented. *In primis* a brief description of the typical atomization behavior dues to impinging jets is showed. Then a complete literature review concerning the topics is proposed.
Chapter 3
In the chapter 3 the experimental setup used in this work is described. Fundamentals of shadowgraphy technique and laser scatterometry, with the corresponding utilized devices, are explained in aim to better understand the basic principles used in the experiments. Schematic sketches of the two different setup implemented are presented , one for ambient pressure condition and one for pressurized environment, focusing on the differences in the used impinge injector units.
Chapter 4
Chapter 4 deals the ambient condition tests, first explaining the choosing criteria for the several Newtonian fluids investigated, and then analyzing the main families of the breakup behavior observed. A complete categorization is made considering all the different definition reported in literature and trying

to strictly uniform the characteristics of the distinct spray patterns. Furthermore, a first result obtained measuring the droplets diameters is showed upon the velocity and dimensionless numbers.

Chapter 5

In chapter 5 an explanation of the constraints dues to the pressurized environment adopted is drawn. These restrictions have been matched with the safety level of each substances decreasing the number of used fluids. Since the type of measurement were completely new for the facility, a custom program was developed to calculate the parameters used in these work. Hence an atomization analysis is given.

Chapter 6

In chapter 6 the discussion of the results is obtained. First the influence of pre-impingement length on the fluid sheet breakup is investigated, and then the variation in fluid physic properties is analyzed using the shadowgraph images by a variation of the Ohnesorge number. A relevant regime diagram based upon Reynolds and Weber number is proposed where the different spray pattern are arranged and categorized by their general behaviors. A detailed study on the peculiar atomization characteristics of glycerine-water mixtures is performed. Similarities with Non-Newtonian gelled propellants atomization behavior is found. Furthermore, an empirical correlation regarding Sauter Mean Diameter of droplets in standard condition environment is proposed.

Chapter 7

The conclusion are drawn in chapter 7 as well as suggestion for future development.

Chapter 2

State of the Art

2.1 Spray Characteristics with a Like-on-like Impinging Injector

The working principle of a doublet like-on-like impinging jet injector is shown in the sketch 2.1. At the impingement point of two equal fluid jets a thin fluid sheet is formed, which is perpendicular oriented to the plane spanned by the two jets.

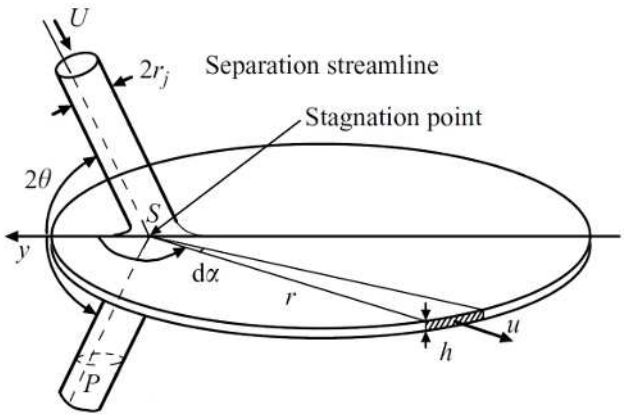

Figure 2.1: Sheet formed by impinging jets (Ref. [20])

Under certain conditions, the sheet shows a wavy structure and decays downstream into ligaments and droplets. Figure 2.2 presents as an example

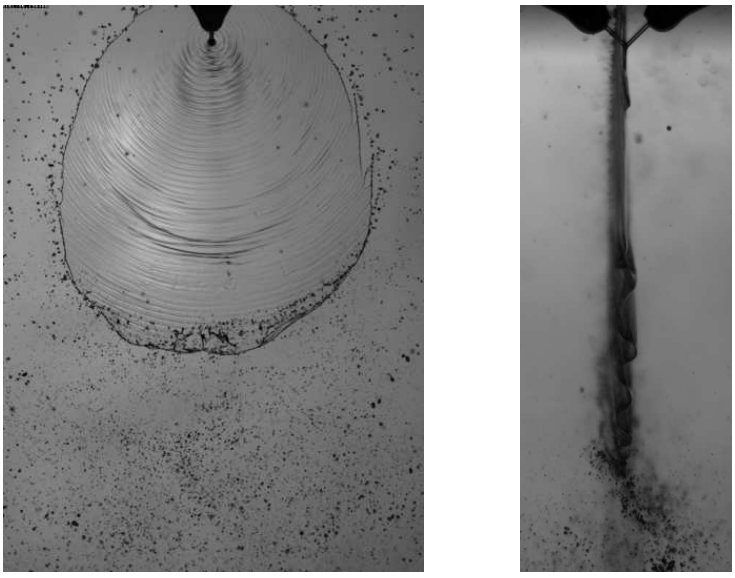

(a) front view (b) side view

Figure 2.2: Example of fluid sheet obtained with n-Heptane ($Re = 5550$, $We = 632$): (a) the presence of waves with different amplitude can be seen at the downstream edge of the sheet; (b) the lateral view shows that a kind of flag-like motion occurs

two typical shadowgraph images for a Newtonian fluid, n-Heptane, at an injector exit velocity of $U_{jet} = 5.2m/s$. From the perpendicular view (left image) it can be seen, that after the impinging point a sheet is created on whose surface waves are developing until the sheet breaks up into droplets. From the parallel view (right image) it can be seen that in this direction the sheet has a rather thin expansion.

The shape of the sheet and the decay process are changing with various parameters, i.e. fluid properties, injector geometries and jet velocities. As example, in Figure 2.3 are shown the results of Ibrahim and Przekwas prediction. As can be seen below $2\theta = 180\,\mathrm{deg}$ (circular shape) a symmetric bay leaf shape is formed. Decreasing the impingement angle the breakup length increases (x axis) up to about 100°, after which it decreases. In the present work a 2θ of 90° is used according to the general values used in rocket engines.

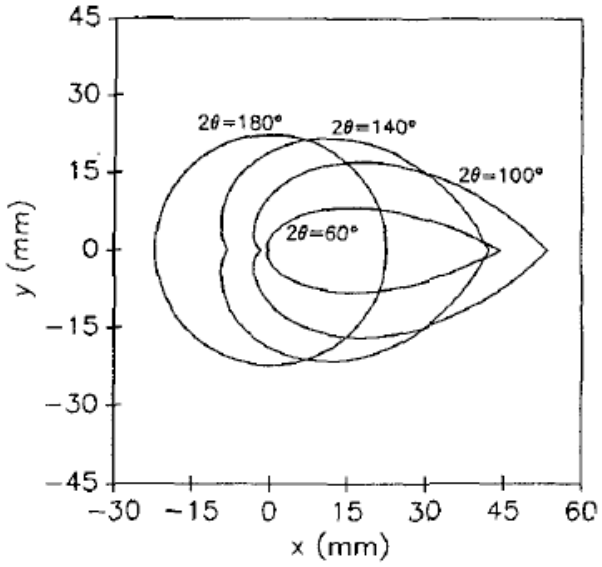

Figure 2.3: Sheet shape prediction for water at low velocities as a function of impingement angle 2θ (Ref. [6]).

2.2 Historical Background

Since the 50'es a large number of studies was conducted with Newtonian fluids regarding impinging jet injectors. Heidmann et-al (Ref. [4]) performed an extensive experimental study on the atomization characteristics of two turbulent impinging jets as a function of orifice diameter, d_o, length-to-diameter ratio, L/d_o, pre-impingement length, l_{pre}, jet velocity, U_{jet}, impingement angle, 2θ, dynamic viscosity, μ_l, and surface tension, σ. The jet velocity was varied from 4 to $30m/s$, the pre-impingement length from 6 to 60 orifice diameter, and the impingement angle from 20 deg to 100 deg. Three sets of precision bore glass tubes were employed with orifice diameters of $0.64mm$, $1.02mm$ and $1.45mm$ resulting in L/d_o ratios of 80, 50 and 35, respectively. Viscosity and surface tension were changed by using various glycerol/water solutions, Varsol and water.

From flash photographs they identified four spray patterns. The first termed the closed rim regime was characterized by a smooth liquid sheet surrounded by a thick rim that contained the major portion of the liquid. This sheet pattern occurred at velocities below $4m/s$. The nest observed spray pattern was

the periodic drop pattern in which waves were evident on the sheet surface. In addition, drops detached tangentially off the sheet periphery at periodic intervals. The velocity range for this pattern was between 4 to $9m/s$. The open rim pattern, also observed between the same jet velocities, was characterized by a thinning sheet, and unlike the closed rim pattern, the outside rim did not meet at the spray centerline. The last spray pattern identified was the fully developed pattern in which waves of drops were shed in a periodic fashion from the sheet edge. Fully developed sprays were observed for jet velocities greater than $10m/s$. They also noted that there were a sharp transition between open rim and fully developed regimes.
In addition, Heidmann et al. (Ref. [2]) measured the shedding frequency of ligaments and drops from the edge of the sheet finding that the wave frequency was linearly proportional to $U_j \cos\theta$. hence the wave frequency decreased with increasing impingement angle, while remaining relatively insensitive to change in orifice diameter and pre-impingement length. An important observation made in this study was the similarity between the measured wave frequency and the frequency of instability modes observed in liquid rocket engines. The breakup length, x_b, was measured as a function of jet velocity (up to $14m/s$) and fluid properties. The breakup length was defined as the distance from the impingement point to the edge of the intact sheet along the centerline. This dimension increased with increasing jet velocity and dynamic viscosity. Heidmann et al. also observed that high viscosity liquids produced more distinct sheets.

In the 1960, Sir Geoffrey Taylor (Ref [5]) performed experiments on laminar impinging water jets with jets velocities to $5.6m/s$. He measured the sheet thickness, the lateral spread, the breakup radii (r_b) of stable sheets formed by jets impinging at included angles of 30°, 60°, and 90°. He also measured and derived expressions for the lateral and vertical reaction forces between the two jets. The sheet shape was determined by stationary antisymmetric waves. The sheet produced in these experiments had closed, pointed tips similar to the closed rim and periodic drop regimes observed by Heidmann et al. ([4]).

Dombrowski and Hooper (Ref. [18]) published an experimental study on turbulent and laminar impinging water jets. In their experiments, they used long precision bore glass tubes ($L/d_o = 400$) with an inside diameter of $0.5mm$. Laminar flow was maintained in the tubes to $Re = 12000$ by contouring the tube inlet and by employing in-line surge chambers. The turbulent flow was ensured by placing a wire in the taper section of each glass tube. Along with flash photographs of the different spray sheets, Dombrowski and Hooper measured the sheet speed using high speed cinematography, and drop size as function of jet velocity and impingement angle. Distinct sheet structure differences were seen between the laminar and the turbulent impinging jet cases. The sheet formed from laminar impinging jets tended to produce much larger and smoother sheets as compared to the sheet formed by turbulent impinging jets. Measured sheet velocities tended to be between the velocity of the jet and the value of $U_j \cos\theta$. They suggested that sheet breakup does not scale with Reynolds number, but is dependent on the jet velocity profile and impingement angle, but in their experiments the only parameter changed in the Reynolds number was the velocity. For turbulent jets, waves formed at the impingement point, termed impact waves, caused the sheet to disintegrate. However, fore the laminar impinging jets, both impact waves and aerodynamic waves affected the sheet disintegration process. The authors also stated that the wavelength of both these waves and the breakup length decrease with increasing jet velocity.

A model for the predictions of the shape and the thickness of the sheet in the low Weber number breakup regime has been derived by Ibrahim and Przekwas (Ref. [6]). The authors considered two breakup regimes depending on the Weber number, with transition occurring at Weber numbers between 500 and 2000. In the lower Weber regime the breakup is due to small disturbances (wave lines) on the liquid sheet, while at Weber number higher than 2000,the sheet disintegration is by the growth of Kelvin-Helmholts instability waves. However, they stated that the computations of the sheet shape and edge thickness can be correlated with the orientation and size of the drops

formed at the edge of the sheet.

During the 90'es, Anderson et al. (Ref. [7], [8], [3]) investigated the spray characteristics of turbulent impinging jets by measuring the sheet breakup length, x_b, maximum spray width, W, and drop size as a function of flow velocity and injector geometry (2θ, d_o,L/d_o and l_{pre}). An analytical model based on linear stability theory was used to predict breakup length and drop size. The experimental apparatus and the operating conditions of the impinging jet system were very similar to those of Heidmann et al..
In this study, the authors found the breakup length to increase with decreasing impingement angle and increasing jet velocity, up to the maximum velocity tested ($18.5m/s$) which agrees with observation made in previous experimental studies. However, the two-dimensional linear stability-based model over-predicted the observed breakup length with increasing jet velocity. Changes in orifice L/d_o did not appreciably affect the spray characteristics, while variation in the pre-impingement length had a measurable effect on breakup behavior; thus, pointing to the importance of the jet condition prior to the impingement. Drop size measurements made with Phase Doppler Particle Analyzer (PDPA) at the spray centerline downstream of the impingement point showed the drop size decreasing with increasing jet velocity and increasing impingement angle. Furthermore, measured drop velocity closely matched the jet velocity indicating that the sheet has nearly the same velocity as the incoming jets.

At the beginning of the new century, Clanet and Villermaux (Ref. [9]) have investigated the smooth regime of the liquid sheet formed by the collision of a round liquid jet impacting a solid circular surface at normal incidence. the paper is devoted to the regime where the sheet interacts with the surrounding medium. This interaction amounts to a shear instability which induces a flag-like, sinuous unstable motion of the liquid which destabilizes and detaches from the continuous portion of the sheet because of the acceleration associated with the passage of the crests of instability at the sheet rim (see Figure 2.4). The critical amplitude of the wave crests for which

the atomization of the sheet occurs is linked to the instability properties of the sheet, which also determines the droplets size d as $d/D_0 \sim \alpha^{-2/3}We^{-1}$ and the sheet radius R as $R/D_0 \sim \alpha^{-2/3}We^{-1/3}$. These laws are valid for $\alpha^{1/2}We > 40$.

Figure 2.4: Liquid sheet sketch $y(r,t)$ close to the rim showing a primary undulation of wavelength λ and the component γ of the acceleration

However, starting from 2002, a group of researchers from the National Cheng Kung University of Taiwan (Ref. [10]), performed a very first attempt in the study of fluid properties effect on the atomization behavior. The authors used an injector diameter of $0.5mm$, length-to diameter ratio of 10, impingement angles of 60°, 90° and 120° and velocity of the jets up to $50m/s$. The 5 working fluids adopted were viscous water-sucrose solution

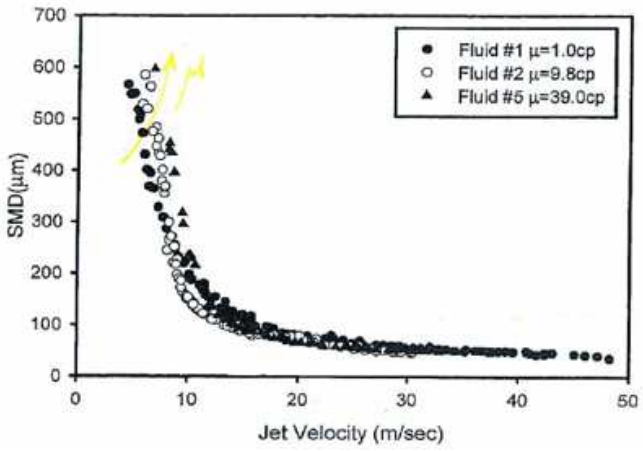

Figure 2.5: Viscosity effect on the mean drop size of impinging jets from Lai et al. [10]

with nearly constant surface tensions. However, the viscosity varied from

1.6 to 14.6cp while the density from 1.082 to 1.245kg/m^3. They observed 10 spray patterns instead of only four patterns defined by Heidmann (Ref. [2]) categorized in three modes, i.e., closed-rim mode, open-rim mode and fully developed mode. As viscosity below 2.1cp, i.e. 20% sucrose solution, flow patterns are similar to those generated by like-doublet water jets. Increasing viscosity up to 6.6cp closed rim liquid sheet can be further divided into dropping mode, cascade closed rim and closed rim with periodic drops modes. Lai

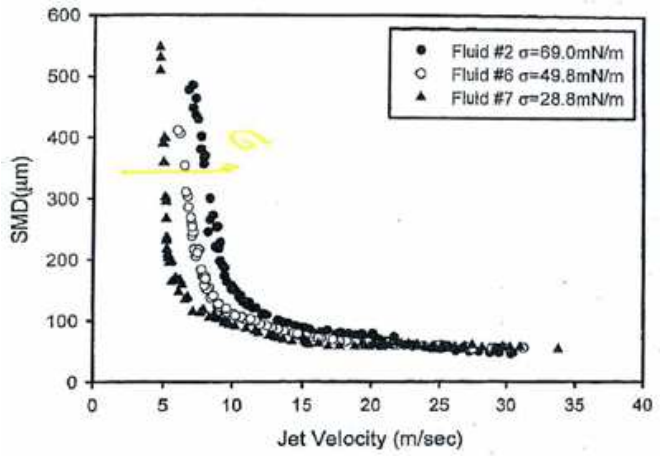

Figure 2.6: Surface tension effect on the mean drop size of impinging jets from Lai et al. [10]

et al. [21] also made a Sauter Mean Diameter measurements founding that the mean drop size approaches an asymptotic value of about 45μm when jet velocity is higher than 30m/s. This asymptotic value is strongly related to the jet diameter of the injector. However, they observed that high viscosity and high surface tension fluids produce larger mean drop size in the lower velocity regime (see Figure 2.5 and 2.6).

Bush and Hasha [17] made a first regime diagram illustrating the observed dependence of flow structures emerging from the collision of laminar viscous jets on the governing dimensionless groups, i.e. Reynolds and Weber number. Seven distinct regimes are delineated in Figure 2.7: $\triangle$, oscillating streams;$*$ sheets with disintegrating rims; $\circ$, fluid chains; $+$, fish-bones; $\diamond$, spluttering chains; $\sqcap$, disintegrating sheets; $\times$, violent flapping. Glycerine-

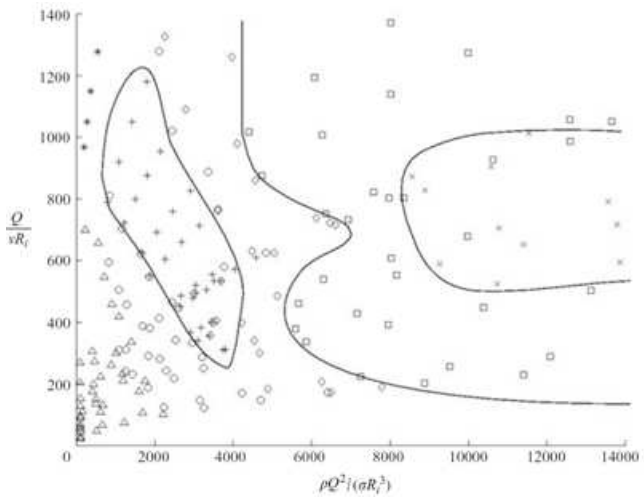

Figure 2.7: First regime attempt made by Bush et al. (Ref. [17])

water solutions with viscosities in the range of 1 to 94cS were examined. For this series of experiments, they fixed the collision angle to $2\Theta = 90°$. Each roughly diagonal trace in figure 2.7 corresponds to a glycerine-water solution with a different viscosity. The lowermost trace corresponds to the fluid with highest viscosity. The progression of the flow structure for each of the fluids was similar. However, they investigated in detailed the new fish-bones and fluid chains patterns.

An important upload in the atomization behaviors categorization have been made by Ashgriz and Li [11]. They identified two major breakup regimes, namely capillary instability regime and Kelvin-Helmohltz instability regime. In the former regime capillary instability dominates the droplet formation from the sheet, while in the latter one the interaction between the sheet and the ambient air causes the sheet breakup. These two regimes are further divided into five subregimes based on the characteristics of the sheet. The authors also derived an equation to estimate the average thickness of the sheet in aim to calculate a sheet Reynolds number. This number is found to decrease with increasing jet Reynolds, thereby showing a laminarization of the sheet. They found that previous model, that consider a parabolic velocity profile of the jets, overestimate the sheet thickness for the area around

the downstream of the centerline.

A very detailed description of physical phenomena underlying the breakup of liquid sheets at low-medium velocities is given in a series of article published recently from a group from the University of Provence in France [16]. The authors quantify and represent analytically the sheet shape, rim size and liquid velocity field. They also observed that external harmonic perturbations of the injection conditions reveal the nature of the rim destabilization and of its coupling with the sheet. They induced a flow perturbation in the incident jets noticing that it lead to sheet thickness modulations which trigger the fragmentation of the rim via the formation of the liquid ligaments.

Since 2004 at DLR Space Propulsion Institute in Germany, research activities on the characterization of both Newtonian and Non-newtonian atomization behavior, flow and spray characterization have been ongoing (Ref. [12], [**?**], [13]).

Chapter 3

Experimental Setup

In the present section an overview of the experimental devices and method for the two different tests series will be described. For the ambient condition campaign the experimental setup developed at DLR for previous works (Ref. [12], [13]) will be used. This setup allows to acquire shadowgraph images, in the planes parallel and perpendicular to the fluid sheet, and the measurements of droplets diameter downstream the injection point. For the pressurized condition campaign a new experimental setup will be assembled combining an existent combustion chamber with the camera system of the previous experiment.

3.1 Feeding system

The liquid is contained in a steel cartridge of about three liters and is forced by an hydraulic feeding system (Figure 3.1) through an injector plate. On the bottom of the cartridge a piston is connected to an hydraulic pump, which can reach a maximum working pressure of $250bar$. The piston velocity can be regulated by acting on the pump setting and provides a maximum fluid mass flow of about $70ml/s$. The top of the cartridge is closed by a plate, with a connection to the feeding pipe and with one pressure sensor.

Figure 3.1: Feeding system

3.2 Cameras system

3.2.1 Fundamentals of shadowgraphy

The shadowgraphy is a process that makes visible the disturbances that occur in a fluid flow, in which light passing through a flowing fluid is refracted by the density gradients in the fluid resulting in bright and dark areas on a screen placed behind the fluid.
The great advantage of shadowgraphy is the extreme simplicity. It is also adaptable to large fields of view. Unlike other widespread techniques (Schilieren for example), the optical quality requirements can often be relaxed (single elements lenses, inexpensive mirrors and so on). Moreover, shadowgrams may be cast on photographic film as well as on a lot of other materials and surfaces. If the lateral scale of schlieren object features is small, shadowgraphy gains the further advantage of high sensitivity. Most of the drawbacks of shadowgraphy stem from its essential ambiguity: a shadowgram is not an image, it is a shadow. There is no 1:1 correspondence between the object and

its shadow (as there is between object and image in schlieren optics, where a lens generates an optically conjugate relationship between the two). Thus shadowgrams are, generally, not true to scale. Only the dark regions (see e.g. 3.2) can yield an undistorted representation of a schilieren object, since they mark where the deflected rays originate, while the bright zones mark where these rays end up [14].

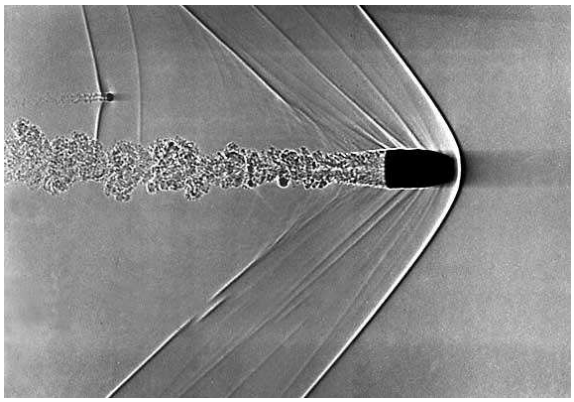

Figure 3.2: Typical Shadowgraph Image

As it can be deduced from Figure 3.2, the shadowgraphy technique permits to see the bow shock wave in air that is normally not visible with our own eyes. In fact, every transparent medium has a refractive index, n, defined as:

$$n = \frac{c_0}{c} \tag{3.1}$$

where c_0 is the universal speed limit of light in vacuum ($3x10^8 m/s$) and c the light speed in the medium. For example air (at $0\,\mathrm{deg}\,C$ and $1bar$) has $n = 1.000292$ when illuminated by light from the Sodium-D spectral line; while Helium, with $n = 1.000035$, is distinctly refractive upon mixing with air, despite the only small difference in n. Generally for gaseous medium there is a linear relationship between the refractive index and the gas density ρ:

$$n - 1 = k_{GD} \cdot \rho \tag{3.2}$$

with k_{GD} the Gladstone-Dale coefficient. This parameter is about $0.23cm^3/g$ for air at standard conditions, for other gases it may vary roughly from 0.1 to 1.5. This coefficient increases slightly with increasing light wavelength λ, thus refractivity is higher for longer λ and so the weakest disturbances become more detectable in infrared than the visible light. However n is only weakly dependent upon ρ, e.g. a change in air density of two orders of magnitude causes only a 3% change of n. Therefore if small gas density variations have to be optically detected, very sensitive optic apparatus is needed. Fortunately the refractivity for a liquid is stronger than gas, e.g. water has three order of magnitude higher than air. This means that working with liquids, like in the present work, less optical sensitivity can be used (Ref. [14]).
The main techniques to take shadowgrams of a particular phenomenon are basically two:

a Direct Shadowgraphy (with diverging and parallel light);

b Focused Shadowgraphy.

The Direct Shadowgraphy technique is the simplest to handle since only a "point" light source, a schlieren object, and a suitable surface upon which cast the shadowgraph are required. A typical diagram of the direct shadowgraphy with diverging light is shown in Figure 3.3.

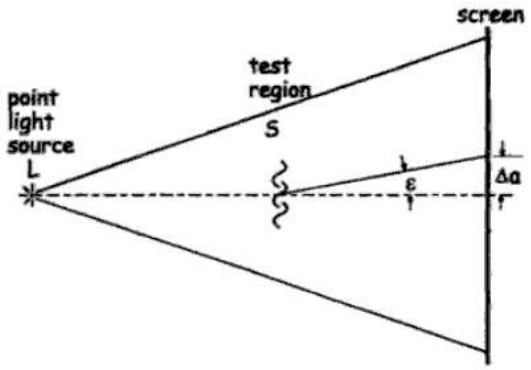

Figure 3.3: Direct Shadowgraphy Technique [14]

The schlieren object S of height d is located at a distance g from the plane of the shadowgram. Illuminated by a light source L at a distance h from that

plane, the schlieren object casts a shadow height d'. The magnification m, i.e. how many times the size of the object appears increased, is given by:

$$m = \frac{h}{h-g} \tag{3.3}$$

For example, in case of $h = 2g$, the shadowgram appears twice the full size. Considering the Figure 3.3, the light ray c, originally straight, suffers a refraction through angle ϵ at the edge of the object; thus the refracted ray c' strikes the screen at a distance Δa from the original position of c, and the light is redistributed. This refraction effect is the essential principle upon which shadography is based, summarized in the expression:

$$\epsilon \cdot g = \Delta a \tag{3.4}$$

As for every photograph based technique, even for shadowgraphy, sensitivity, maeaning the contrast and the definition that can be obtained for every taken picture, is really important. According to Schardin [14], the contrast of the direct shadowgram in diverging light is equal to the ray displacement relative to the size of the shadow:

$$\frac{\Delta a}{d'} = \frac{\epsilon}{d} \cdot \frac{g}{m} \tag{3.5}$$

Since $\frac{\epsilon}{d}$ characterizes only the schlieren object, the other terms in the second member represents the entire effect of optical geometry on sensitivity. Differentiating with respect to g, this term is found to have a maximum at $\frac{g}{h} = \frac{1}{2}$. Schardin thus stated two principle for high sensitivity in direct diverging light shadowgraphy. The first is to make h as large as possible and the second to locate the object investigated halfway between the light source and the screen. In reality other common problems have to be solved to set up a perfect shadography apparatus (diffraction blur,..), but the Schardin principle represent good basic guidelines.

The Focused Shadography technique is usually more advantageous since it allows variable magnification of the shadowgram (for further details on the theory behind see Ref. [14]). For example the ability to demagnified the shadowgram to a convenient size is important in light starved application, or

the possibility to distance the shadowgram from the object as well. Moreover it is possible to do "contact shadowgraphy" with focusing optics even when actual contact with the object is impossible. Finally, another advantages lies in the ability to adjust the sensitivity and resolution simply by focusing a lens while observing the shadowgram, rather than having to vary the distance g. Magnification and sensitivity are thus decoupled by a proper choice of focusing lens. The principal limitations came from the limited field of view, dues to the fields lens, and the incongruence of the images if a small focusing lens aperture causes a cut off of refracted rays.

3.2.2 PCO.200 camera

For the visualization of the spray patterns the focused shadowgraph-technique has been used, together with two PCO.200 cameras, one parallel and one perpendicular to the plane of the injectors, and two Nanolite spark lights as light sources. The employed CCD cameras have a maximum resolution of 2048 x 2048 pixel with a corresponding frame rate of 14.7 fps and 14 Bit A/D converter. The trigger, that connect the cameras with the flashbulbs, covers a range of 0-25 Hz, hence the maximum frame rate of the camera. The light beam of the Nanolites passes through a lens system, which increases the illumination intensity and regularity of the light. An average of more than 50 pictures has been determined to ensure stationary conditions for every experiment and stored in the M11.1 HP station.

Figure 3.4: PCO.2000 Camera

3.3 Laser system

3.3.1 Fundamentals of laser scatterometry

Any particle hit by a coherent light beam will absorb some of the incident radiation, turning, it into heat, and will scatter the rest. Scatterometry is based on the scattered portion of the incident energy, divided into three types: diffracted light, reflected light and refracted light. The optical properties, refractive index and, above all, particle size of the particles surrounding the ambient, determine how the light is scattered and absorbed. The technique of laser diffraction is based around the principle that particles passing through a laser beam will scatter light at an angle that is directly related to their size. As the particle size decreases, the observed scattering angle increases logarithmically. The observed scattering intensity is also dependent on particle sizes and diminishes, to a good approximation, in relation to the particle's cross-sectional area. Large particles therefore scatter light at narrow angles with high intensity, whereas small particles scatter at wider angles but with low intensity.

The process described is far based on the idea that all the particles have a spherical shape, but, usually, the shape of the particles is much less regular (Figure 3.5). The basic problem in particle sizing is that the three-dimensional object needs to be described with only one number. The idea is to transform the investigated shape into a sphere since it is the only shape that can be fully characterized by a single parameter, the diameter. The equivalent sphere theory lets measure some properties of our particle and assumes that this may refer to a sphere from which it can be derived the unique number that will describe the particle itself. Usually the most common properties considered are weight or volume since these parameters are not related with geometric dimension of the object itself. This technique is very powerful because we can immediately notice if some changes in shape or size occur at the reference object. This involves a lot of uncertainties with the original particle size, especially when one dimension of the particle is clearly less important than the others and it is common to discard it. meanwhile

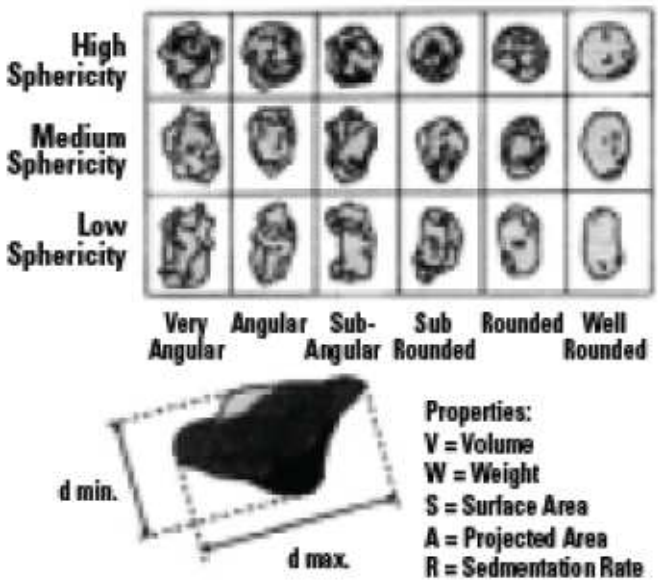

Figure 3.5: Categorization of different particle sphericity

considering the equivalent sphere this never can happen. When a change occurs in a negligible dimension, the reference object can be seen like a bi-dimensional projection of it and so there are different measurable diameters that can be used as characteristic. if the maximum length of the particle is taken, we are saying that the particle is a sphere of this maximum dimension, otherwise using the minimum diameter this will give another solution for sizing the particle.

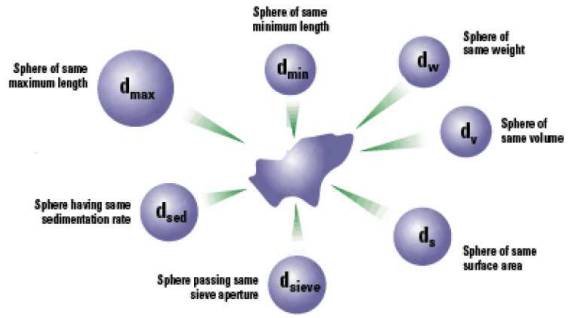

Figure 3.6: Different standard particle dimensions

Each characterization technique measuring a different property will give

us different results from another way of analysis, which could considers another parameter as the main dimension as can be seen from Figure 3.6.

3.3.2 Malvern Spraytec

A Malvern Spraytech laser was used to measure the average droplets diameter, positioned about $22 - 23.5cm$ downstream the impingement point.

Figure 3.7: Malvern Spraytech laser

It belongs to the family of Ensemble Laser Diffraction (ELD), a technique that measures a group of particles as a whole distribution. Its typical optical configuration can be seen in Figure 3.8. The laser diode generates a laser beam with 670nm wavelength passing through the measuring volume. Here a part of the light is absorbed and another part s scattered. The resulting beam is focused by a lens on a detector which measures intensity and position of the incident beams and determines the average droplets dimensions. The beam power detector behind the scattering detector is used for calibrating the instrument.

If the instruments is aligned and calibrated, most of the sources errors are removed, but by dense sprays multiple light scattering can occur. This is definitely the biggest source of errors. The scattered light from a drop might be scattered again by other drops before reaching the lens. To avoid multiple light scattering, the investigation volume is reduced using two plastic tubes, visible in Figure 3.9. Moreover a slight air flow is injected in the tubes to avoid the sedimentation of droplets during the tests.

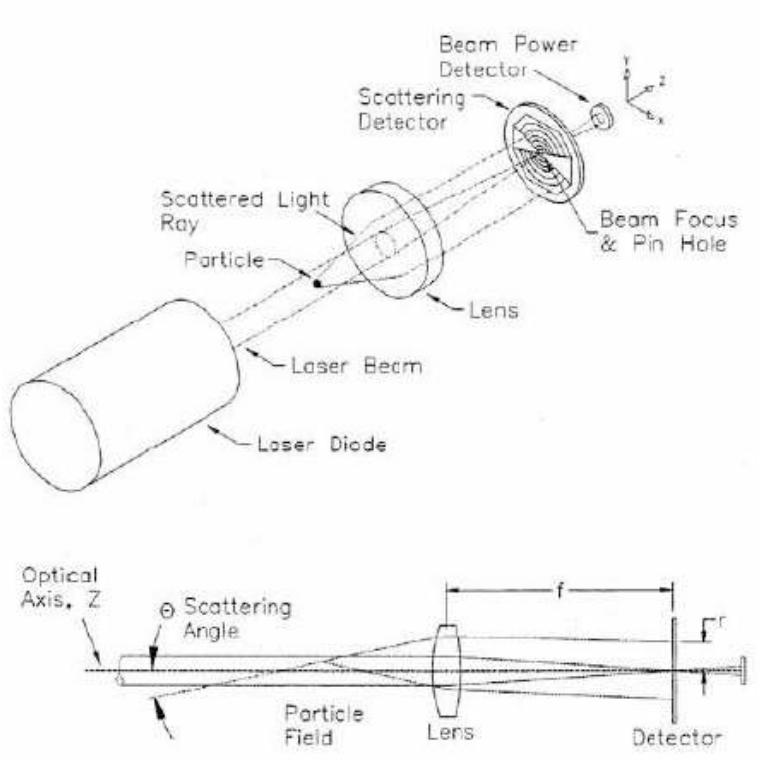

Figure 3.8: Ensemble Laser Diffraction

Figure 3.9: Malvern analysis volume reduction

3.4 Ambient Condition Setup

The whole experimental setup is presented in Figure 3.10. It consists of a cartridge with the fluid to be investigated, a hydraulic driving unit and a modular injector unit. The two sensor of pressure are positioned one at the top of the cartridge and one at the nearly exit of the nozzle exit so a pressure drop can be measured. In this study the measurements of pressure has been taken in account to understand when stationary condition happens. The temperature of the cell and the environment is assumed equal and has been measured by a thermometer.

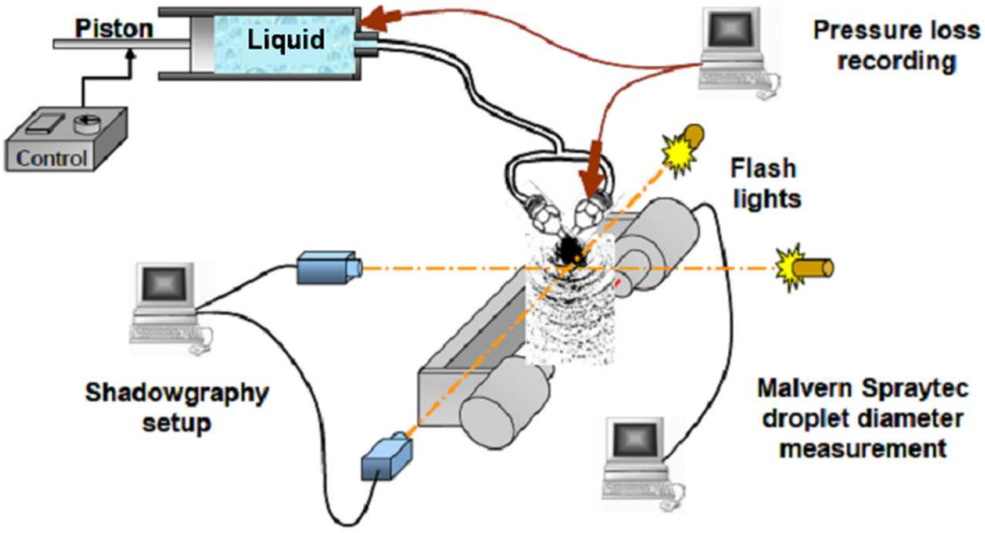

Figure 3.10: Experimental setup: Ambient Condition

3.4.1 Injector Modular Unit

The injector arms of the injector unit are mounted on movable rotary tables so that the impingement angle as well as the pre-impingement length can be varied easily. For the present work an impingement angle $2\theta = 90°$, a pre-impingement length $L_{pre} = 5mm$ and an injector diameter $D_0 = 0.7mm$ have been chosen. The injector tips (nozzles) can easily be changed for the variation of the nozzle exit diameters and the internal injector geometry. The high ratio $l/D_0 > 10$ of the internal injector channel as well as the internal

wall inclination angle of $\alpha = 20°$ have been chosen both to reduce influences of separation by the formation of a vena contracta, etc. in the intake to the injector channel and to induce a more fully developed velocity profile at the injector exit (Figure 3.11).

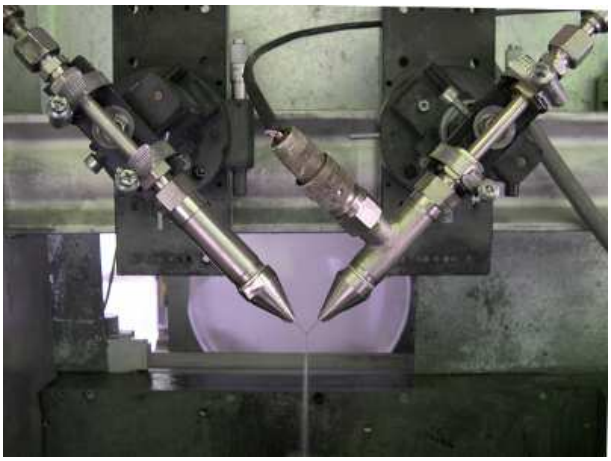

(a) Modular unit

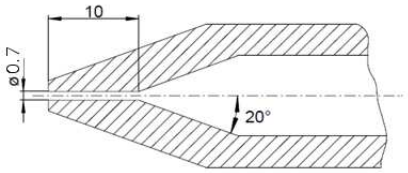

(b) Nozzle internal geometry

Figure 3.11: Injector modular unit

3.4.2 Experimental Procedure

In the following are listed the steps to conduct the experiments:

1. Mount injector nozzles, feed the injector line connecting the water faucet, turn on the facility heater to reach a stationary temperature of $20°C$ in the environment;

2. Start-up of the control room computers;

3. Acquisition system adjustment for injector geometrical constraints and symmetry;

4. Check laser scattering;
5. Fill the cartridge: wear proper gloves, mask and glasses in case of hazardous species;
6. Fix the cartridge to the piston, put on the cover and connect the pressure gauge;
7. Clean the injector line with high pressure air and then mount the feeding system;
8. Start-up the basic/unix workstation, set the parameters of the tests;
9. Perform tests: if the cameras get dirty increase the distance scrolling on the bench arm and focus/align again;
10. Clean all devices, dismount injectors and elaborate encoder and pressure sensor data in the custom Basic program of $M11.1$.

3.5 Pressurized Condition Setup

For the campaign a new experimental setup has been created, combining an existent combustion chamber with the acquiring system used in the previous experiments. A first sketch can be seen in Figure 3.12.

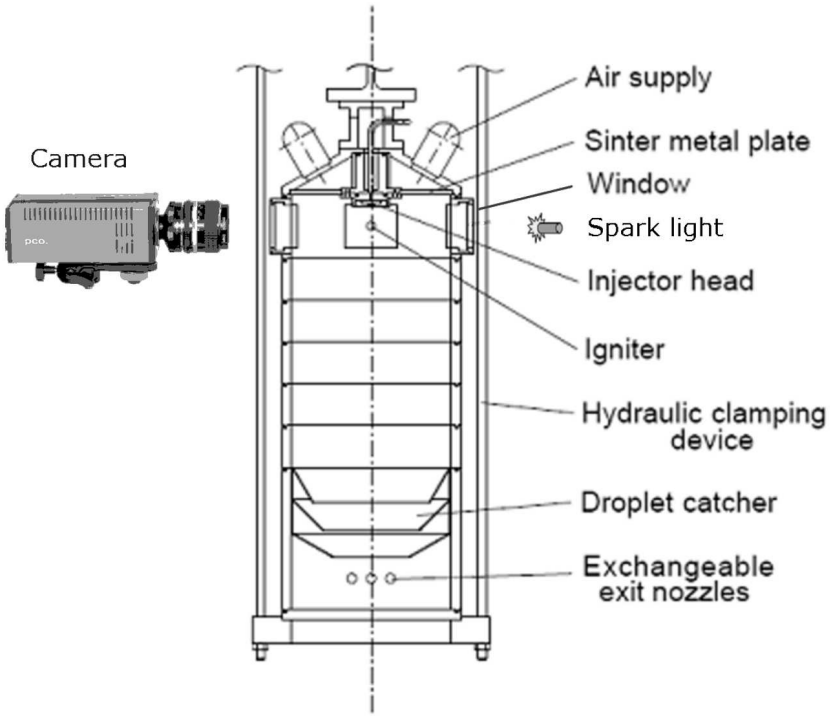

Figure 3.12: Experimental setup: Pressurized condition

3.5.1 Combustion Chamber

The combustion chamber (CC) is a stainless steel, non cooled, cylindrical chamber (Figure 3.12). It is made of different removable rings enabling to modify the length of the chamber. During the present work the length of the combustion chamber was $80cm$. The internal diameter of the chamber is of $30cm$ and the thickness of the wall is of $4cm$. At the bottom disk are located three holes. On each a hole a nozzle can be mounted. By using the available nozzles (Figure 3.2a) it is possible to obtain a quite large diameter

range of equivalent nozzles between a minimum of $12mm$ and a maximum of $62mm$. In this work all the three holes has been blocked in aim to have a fixed pressure during the tests. A tap has been mounted in one of the holes to take the liquid at the end of the test.

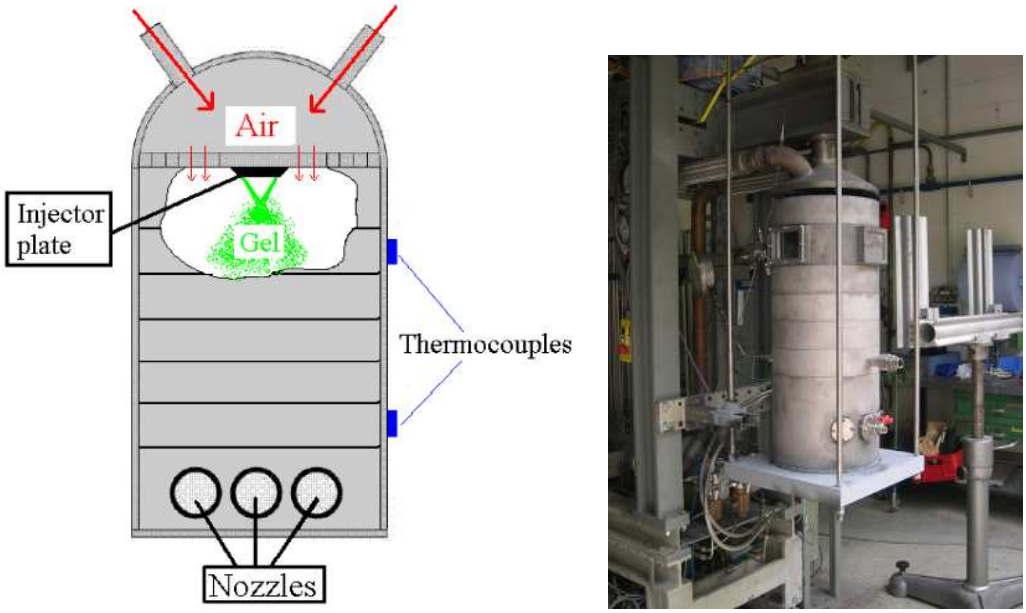

Figure 3.13: Combustion chamber

3.5.2 Injector Unit

The geometry of the impinging injector unit used is shown in Figure 3.14. The diameter of the two holes of the injector is of $0.7mm$ and the plate provides an impinging angle of 90°. The distance between the injection and the impinging point is $5mm$. Thus the same geometrical constraints of the Ambient Condition campaign have been used.

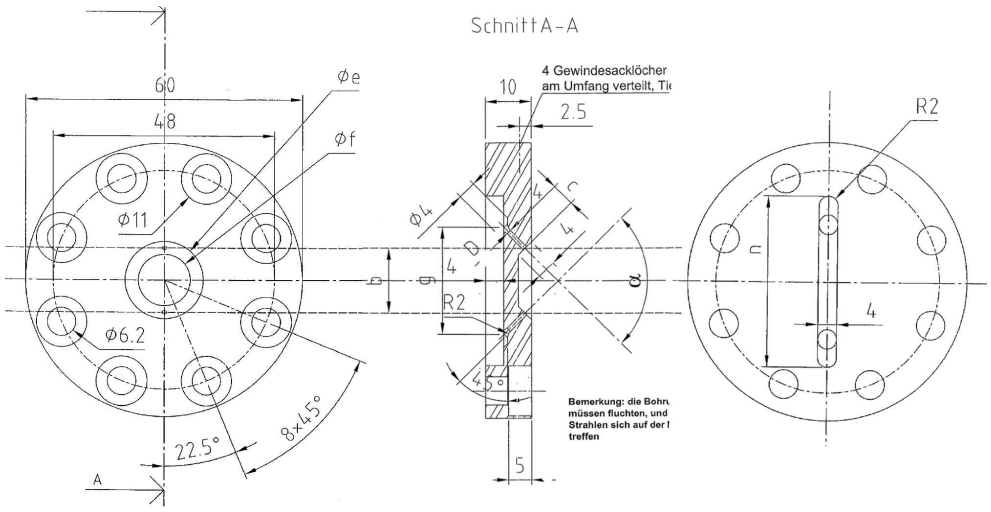

Figure 3.14: Injector Plate

Chapter 4

Ambient Condition Campaign

4.1 Fluids Scan and Decision

In the present work eighteen different fluids are investigated basing the choice criteria on covering the biggest range of physics properties such as density, viscosity and surface tension. Since the test facility works in an open environment, the search is conducted checking the Material Safety Data Sheet of every species candidate (Ref. [32], [33], [35]), especially looking for non-toxic Newtonian liquids.
Furthermore, as analysis that involves different parameters, it's useful to use dimensionless numbers that represent both the fluids properties (σ, μ, ρ) and the operational condition (U_{jet}), e.g. Reynolds and Weber numbers. In particular to relate the viscous force to the inertia and surface tension effects, the Ohnesorge number can be used, noticing how it represent a characteristic of a considered fluid once the injection diameter is fixed. In the sprays'studies, in fact, this number gives an information on the substance atomization behavior. Generally the lower is the Oh the easier is the atomization. The

dimensionless numbers can be written as:

$$Re = \frac{\rho \cdot U_{jet} \cdot D_{inj}}{\mu} \tag{4.1}$$

$$We = \frac{\rho \cdot U_{jet}^2 \cdot D_{inj}}{\sigma} \tag{4.2}$$

$$Oh = \frac{\mu}{\sqrt{\rho \cdot \sigma \cdot D_{inj}}} \tag{4.3}$$

where U_{jet} is the velocity of the jets and D_{inj} the injector exit diameter.

One of the aims of this work is to arrange the different spray patterns on a logarithmic regime diagram in dependence upon Reynolds and Weber numbers. The relationships between the variables described before can be obtained as follow:

$$We = Oh^2 \cdot Re^2 = c \cdot Re^2 \tag{4.4}$$

Passing to the logarithm:

$$\begin{aligned} Log(We) &= Log(Oh^2 \cdot Re^2) \\ &= 2Log(Oh) + 2Log(Re) \\ &= C + 2Log(Re) \end{aligned} \tag{4.5}$$

Thus every substance lies theoretically on a diagonal line and the Ohnesorge increases moving from right to left, as can be seen in Figure 4.1 that represent the work made by Ciezki et al in 2005 at DLR-Lampoldshauzen ([12]). The orange arrows individuate the gap to fill to obtain a broader investigation.

After a trade-off based on the criteria exposed above the chosen fluids are shown in Figure 4.2 and listed in Table 5.1. As can be noticed a wider range of Oh number ($0.0027 < Oh < 3.83$), as well as Reynolds ($10^1 < Re < 10^5$) and Weber ($10^1 < We < 10^5$), is guaranteed. Of peculiar interest are the low Oh fluids because of the same properties of the common liquid propellants used in propulsion system, and the high viscosity region (i.e. high Oh) because of possible similarities with gelled propellants atomization characteristics.

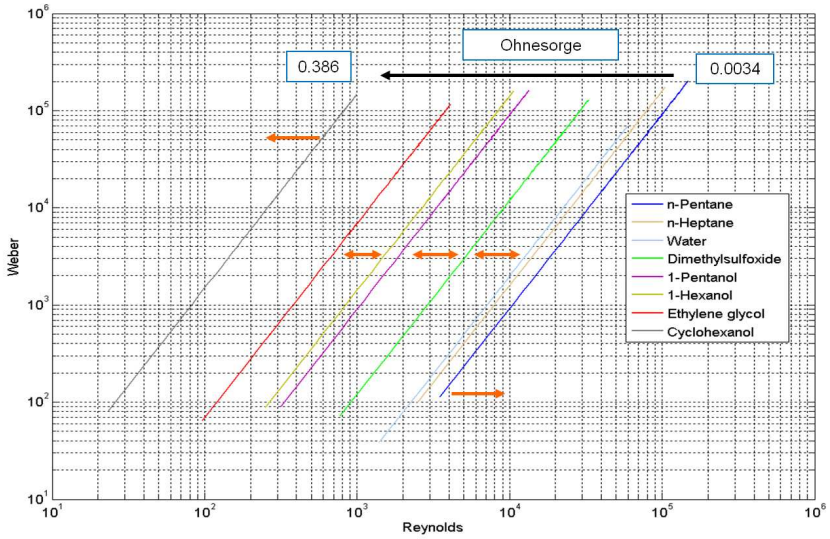

Figure 4.1: Fluids investigated in previous work (see e.g. Ciezki et al. [12])

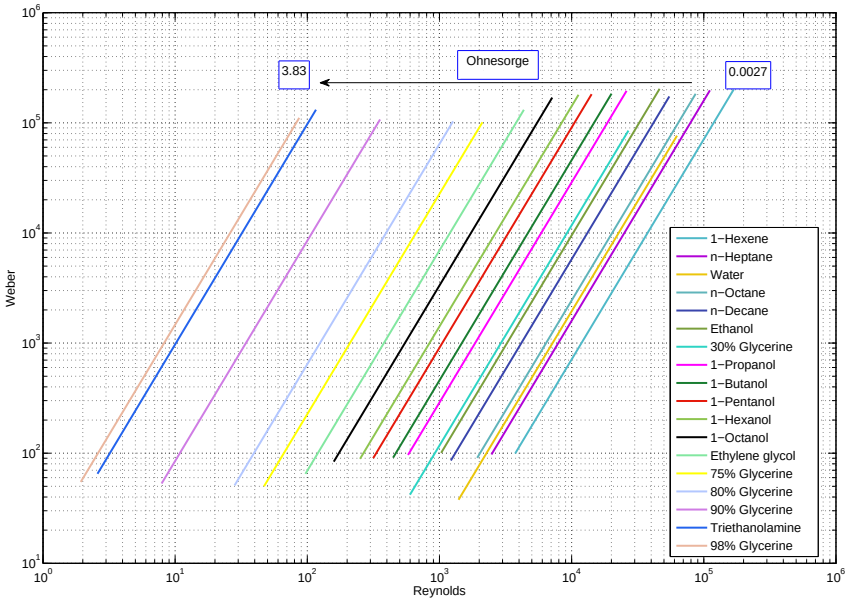

Figure 4.2: Fluids investigated in the current work

The influence of ambient temperature is taken in account interpolating viscosity and surface tension from the data found in literature [15]. In figure 4.3 can be seen how for viscosity an exponential low allows a correlation

coefficient $R^2 \simeq 0.99$. This parameter indicates the goodness of the regression and for all the species it's always more than 0.98. The same values are detectable the surface tension even if the interpolation, in this case, is linear. The variation of density in function of temperature is negligible.

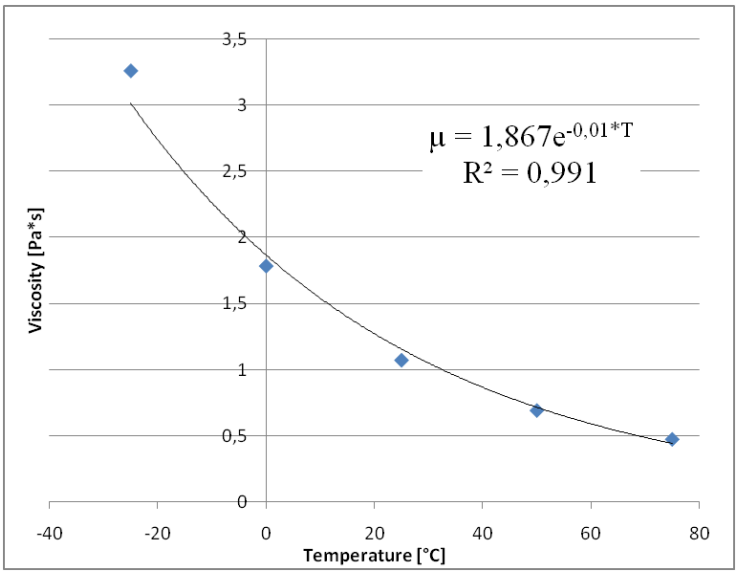

Figure 4.3: Example of μ interpolation: Ethanol

Liquid	**Formula**	μ **[mNs/m^2]**	σ **[mN/m]**	ρ **[kg/m^3]**	**Ohnesorge**	**Hazardous**	**CAS**
1-Hexene	C_6-H_{12}	0.252	19.00	673.0	0.0027	Xn+F^++N	592-41-6
n-Heptane	C7-H16	0.387	19.65	683.6	0.0040	Xn+F^++N	142-82-5
Water	H2O	1.002	74.00	998.0	0.0044		
n-Octane	C8-H18	0.508	21.62	700.0	0.0049	Xn + F	111-65-9
n-Decane	C10-H22	0.838	23.83	730.0	0.0076	Xn + N	124-18-5
Ethanol	C2-H6-O	1.074	21.97	789.4	0.0097	Xn + F	64-17-5
30% Glycerine	30	2.51	71.50	1072.7	0.0108		56-81-5
1-Propanol	C3-H8-O	1.945	23.32	803.5	0.0170	Xi + F	71-23-8
1-Butanol	C4-H10-O	2.544	24.93	809.8	0.0214	Xn	71-36-3
1-Pentanol	C5-H12-O	3.619	25.36	814.4	0.0301	Xn	71-41-0
1-Hexanol	C6-H14-O	4.578	25.81	819.0	0.0376	Xn	111-27-3
1-Octanol	C8-H18-O	7.288	27.60	825.4	0.0577	Xi	111-87-5
Ethylene glycol	C2-H6-02	16.1	47.99	1113.0	0.0833	Xn	107-21-1
75% Glycerine	75	35.5	66.72	1192.0	0.1505		56-81-5
80% Glycerine	80	60.1	66.41	1208.5	0.2536		56-81-5
90% Glycerine	90	219	65.17	1235.1	0.9226		56-81-5
Triethanolamine	C_6-H_{15}-NO_3	609	48.40	1124.2	3.1205	Xi	102-71-6
98% Glycerine	C3H8O3	911	64.17	1256.4	3.8348		56-81-5

Table 4.1: Table of fluids data

4.2 Breakup behaviors

In the present section the results of the tests in an ambient condition will be described. Seven different main families of atomization patterns have been defined and, although they're not identical for all fluids, similarities can be found.

4.2.1 Closed Rim

From the impingement point, where the jets collide, the liquid expands radially creating a flat and thin sheet, perpendicular to the jets collision plane, bounded by a distinct and pronounced rim. This rim collects the major portion of the liquid flow as it is described in Ref. [2]. At the lower end of the sheet the two arms of the rim impinge under a distinct angle. At this tip is formed either a single stream, which breakup into droplets, or another smaller sheet normal to the previous one, which may subsequently decay into droplets.

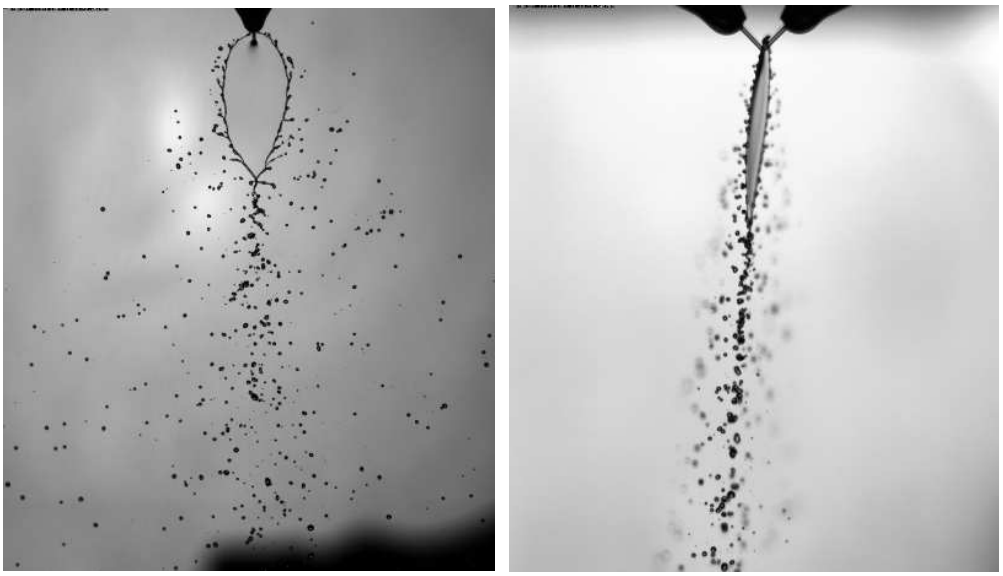

(a) front view (b) side view

Figure 4.4: Closed rim: Decane (Oh=0.0076), U_{jet}=2.6m/s, Re=1316, We=145

As remarked in the introduction, distinct characteristics in the same breakup behavior can be found going in deep with the investigation.

Sheet with stochastic spreading of droplets

This behavior is typical for Newtonian liquids with low Ohnesorge numbers, ranging from that of 1-Hexene (Oh= 0.0027) to that of n-Decane (Oh= 0.0076), at low jet velocities. Figure 1 presents typical shadowgraph images showing perpendicular on the fluid sheet. The sheet appears either smooth or perturbed by small waves. Along the rim disturbances grow with increasing sheet plane angle θ (which is presented in the left image of Figure 4.5) until they lead to the formation of ligaments, which break up into droplets in a stochastic manner. It shall be noted in this context that for the investigated fluids with $0.0027 < Oh < 0.0076$ no stable rim without droplet formation could be observed due to a lower limit of jet velocities, which could be realized with the experimental setup. Bremond et al [16] showed that the

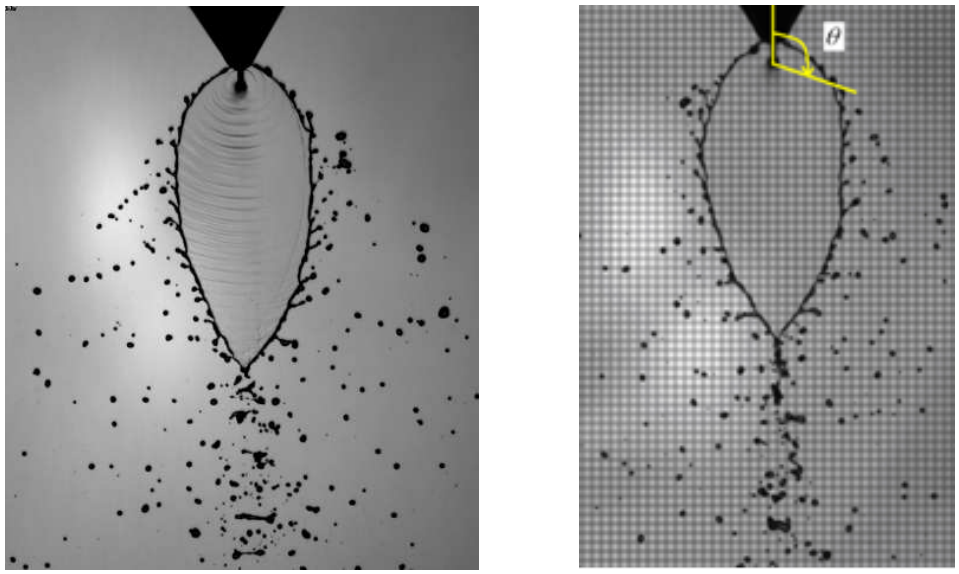

(a) Heptane (Oh=0.004): U_{jet}=1.3 m/s, Re=1349, We=39

(b) Octane (Oh=0.0076): U_{jet}=2.6m/s,Re=2268,We=152

Figure 4.5: Closed rim: stochastic spreading of droplets

perturbations of the sheet are transmitted from the jets to the rim through

sheet thickness modulations. They explained that the instability in the rim is a capillary instability of a Plateau-Rayleigh type. They also pointed that viscous slowing may possibly retard the instability of the rim. If the viscous forces in a capillary (here in particular the rim) are strong enough they may retard the growth of instabilities.

Fluid chains

Increasing the Ohnesorge value of the liquid a steady flow structure composed of thin fluid sheets bound by relatively thick cylindrical rims is generated by the oblique collision of equal laminar jets. Individual links in the chain are mutually orthogonal and decrease successively in size until the chain coalesces into a cylindrical stream. Fluid chains have been well described in Bush and

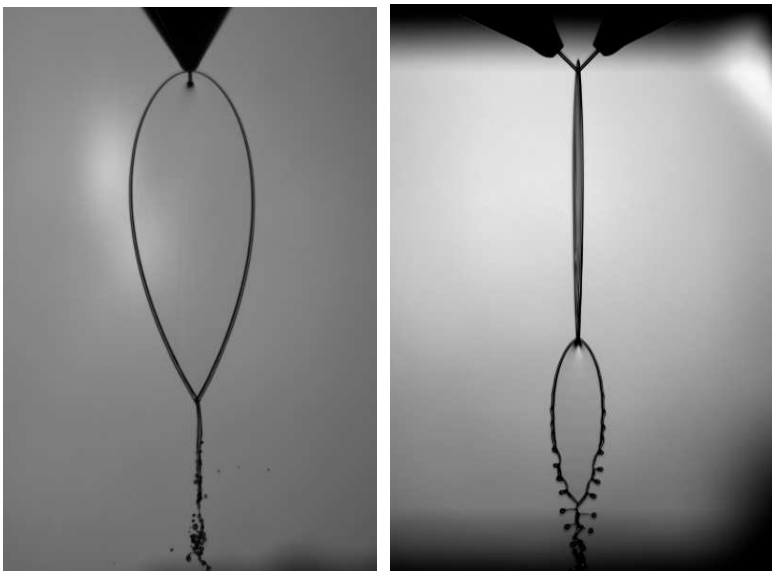

(a) front view (b) side view

Figure 4.6: Closed rim: fluid chains with Butanol (Oh=0.0214): U_{jet}=2.6 m/s, Re=427, We=150

Hasha [17]. They stated that the curvature force associated with the surface tension acts normal to the edges of the fluid sheet and so acts to limit its lateral extent. Moreover, the curvature force causes the sheet to retract and ultimately close, thus forming the apex of the first link. Fluid accumulates

at the edges of the sheet forming a relatively thick rims. When these rims collide at the apex of the link, they give rise to another thin sheet in the plane perpendicular to the first link. The process repeats, producing mutually orthogonal links that decrease progressively in size until the chain coalesces into a cylindrical stream through the action of viscosity. This behavior is typical for every Closed Rim pattern with fluids from Ethanol (Oh=0.0097) to 90%Glycerine (Oh=1.1). The so called fishbone structures could be seen in the last orthogonal sheet.

Fishbones

This breakup mode was observed for fluids with medium Ohnesorge numbers, i.e. from ethanol (Oh= 0.0097) to Ethylene glycol (Oh= 0.0833). Similar jet velocities were used for these experimental conditions as for the breakup mode presented in the previous subchapter.

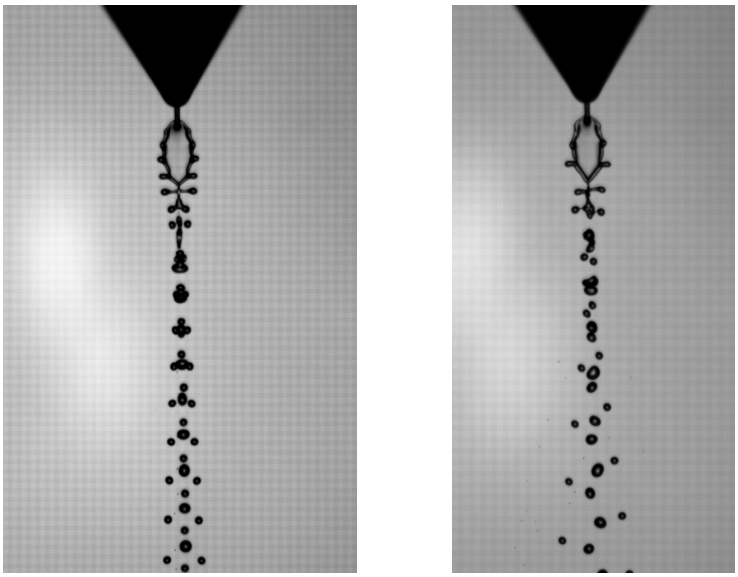

(a) Pentanol (Oh=0.0301): U_{jet}=1.3 m/s, Re=158, We=37

(b) Propanol (Oh=0.0172): U_{jet}=1.3 m/s, Re=296, We=39

Figure 4.7: Closed rim: fishbones structures

It can be seen in the images of Figure 4.7 that also in this breakup

mode disturbances grow along the rim with increasing sheet plane angle θ. Under the present conditions the ligaments, which are connected with the sheet and which show thickening at their ends, are formed in a periodic and symmetrical manner until droplets may be separated. These droplets are moving downstream in a widely symmetrical manner, whereas the angle under which they are moving downstream is significantly smaller than for the in the previous subchapter presented breakup mode with the stochastic separating droplets from the rim.

The fishbone structures breakup mode was first observed by Bush et al. with ethanol [17]. It should be mentioned in this context that the fishbone structures could be observed with ethanol only in the transient phase of the startup of our experiment. Bremond et al. [16] showed that a small difference in the velocity of the two impinging jets may lead to the formation of fishbone structures. In our study fishbone structures were manifested in two different ways. With Propanol, Butanol and Pentanol the fishbone structures could be observed for the entire length of the test. For Hexanol, Octanol and Ethylene Glycol the fishbone structures could only be observed at the start and at the end of the test. According to Bush et al and Bremond et al the source of this instability is Rayleigh-Plateau capillary instability of the rim. They showed that the flapping of the sheet is produced by the instability in the rim and not by aerodynamic instability of the sheet. If the flapping would be caused by aerodynamic instabilities an increase in injection velocity would increase the flapping, which is the opposite of what was observed: the sheet returned smooth and stable for slightly higher velocities.

4.2.2 Open Rim

The sheet is not totally surrounded by a distinct rim. A flapping motion of the lower part of the sheet, which is caused by a Kelvin-Helmholtz-type instability (Ref. [28], [29], [30]), breaks up the rim into ligaments and droplets so that the two arms of the rim aren't anymore in contact. On the side view image it can be seen how this instability generates waves, which lead to the breakup. Also larger droplets could shed from the rim according to the

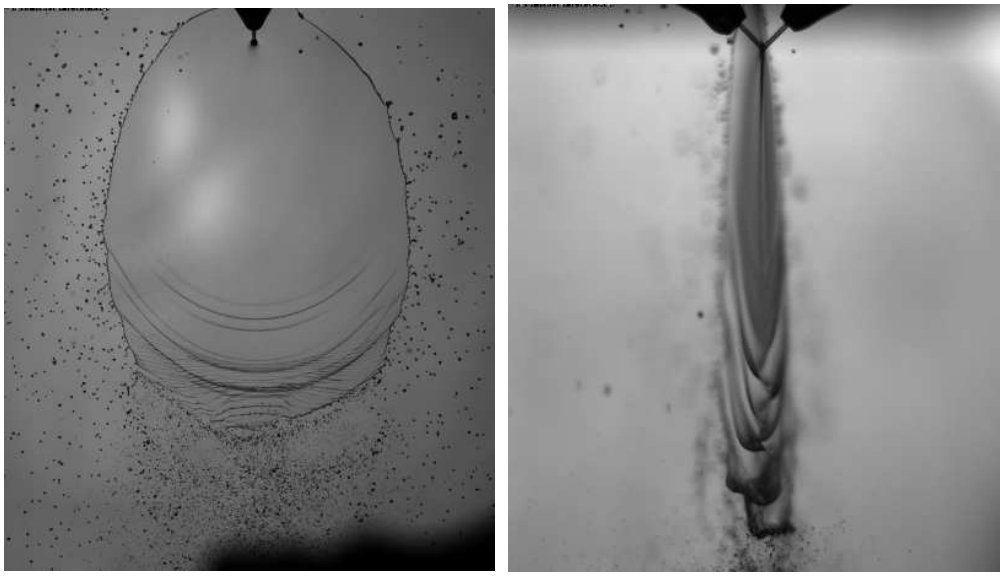

(a) front view (b) side view

Figure 4.8: Open rim: Decane (Oh=0.0076), U_{jet}=7.5m/s, Re=3244, We=901

capillary instability effect (see Ref. [16]). Increasing the injection velocity an expansion of the sheet width with slight reduction of breakup length always happens (see table 4.2).

The atomization process at the edge downstream presents peculiarities increasing the Ohnesorge of the fluid. After a Oh approximately of 0.01 the two arms of the rim becomes more stables and starts to appear at the breakup edge a vertical thinning from which filaments of fluid decay in droplets. Then, increasing the jet velocity, the sheet becomes broader and the capillary instability phenomena affects also the rims that starts to shed droplets. Also the breakup mechanism downstream returns to be similar to the previous one seen for the low Ohnesorge liquids. From the side views it's possible to see how the aerodynamic waves augment in amplitude while the breakup length decreases. Figure 4.9 shows the behaviors described above regarding the Hexanol. Same considerations on the azimuthal corrugations have been made by Villermaux and Clanet in Ref. [9].

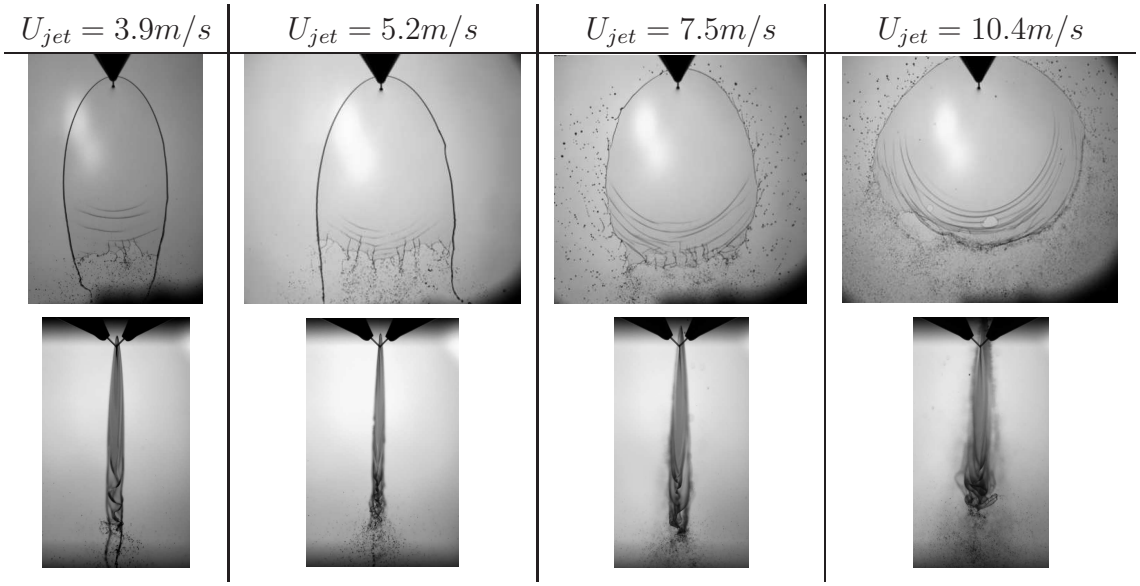

Table 4.2: Open Rim behavior increasing velocity: front and side views, Hexanol

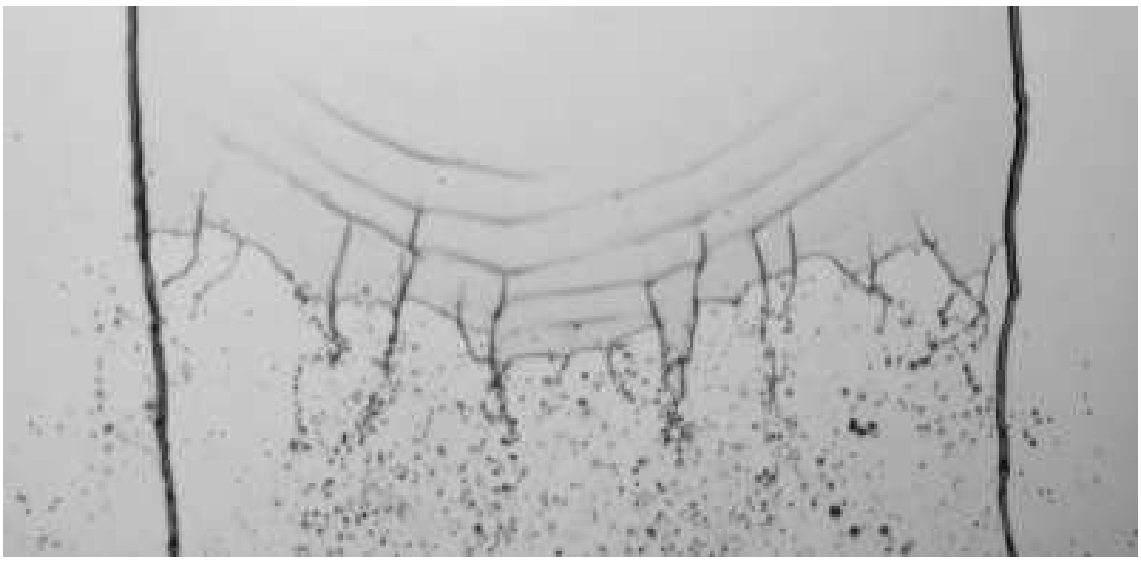

Figure 4.9: Open rim: Hexanol (Oh=0.0376), U_{jet}=5.2 m/s, Re=611, We=591

4.2.3 Rimless Separation

Distinct rims aren't visible anymore. The rupture of the almost circular liquid sheet starts at the sides with the separation of parts of the sheet in the region of the Kelvin-Helmholtz-type instabilities. A direct shedding of droplets from the sheet always occurs and parts of sheet separate periodically decaying farther downstream (see Figure 4.11).

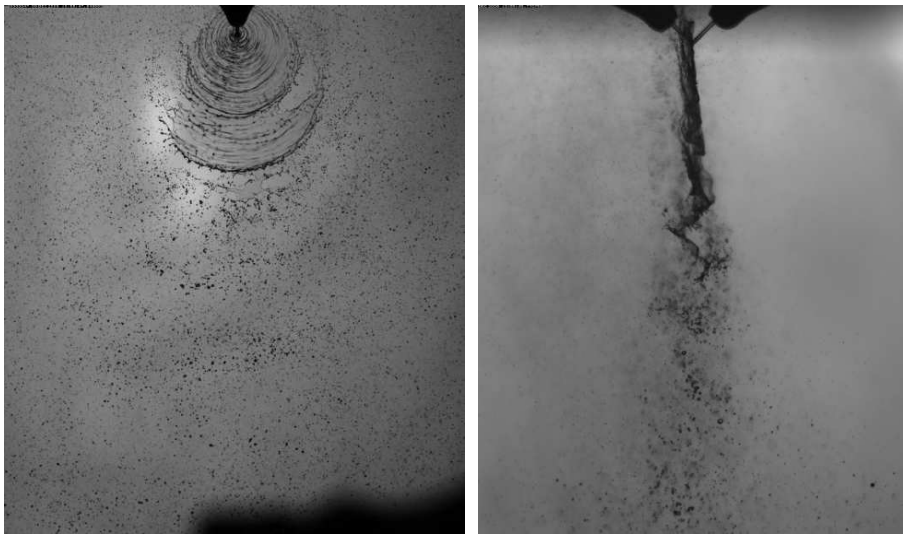

(a) front view (b) side view

Figure 4.10: Rimless Separation: Octane (Oh=0.0027) U_{jet}=5.2 m/s, Re=8650, We=673

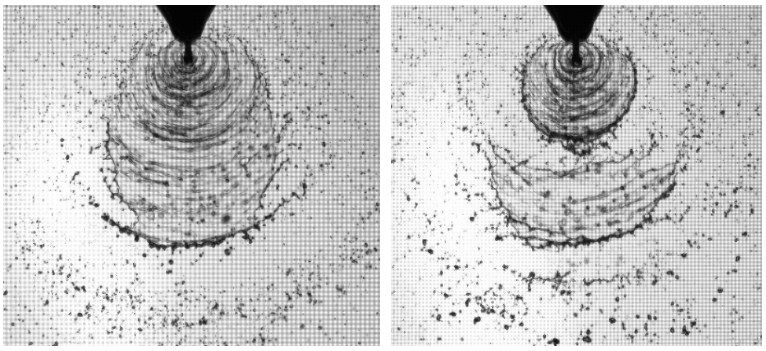

Figure 4.11: Consecutive pictures that show periodic separation of part of the sheet: Hexene (Oh=0.0027) U_{jet}=5.2 m/s, Re=8650, We=673

4.2.4 Smooth Sheet Ligaments

This breakup shows some similarities to the rimless separation mode. But instead of the droplet direct decay from the sheet, a periodic separation of bow-shaped structures (also called ligaments) from the sheet occurs, which subsequently decay into droplets downstream.

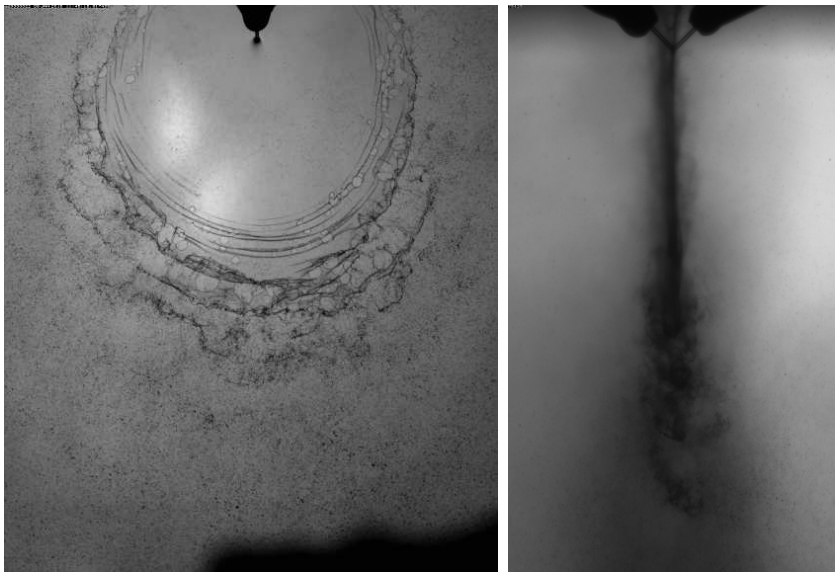

(a) front view (b) side view

Figure 4.12: Smooth Sheet Ligaments: Ethylen Glycol (Oh=0.0833) U_{jet}=24.7m/s, Re=1095, We=9899

The separation of these ligaments is supported by the occurrence holes in the sheet, which grow in size. It seems that these holes (Figure 4.13) appear after the highest amplitude of the wavy structures present on the sheet.

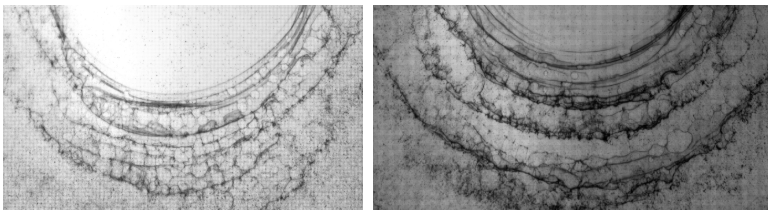

Figure 4.13: Smooth Sheet Ligaments: rupture in ligaments by holes

4.2.5 Ruffled Sheet Ligaments

In this mode the inner part of the sheet is not anymore smooth. Wavy structures occur directly on the sheet, which size (in particular the breakup length) is difficult to detect on the images. The bow-shaped ligaments, which are moving periodically downstream, seem to be separated significantly earlier from the sheet so that the sheet size seems to be significantly reduced. On the side view image, it can be noticed that the spreading angle of the droplets is significantly larger than for the smooth sheet ligaments mode. Furthermore, it can be observed that the two jets start to pronounce a turbulent behavior.

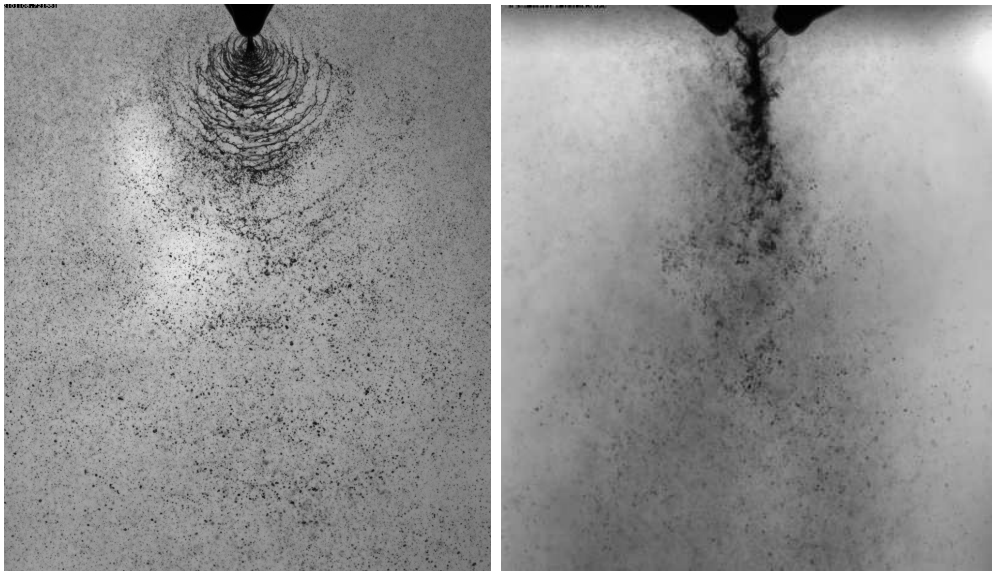

(a) front view (b) side view

Figure 4.14: Ruffled Sheet Ligaments: Decane (Oh=0.0076) $U_{jet} = 16.9m/s$, $Re = 8617$, $We = 6124$

4.2.6 Fully Developed

A direct decay into droplets without any ligaments formation seems to occur comparatively near the impingement point of the two jets, which state of flow can be assumed as turbulent. These separated droplets are mainly concentrated in bow-shaped "clouds", so that waves of droplets spread downstream

periodically. From the side view of Figure 4.15 it can be noticed that the sheet is completely absent and droplets shed in all the directions. As will be shown later on, this regime corresponds to the operative point of all the rocket propulsion engines.

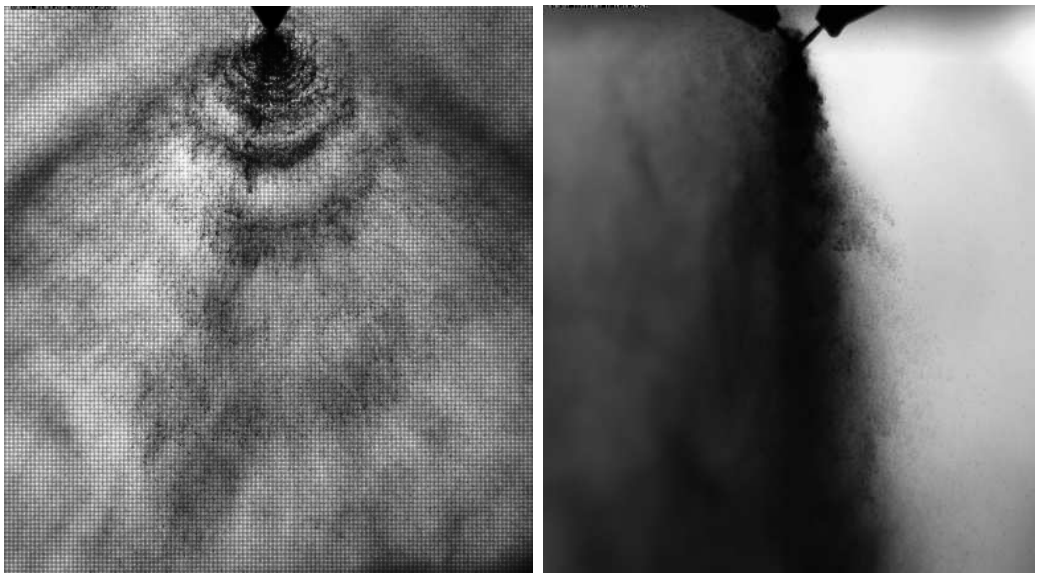

(a) front view (b) side view

Figure 4.15: Fully Developed: n-Octane (Oh=0.0049) $U_{jet} = 58.5m/s$, $Re = 51025$, $We = 76719$

It has to be mentioned that a very particular behavior has been observed for the very low Ohnesorge substances at highest velocities. An example is given in Figure 4.16 where a violent spreading of droplets cloud by "lines" is present for both the fluids. A detailed study on this peculiar behavior is necessary.

4.2.7 Aerodynamic Instability

No droplets were separated from the sides of the rims of the liquid sheet at low jet velocities, the sheets are long and narrow and their surface is smooth. At a distinct higher velocity the sheet starts to be subjected to an aerodynamic instability that generates a flapping motion of the sheet. The

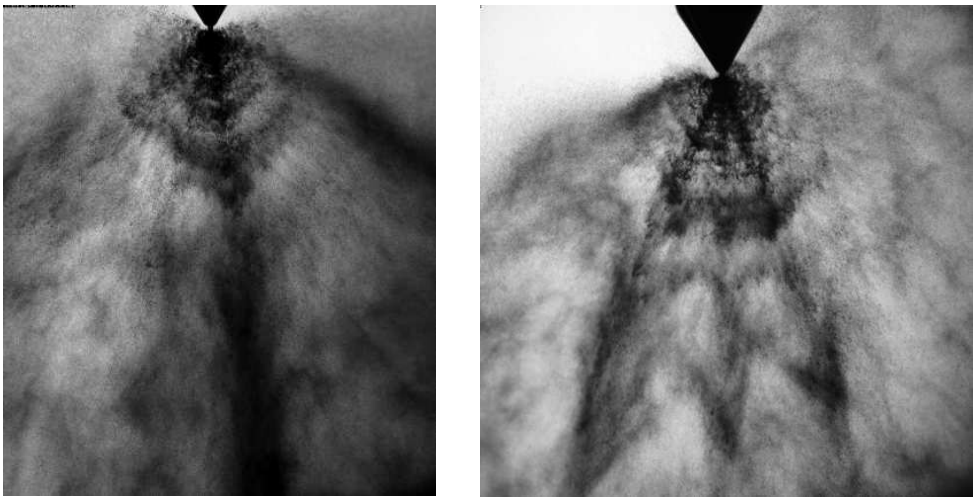

(a) Decane (Oh=0.0076) $U_j = 79.3m/s$, $Re = 39576$, $We = 134071$

(b) 1-Hexene (Oh=0.0027) $U_{jet} = 67.6m/s$, $Re = 110141$, $We = 112527$

Figure 4.16: Fully Developed peculiarity: violent spreading by lines

side view of Figure 4.17 clearly shows this flapping.

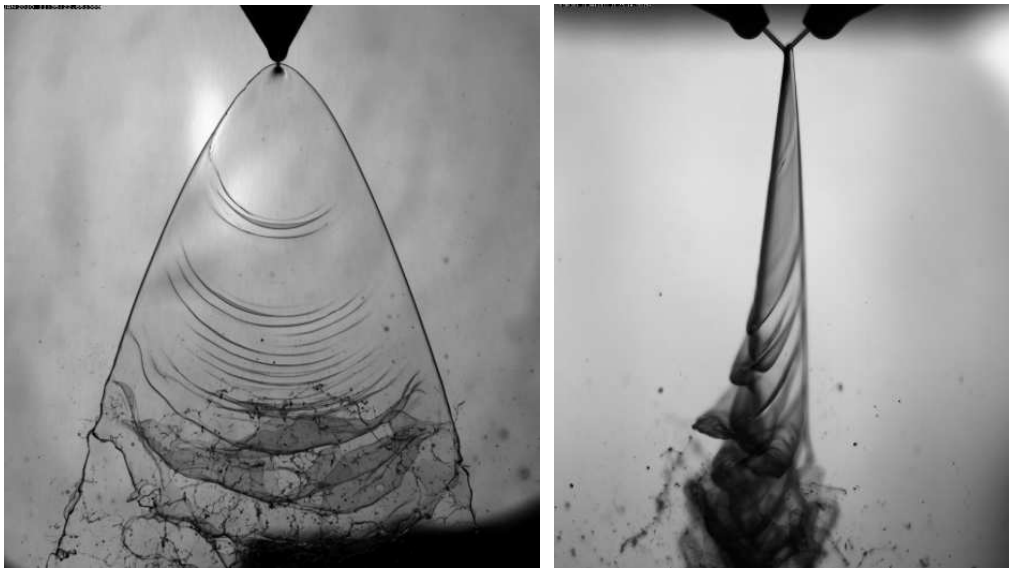

(a) front view

(b) side view

Figure 4.17: Aerodynamic Instability: Triethanolamine (Oh=3.12), $U_{jet} = 28.6m/s$, $Re = 31$, $We = 13321$

It should be noticed that the upper part of the sheet is still stable, with a smooth and thick rim and a flat sheet. No capillary instability could be observed in this region. The breakup of the sheet results from an aerodynamic instability of the Kelvin-Helmholtz type. It was first analyzed in the context of liquid sheets by Squire [28]. A detailed explanation of this phenomenon was given by Clanet et al [**?**]. The instability arises when the liquid sheet moves in a still medium. On both sides of the sheet disturbances are generated from the shear stress that arises due to the speed difference between the sheet and the surrounding ambient air. The coupling of these disturbances by the pressure inside the liquid allows only two destabilization modes: an antisymmetric, sinuous mode and a symmetrical dilatation mode. Clanet and Villermaux showed how for a thin liquid sheet moving in a much less dense environment the sinuous mode is the mode that leads to instability, having a higher grow rate than the symmetric mode.

4.3 Test Example

In the following an experimental test regarding Ethanol is showed. As can be seen every experiments has been analyzed first in an excel tale (Table 4.3), calculating and interpolating the different properties. Then each test has been graphed on the Re-We both with the typical test shadowgraph images (Figure). The result for Ethanol can be seen in Figure 4.18. For all the the other test images please see

BAI	**Pump**	**T [°C]**	U_{jet} **[m/s]**	ρ **[kg/m3]**	μ **[mPa s]**	σ **[N/m]**	**Re**	**We**	D_{32} **[μm]**	**Breakup**
61	0,45	18	1,3	789,4	1,33	12672,47	541	42		cr
74	0,48	19	1,95	789,4	1,30	13461,87	828	95		cr
62	0,5	18	2,6	789,4	1,33	12672,47	1083	168		cr
69	0,55	18	5,2	789,4	1,33	12672,47	2166	671	114,29	or
68	0,6	18	6,5	789,4	1,33	12672,47	2707	1049	103,11	or
76	0,65	17,5	7,8	789,4	1,34	12277,77	3218	1507	96,74	or
63	0,7	17,5	9,1	789,4	1,34	12277,77	3755	2051	89,98	sl
70	0,8	18	13	789,4	1,33	12672,47	5415	4194	80,07	sl
73	0,8	20	13	789,4	1,28	14251,27	5625	4226	82,49	sl
72	0,85	20,5	14,3	789,4	1,27	14645,97	6246	5123	84,47	sl
71	0,9	21	16,6	789,4	1,25	15040,67	7320	6916	83,31	l
64	1	18	19,5	789,4	1,33	12672,47	8122	9437	74,62	l
65	1,2	18	27,3	789,4	1,33	12672,47	11371	18496	67,95	l
66	1,5	18	42,9	789,4	1,33	12672,47	17869	45673	52,01	l
77	1,7	19	54,6	789,4	1,30	13461,87	23178	74260	41,81	fd
67	2	18	70,2	789,4	1,33	12672,47	29240	122298	34,45	fd
75	2,5	17,5	83,2	789,4	1,34	12277,77	171467	312	30,45	fd

Table 4.3: Example of Excel work-sheet used to calculate the parameter of interests (Ethanol)

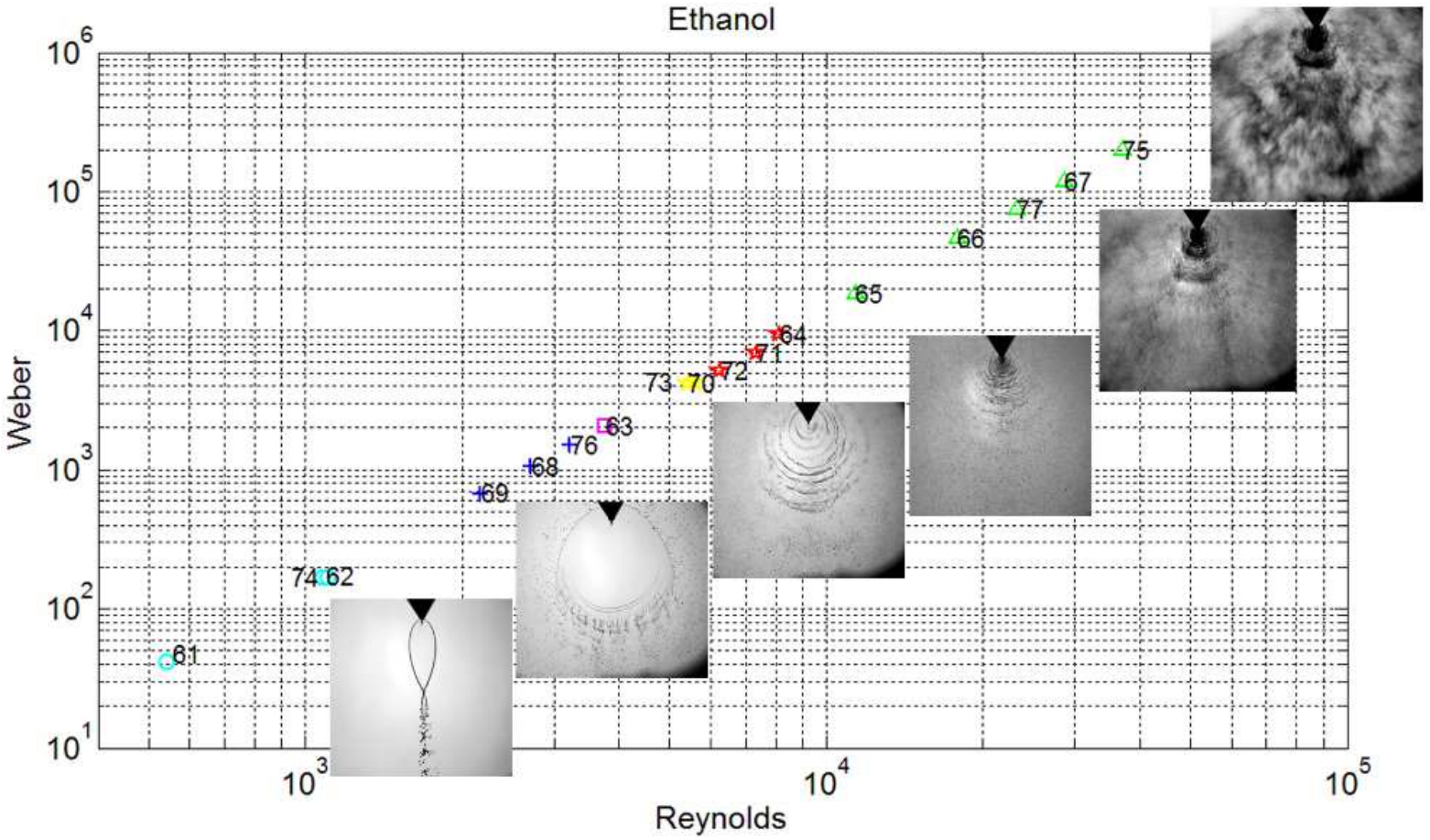

Figure 4.18: Image of Re-We test example: Ethanl

4.4 Droplets Measurement

A droplets measurement has been made for each fluids tested using the Malvern Spraytech laser and a typical output data is shown in Figure 4.19. As can be seen the software RTSizer 5.4 gives the different droplets diameter quantities, e.g. $Dv(10)$, $D_{3,2}$, $D_{4,3}$, etc. and through the Time History window it can be calculated an average PSD (Particle Size Distribution) in a chosen interval.

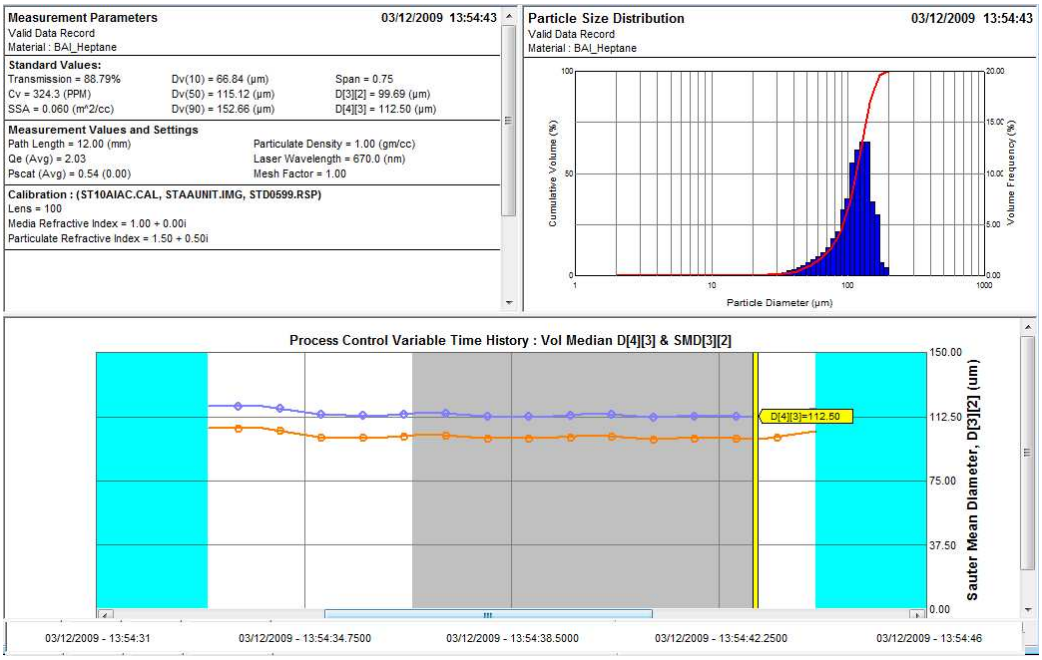

Figure 4.19: Typical Malvern output using RTSizer (Average plot)

In the present work an average during the stationary state is always considered, this means a size of droplets almost constant in the time range. In the current work the droplet diameter has been referred to the $D_{3,2}$ value, also called Sautem Mean Diameter. This number represents an average size of droplet diameter where the volume surface ratio of the particle it's assumed the same of the probe and is expressed like:

$$D_{3,2} = \frac{\sum d_i^3}{\sum d_i^2} \tag{4.6}$$

It's a parameter commonly used in atomization and combustion field for its good relationship with the heat and mass transfer. In the pictures below the SMD vs jet velocity, vs Reynolds and vs Weber are plotted. As can be seen in Figure 4.20 the general diameter trend is to decrease increasing velocity. In particular seems there's no marked influence of the fluid properties till an $Oh \simeq 1$.

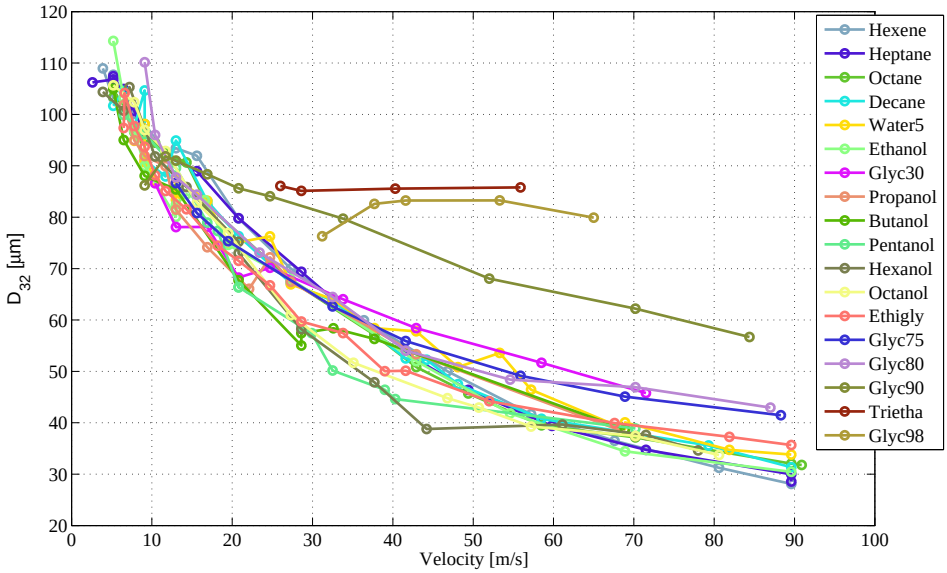

Figure 4.20: Sauter Mean Diameter vs U_{jet}

Moreover it can be noticed the Triethanolamine and 98% Glycerine mixture have almost a constant droplets size, so they won't be considered in the relations that will be shown later on.

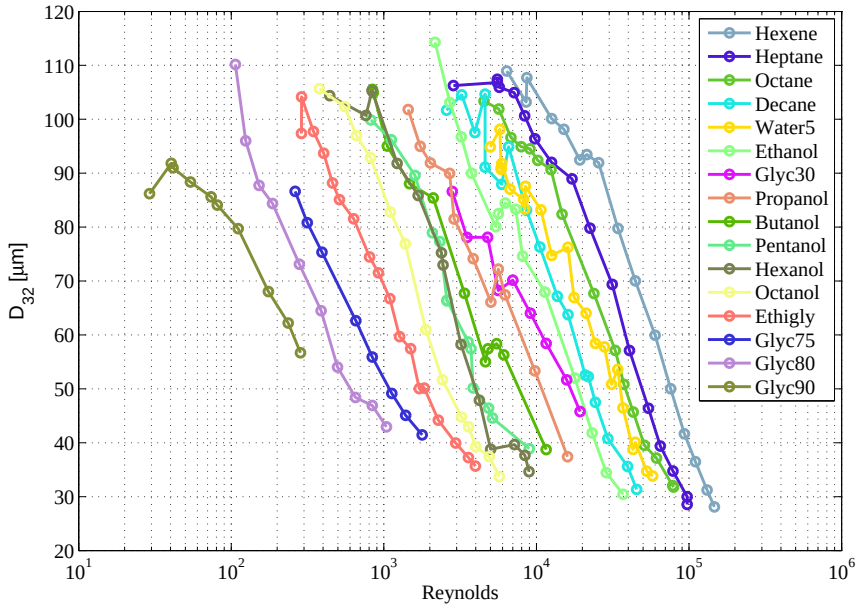

Figure 4.21: Sauter Mean Diameter vs Reynolds

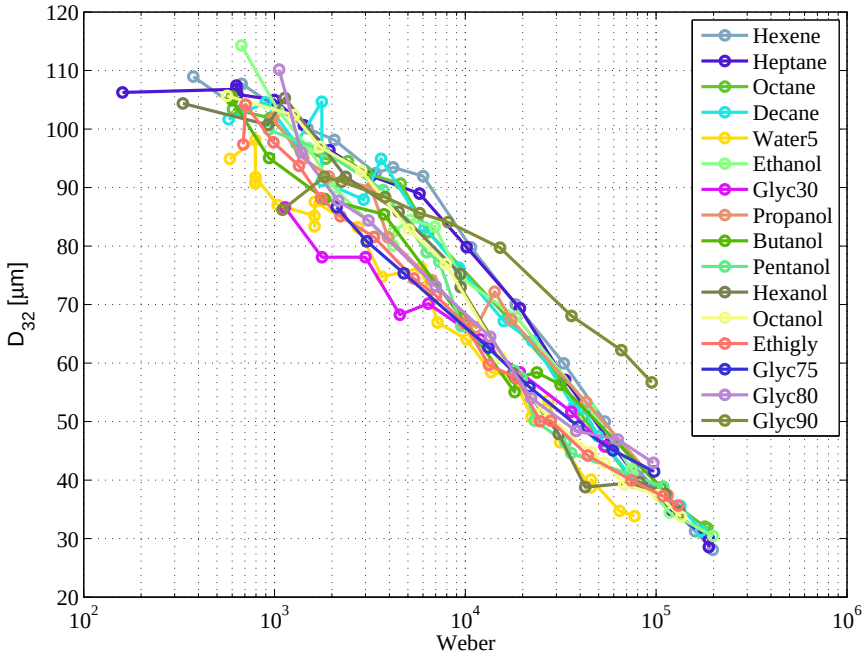

Figure 4.22: Sauter Mean Diameter vs Weber

Chapter 5

Pressurized Condition Campaign

The main object of this section is to examine the general effect of pressure on the breakup behaviors. Since the pressure inside the chamber increases during the combustion processes, it could be useful to study how an augment of the ambient pressure affect the atomization characteristics with cold flow experiments. In the years Jung et al. [22] and Dombroski et al. [19] studied the influence of high environment density on the impinging injector spray behavior of water and few sucrose solutions. Nevertheless questions are still open.

5.1 Fluids Decision

Safe handling and storage procedures have to be respected since most of the fluids used in the open environment tests are harmful. Generally according to the Material Safety Data Sheet (see [35], [32]) a ventilated area must be guaranteed. In case of a close apparatus, like the one used in this section, only the not stinky fluids can be used. As can be seen in Figure 5.1 only seven species have been examined.

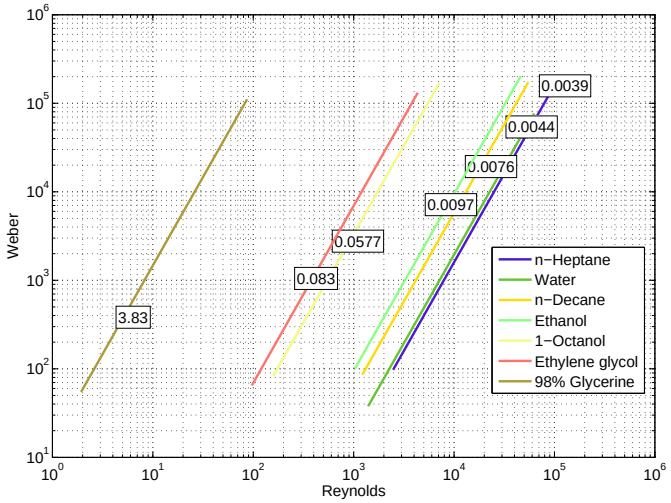

Figure 5.1: Fluids investigated

5.2 Developing of MATLAB program for test analysis

Since the experimental setup used is completely new, a program to analyze the sensors data has been developed using Matlab R2009a. For the first step the program receives in input the text file that is computed by the M11 acquisition system. The pressures and temperatures of both cartridge and pressurized chamber, the piston's displacements and the acquisition time are stored each in different columns. Once the txt file is uploaded, the program allows to visualize the data (e.g. Figure 5.2), in particular an interactive input window is used in the pressure/displacements vs time graph (e.g. Figure 5.3). In this way the user can choose the initial and final points into which the mean values of piston velocity has to be considered. The velocity of the jets it's calculated using the continuity equation since the gradient of pressure realized still allows to use the incompressible hypothesis. The program, named *elaborate_data.m*, saves in a *.txt* file the data elaborated. An example is given in Table 5.1. The temperature of the liquid it's useful for further numerical estimation of viscosity and surface tension as well as the velocity of the jets and density of pressurized air may be utilized for dimensionless

numbers analysis.

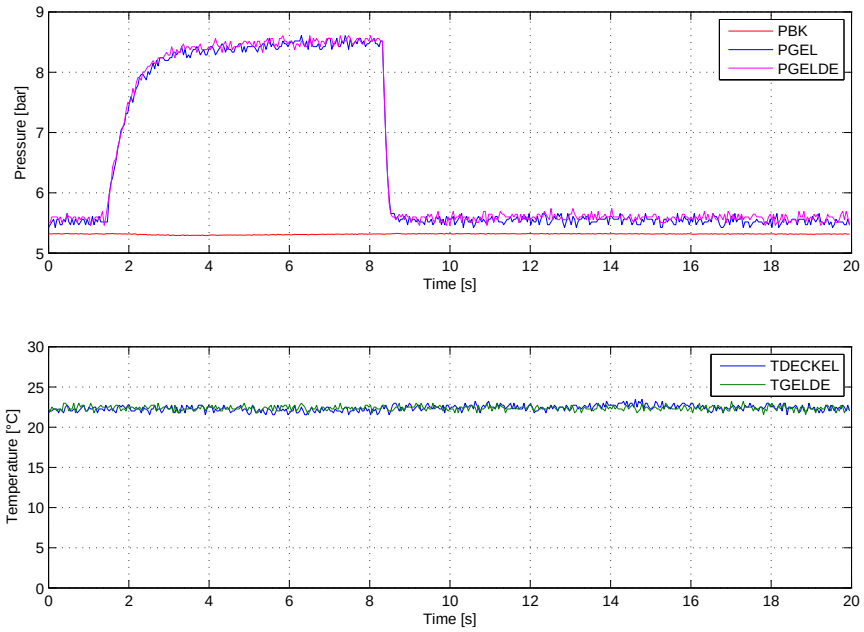

Figure 5.2: Test example of Ethanol @5*bar*: Pressure and Temperature diagram

T_{liq} [°C]	U_{jet} [m/s]	ρ_{air} [kg/m^3]	Breakup	Test
23.820447	6.301272	6.816371	or	BAI0349.txt
23.441833	9.059828	6.736812	or	BAI0350.txt
23.375195	8.920601	6.623654	or	BAI0351.txt
22.782935	12.633592	6.528509	sl	BAI0352.txt
22.935935	22.729662	6.427309	fd	BAI0353.txt
22.776876	36.178032	6.364757	fd	BAI0354.txt
22.368844	50.844824	6.254338	fd	BAI0355.txt
20.205762	16.327257	6.970086	sl	BAI0363.txt

Table 5.1: Example of file.dat used to elaborate results

In order to complete the atomization characteristics of each fluid investigated, after a detailed look of the pictures acquired during the spray tests,

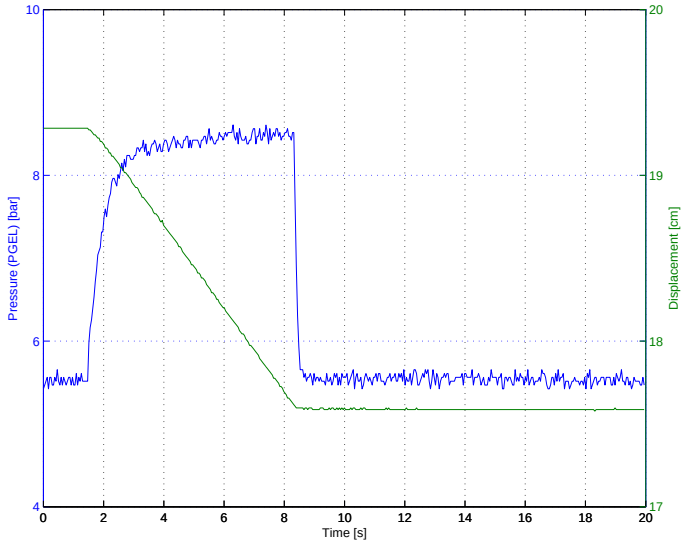

Figure 5.3: Interactive window of Ethanol @5*bar*

one column (called Breakup) with abbreviation of the atomization patterns should be created. Thus the calculated *file.dat* it's ready to be processed using *graphics.m*. This code allows to manage the numerical data both with the string breakup abbreviation recalling the *txt2calc.m* function. Then the elaboration considers the influence of temperature on the fluid properties and uses the dimensionless numbers, the jet velocity and the breakup markers, calculated by the subfunction *calc.m*, to realize graphs that will show every test characteristics.

5.3 Pressurized Atomization Behaviors

The tests have been made using three different ambient pressure, e.g. 1, 5 and 10 bar, increasing the injection velocity and using air as ambient gas. It's useful to remind that the ideal gas law it's still valid, thus to an increase of air ambient pressure corresponds an increase of gas temperature and density. In fluid dynamics studies, in fact, it's often reported the ambient density as working variable. In this work we will feel free to use both pressure

and density as the parameter we are varying to investigate the atomization behaviors, since the ΔT can be taken in account.
Figures 5.5 and 6.15 show a representative series of shadowgraph images of the impinging injector operating with Ethanol and Octanol, increasing velocity from up to down and ambient pressure from left to right.

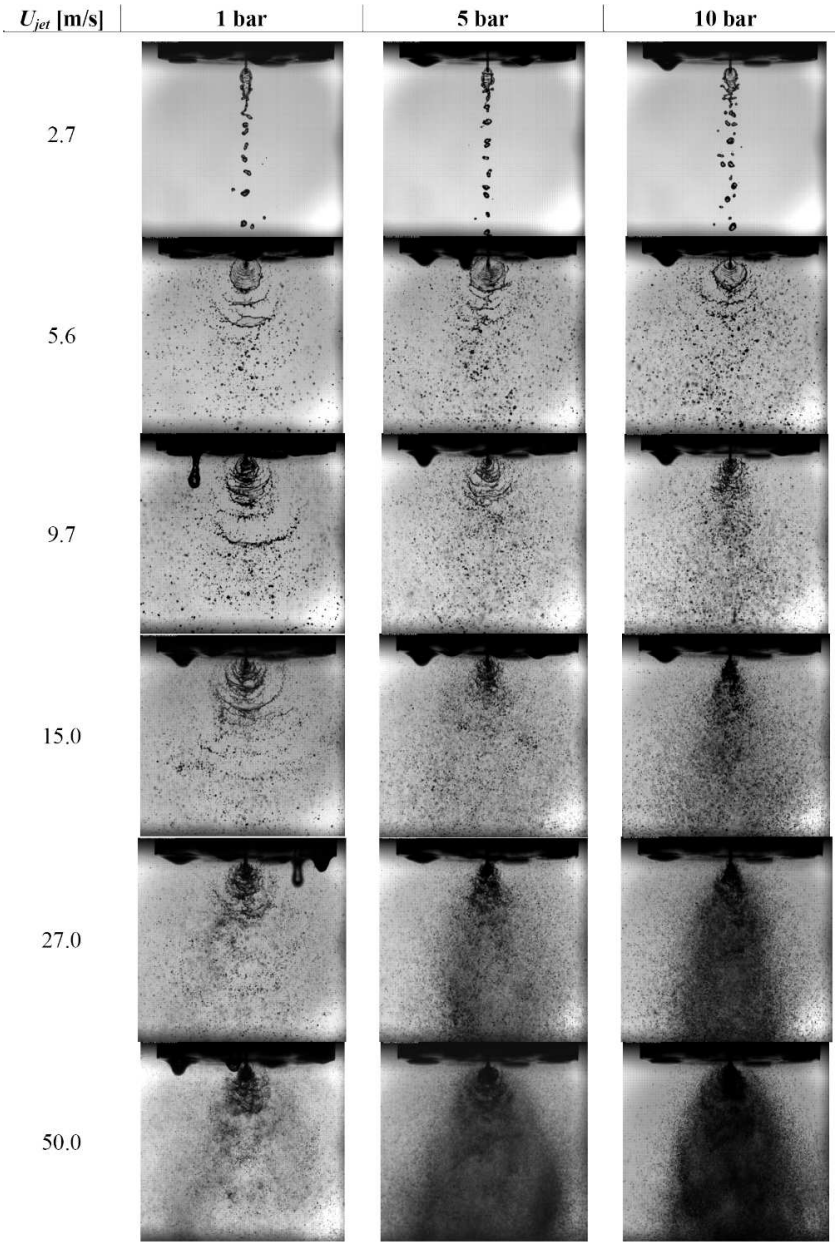

Figure 5.4: Pressure test: n-Heptane

As can be clearly seen from both the pictures, increasing the velocity the breakup behaviors are still reconcilable to the seven main regimes previously found. This means that, even if the injector internal geometry

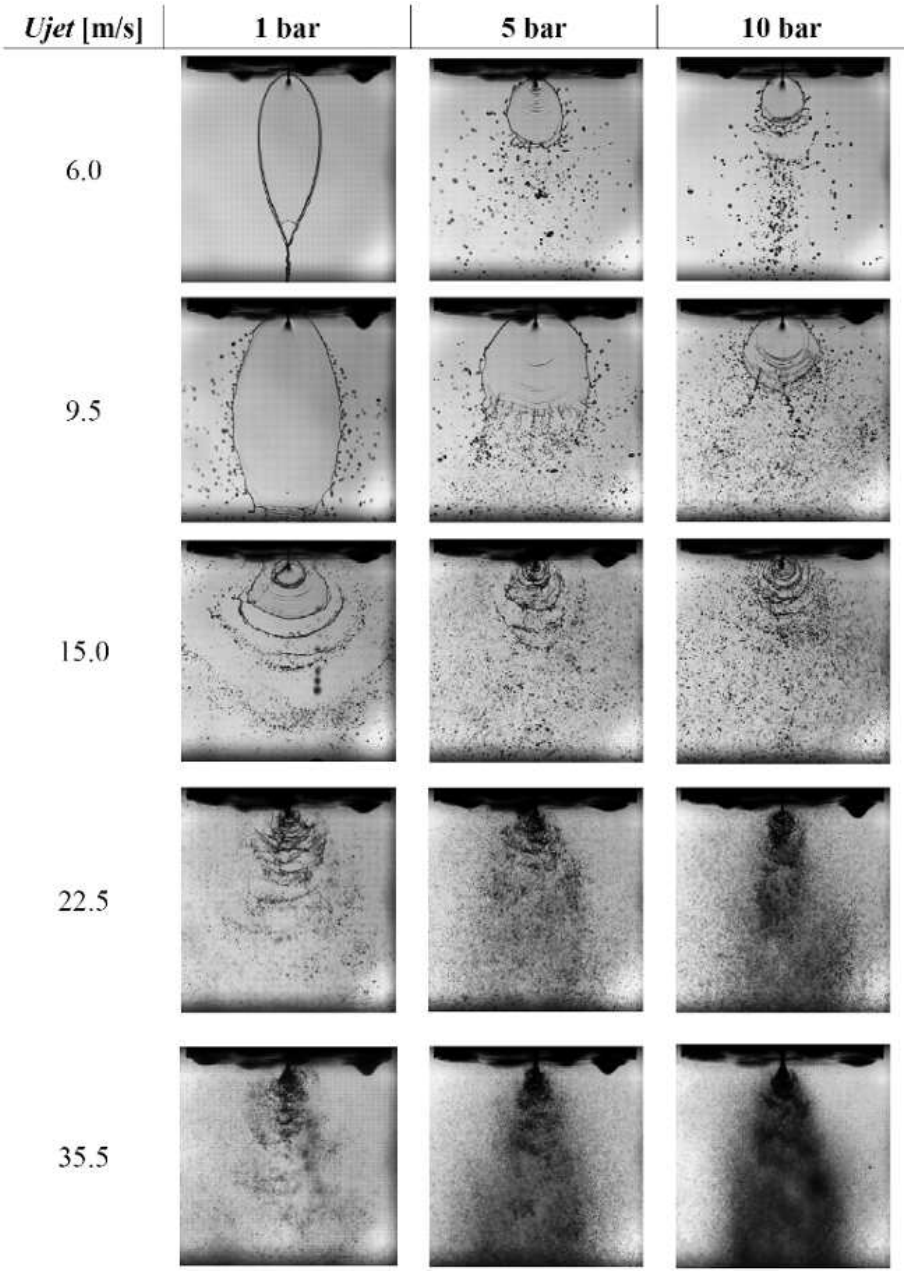

Figure 5.5: Pressure test: Ethanol

changes, the atomization mechanisms strongly rely on injection diameter,

pre-impingement length and diameter to channel length ratio. It has to be mentioned that the same patterns in ambient pressure (1 bar column) appears in the previous campaign at slightly lower velocities (i.e. liquid Weber and Reynolds). This is probably due to the sharp edges of the injection channels that anticipate the turbolent behavior of the velocity profile at the exit. It's important to see that often the upper part of the sheet impinge against the injection plate. Nevertheless this impingement doesn't affect the spray pattern for each velocity and pressure condition investigated.

Chapter 6

Discussion

6.1 Influence of Pre-Impingement Length

Many studies (Ref. [**?**], [8]) have emphasized the importance of the pre-impingement length on the atomization behavior of the sheet formed by the impingement of two cylindrical jets. A perturbation of the jets strongly affects the characteristics of the sheet both for capillary and longitudinal instabilities present in the jet. In aim to study only the effect of fluid properties varying the jet exit velocity, an investigation on the better pre-impingement length to use has been performed with water.

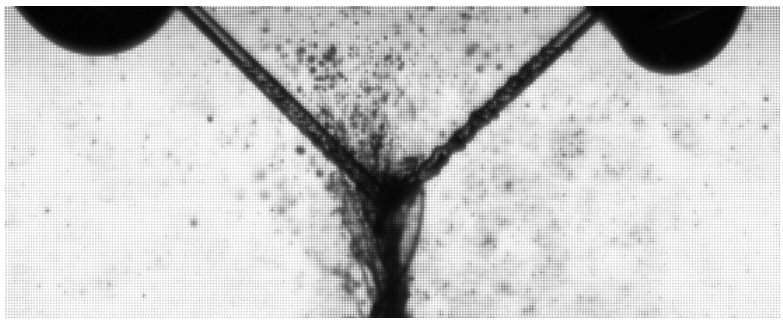

Figure 6.1: Water 10 mm jets: $U_{jet} = 10.4m/s$

Figure 6.1 and 6.2 represent images on the jet behavior at a jet exit velocity of $10.4m/s$ with a pre-impingement length, l_{pre}, of 10 and $5mm$. As can be clearly seen perturbations occur in the jet for $l_{pre} = 10mm$, while the

instability effects seem to be negligible for $5mm$ test.

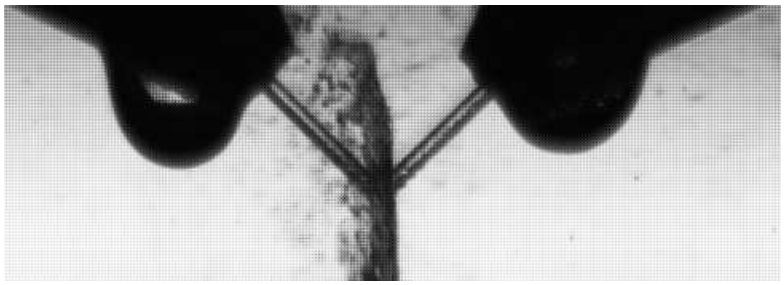

Figure 6.2: Water 5 mmjets: $U_{jet} = 10.4m/s$

As can be seen in Figure 6.3 the ruffled behavior of the jet before the stagnation point reflects on the formed sheet that breakup periodically in parts of sheet or ligaments. This periodic atomization it has been found in the transition region from rimless separation to ruffled sheet ligaments pattern. Decreasing the impinge length an almost stable rimless separation mode happens (Fig.6.3(b)). To reduce the effect of the several geometrical parameters which influence the spray behavior, also for a transition region as in this case, a pre-impingement length of $5mm$ it has been used both in the ambient and the pressurized condition experiments.

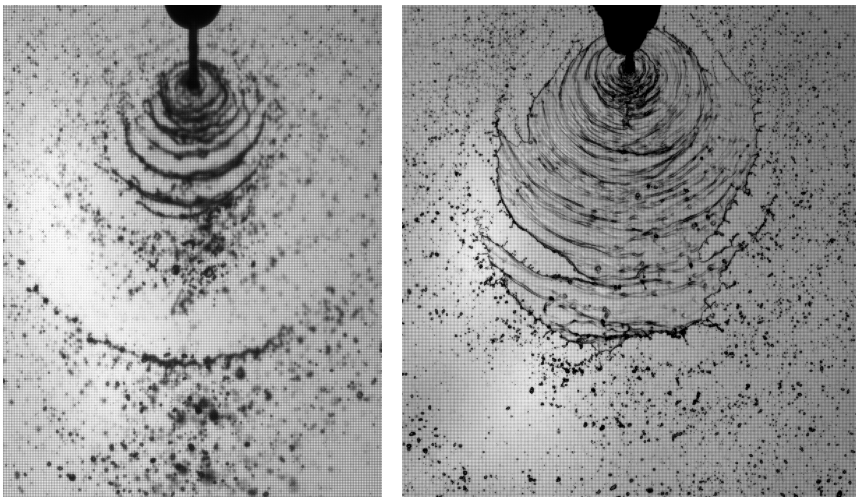

(a) $l_{pre} = 10mm$ (b) $l_{pre} = 5mm$

Figure 6.3: Front view of water sheet formed by two different pre-impingement length at a jet velocity of $10.4m/s$

6.2 Influence of Ohnesorge number

Table 6.4 presents typical shadowgraph images of the atomization of four distinct fluids with different Oh numbers. For all fluids tested different breakup patterns could be observed with increasing jet velocity, and thus increasing Re and We numbers. For n-Heptane (left column), which is a fluid with a very low Oh number, at low injection velocities (and thus low Re and We) a flat sheet with a distinct rim is produced perpendicularly to the plane of the two impinging jets. From the rim which surrounds the whole sheet, droplets separate in a stochastic manner. Going to higher velocities (and Re and We) a flapping motion of the lower part of the sheet breaks up the rim so that the two sides of the rim aren't anymore in contact. The rim disappears completely for further increases in velocity and the sheet becomes ruffled. For the higher injection velocity no sheet can be observed, and the jets atomize in droplets very close to the impingement point.

Tests with Glycerine (right column), which is a fluid with a very high Oh number, show that the jets do not impinge at the lower velocities due to the bending of the jets by gravitation. An increase in the velocity leads to the impingement of the jets and to the formation of a smooth sheet with a thick rim perpendicular to the jets. The shape of the sheet is very elongated. For further increase in velocity the lower part of the sheet starts to flap. At the higher injection velocities the sheet increases in width. The inner part of the sheet remains smooth up to a distinct bow-shaped line. Downstream (going to the outer region) starts an increasing flapping of the sheet, which leads to a breakup into droplets as can be seen on the lowest image in the column. Furthermore it can be seen that the distinct rim remains up to high velocities and vanishes not till the breakup region.

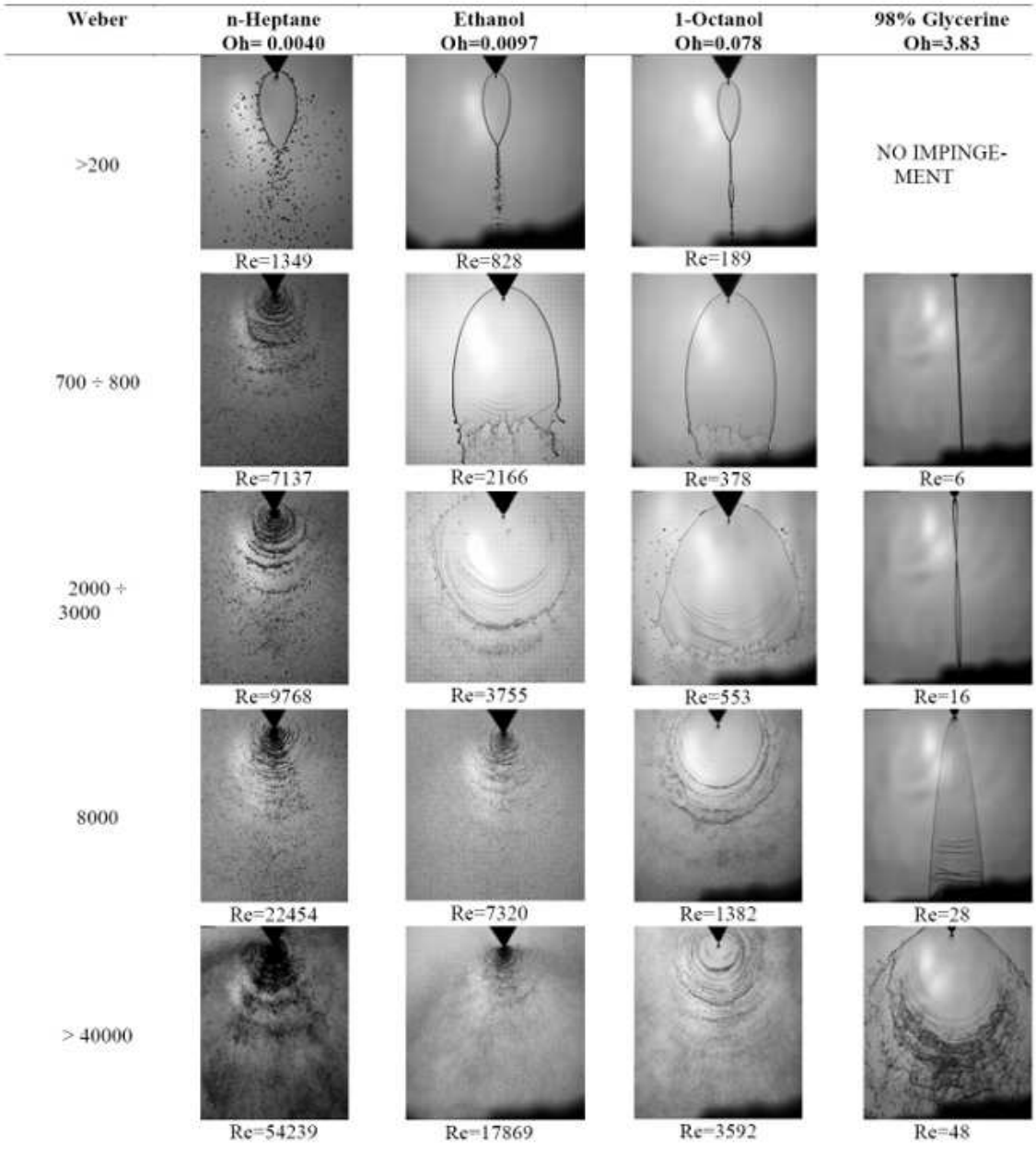

Figure 6.4: Influence of Ohnesorge number on the breakup behaviors

6.3 Regime Diagram

As explained in the Section 4.1, the experiments can be positioned in a Reynolds vs. Weber diagram, which is presented in Figure 6.5. Tests conducted with the same liquid for increasing injection velocities are laying on a straight line in this log-log diagram due to the equation $We = Oh^2 \cdot Re^2$. The Ohnesorge number of the used fluids increases moving from right to left in a range from 0.027 (Hexene) to 3.83 (99% Glycerine solution). The data points in the diagram have different symbols and are additionally color-coded to show the respective breakup regime.

It can be seen that the Closed Rim (CR) mode occurs for all fluids. It is detectable in the region of $102 < Re < 104$ below a constant Weber number of approximately $We < 300$. The low Weber indicates that in this region the surface tension forces are dominant in comparison to the inertial forces for fluids of approx. $Oh < 0.1$. Taylor [5] stated that the surface tension forces are that what holds together the rim, which may be an explanation why distinct rims can be observed in the low We region. Moreover in the left part of the diagram (approx. $Re < 50$) where the liquids with the highest Oh are located, the CR regime expands to a higher Weber number.

The Rimless Separation mode presents the transition between the Open Rim mode and the two modes with ligaments structures (Smooth Sheet and Ruffled Sheet) for fluids with Ohnesorge numbers in the range $0.044 < Oh < 0.25$. This mode occurs in a small band, whose position in the diagram decreases slightly with increasing Re. The Smooth Sheet with Ligaments pattern was found above a nearly constant Weber number $We \cong 4103$ in the Reynolds range from 8101 to 5103. For higher Re the Ruffled Sheet with Ligaments structure mode occurs. The different behavior of the sheet for these two patterns may probably be related to the fact that the injector flow conditions of the impinging jets are laminar for the Smooth Sheet mode and turbulent for the Ruffled Sheet mode. This agrees with the observation that above a certain Re all sheets are ruffled.

The Fully Developed regime is located in the high-est Re and We region, at approx. $Re > 5103$ and $We > 1104$. It can be assumed that on the one hand the state of fluid flow in the injector tip passages is turbulent. On the other hand the influence of the surface tension forces is low in comparison to the inertial forces. In the limited region of very low Reynolds (and relatively high Ohnesorge) numbers a breakup pattern, which was called "Aerodynamic Instability Breakup mode", could be identified for the three liquids with the highest Oh.

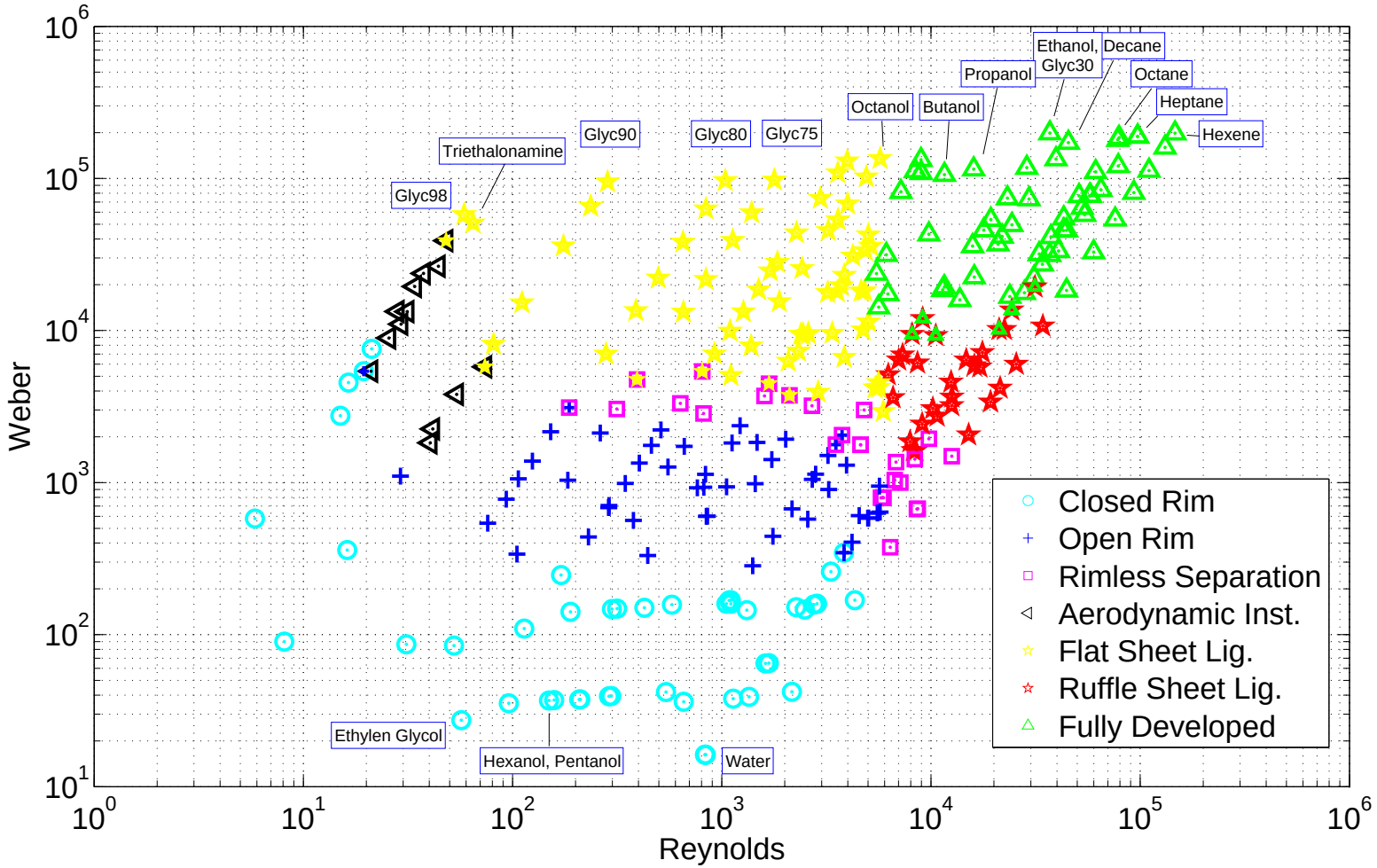

Figure 6.5: Regime Diagram

6.4 Glycerine Mixture

In the current work, in order to investigate a broader range of physics properties of Newtonian fluids, few glycerine mixture have been used. Thanks to mixture of glycerin and water it has been possible to study new Re-We regions reaching distinct Oh numbers using totally safe liquids. Actually the Oh reachable are between the 98% Glycerine (3.83) and the Water (0.0048). The physics properties variation has been estimated using literature's sources (Ref. [34], [15]) and four different mixtures have been produced. Same procedure was used by Dombrowski and many others (Ref. [18], [17]) since the beginning of impinging injector experiments.

30%Glycerine Oh=0.0107	75%Glycerine Oh=0.1505	80% Glycerine Oh=0.2536	90% Glycerine Oh=0.9226
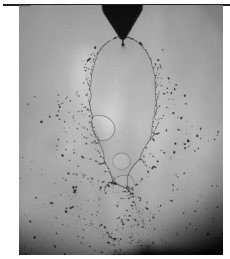	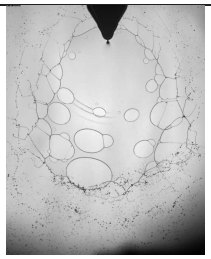	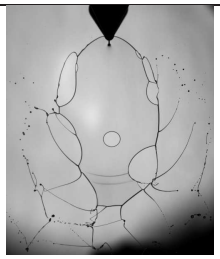	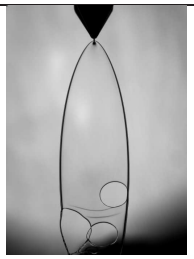
			

Table 6.1: Different glycerine mixture $5.2m/s < U < 9.1m/s$

From Table 6.1 can be noticed how at low injection velocity (and so Re-We low region) the breakup behavior presents a stochastic formation of holes in the inner part of the sheet for every mixture realized. The cause of this perforation is never fully established although it was suggested ([19]) that they were probably caused by drops impinging on the sheet. Also Bush and Hasha (Figure 6.6 (a)) meet the appearance of the holes suggesting, under

personal communication of C. Clanet, that may result from the working fluid being a mixture.

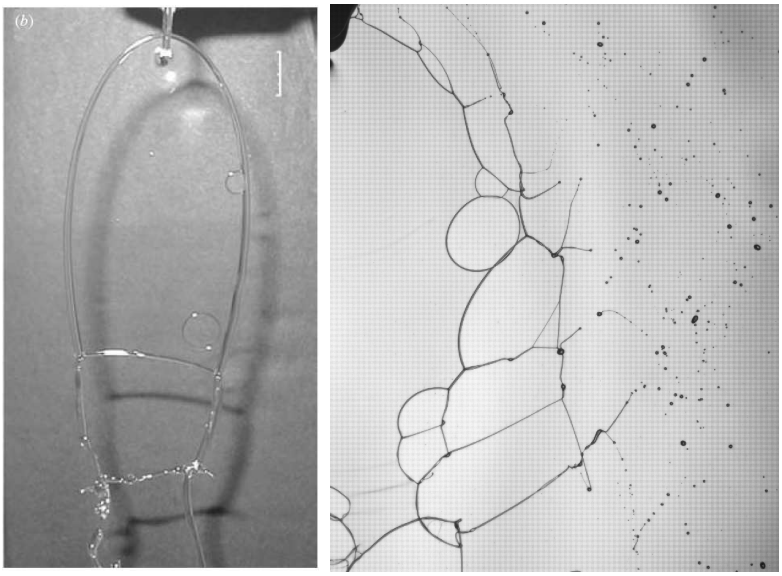

(a) Bush and Hasha [17] (b) 80% Glycerine, $U_{jet} = 9.1m/s$

Figure 6.6: Peculiarity of glycerine mixture: (a)previous work and (b) our experiments

Furthermore a particular rupture of the bounding rim occurs. In Figure 6.6 (b) represents a zoom of the fragmentation process considering an 80% Glycerine mixture: part of the fluid contained in the thick rim detaches from the sheet forming almost radial ligaments of fluid that decay in large droplets in the outer environment. These ligaments may rest attached on the sheet. It can be also noticed how a bounding rim is recreated between the attachment points of the ligaments probably dues to the surface tension effect, but the shape of the sheet is no more regular.

As can be seen from Table 5.1 the Ethanol and Glycerine 30% have almost the same Oh, so it's thought that could be interesting to compare the breakup behaviors at same Reynolds and Weber numbers. In this way it can be seen the peculiar characteristics of their spray patterns including the differences at low velocity mentioned above. In fact, as shown in Figure 6.7, at low Re-We numbers the presence of holes in the 30%Glycerine mixture occurs

while increasing the injection velocity the atomization patterns are strictly similar.

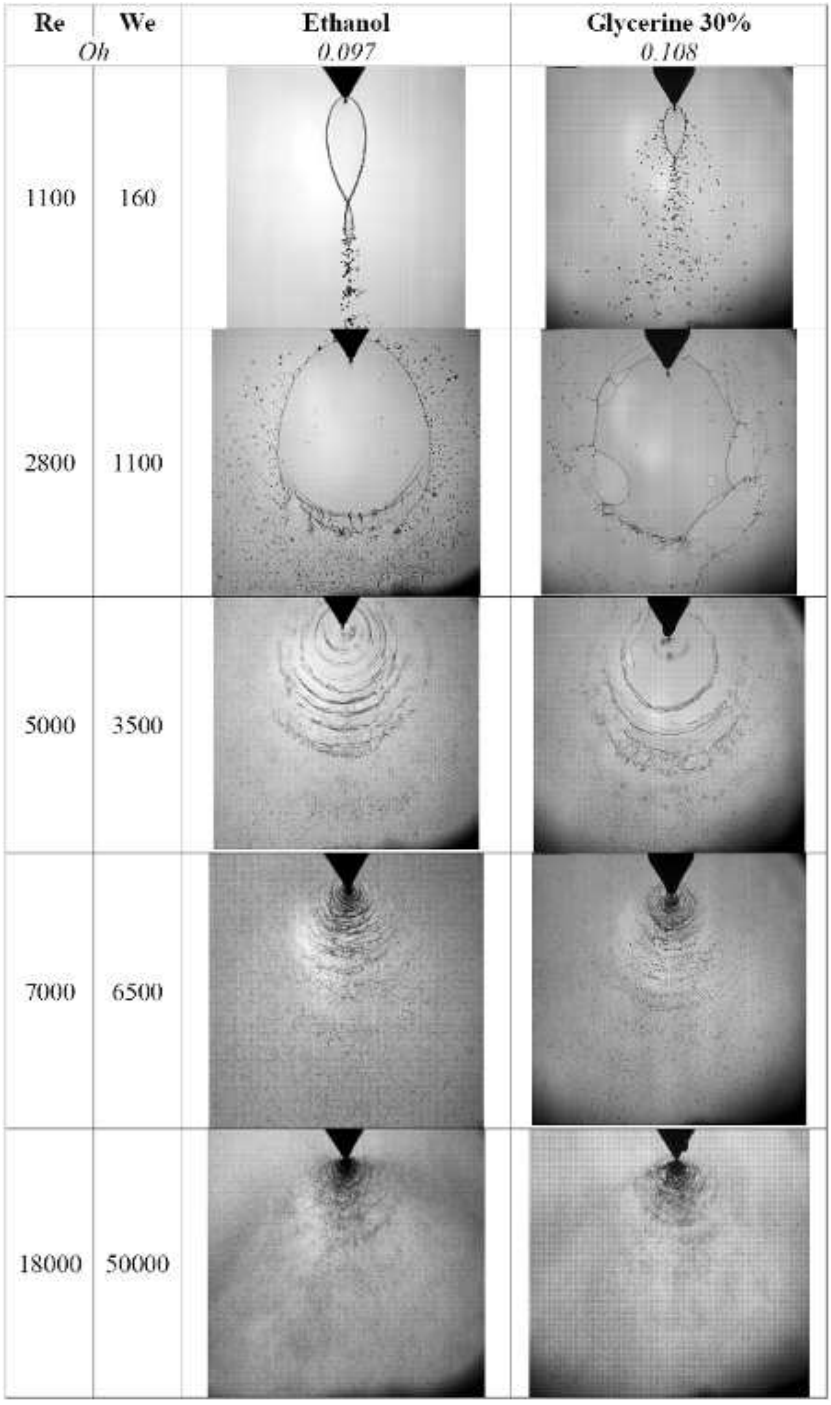

Figure 6.7: Breakup behaviors of Ethanol and 30%Glycerine mixture

6.5 Similarities with Gelled Propellants

Also for the atomization of gelled fuels impinging jet injectors are interesting. Due to fact that high shear rates are produced both in the taper inside the injector tip and in the region around the inter-section point of the fluid jets the shear viscosity of these gelled fluids is strongly decreased partly up to an extensive liquefaction (Ref. [24]). It should be mentioned here that gelled fuels and propellants are of interest for rocket and ramjet propulsion systems, because of their safety and performance benefits. Due to their non-Newtonian flow behavior they offer the possibility to design engines, which can be throttled similar to engines with liquid fuels and which have simple handling and storage characteristics similar to engines with solid fuels (Ref. [23]). For this reason it has been found interesting to analyze the spray pattern of fluids with high viscosity (e.g. Ohnesorge) considering how it could be related to gelled propellant behavior using impinging injector.

6.5.1 Gel Rheological Behavior

Gelled fuels are shear-thinning fluids, which show a decreasing shear viscosity μ with increasing shear rate $\dot{\gamma}$, whereas Newtonian fluids have a constant value. Figure 6.8 presents this dependency for a paraffin-gel as an example in a log-log diagram. It can be seen, that the viscosity values of the paraffin gel are orders of magnitude higher at low shear rates than the un-gelled liquid paraffin of constant viscosity (dashed line). The rheological properties of gelled fuels can be estimated with a rotational and a capillary rheometer. Furthermore gelled propellants show a distinct yield stress τ_0 and a limited minimum constant viscosity μ_∞ (upper Newtonian plateau), which can be assumed in a first step as the viscosity of the basic un-gelled liquid.
Those rheological properties allow building throttleable engines similar to engines with liquid fuels without loosing the handling and storage advantages of engines with solid fuels. Under storage conditions the gel has a semi-solid state and is not capable of flow. Its viscosity, however, decreases if there are high shear stresses applied to the gel so that it is possible to feed it from the tank through pipes and injectors into the combustion camber.

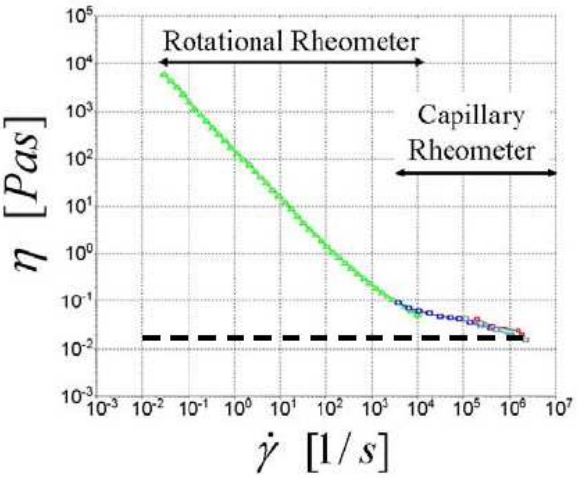

Figure 6.8: Viscosity of paraffin-gel

The rheological behavior of a non-Newtonian shear-thinning fluid is commonly described in the simplest form by the power-law equation (Eq. 6.1).

$$\mu = K \cdot \dot{\gamma}^{n-1} \tag{6.1}$$

Since this equation does not include the yield stress τ_0 of the gel neither the limit for the minimum viscosity μ_∞, it fits only to the experimental data in the range of medium shear rates. The Herschel-Bulkley-equation, however, considers the influence of the yield stress to the viscosity behavior and thus fits to the data for low and medium shear rates. An extended version of the Herschel Bulkley equation shows Eq. 6.2.

$$\mu = \frac{\tau_0}{\dot{\gamma}} + K \cdot \dot{\gamma}^{n-1} + \mu_\infty \tag{6.2}$$

This formula includes in addition to the power law and the yield stress influence the limit of minimum viscosity and fits to the experimental data in the entire shear rate range. The laminar, fully developed and steady pipe flow behavior of gels with a viscosity behavior described by the Extended Herschel-Bulkley equation has been described in detail by Madlener and Ciezki ([25]).

6.5.2 Atomization Peculiarities

The aerodynamic instability described in the section 4.2.7 is often also the mechanism that leads to the breakup of sheets formed from non-Newtonian fluids, as can be seen in Figure 6.9. Negri, Bailardi and Ciezki [13] recently observed that all the investigated polymeric solutions with high polymeric weights break up at medium velocities in this mode.

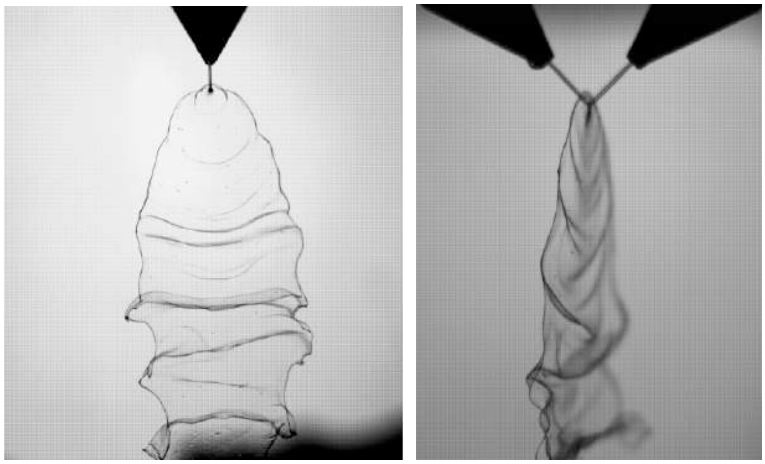

(a) front view (b) side view

Figure 6.9: Breakup of non-Newtonian fluid dues to aerodynamic instability: Water + 3.1% Methocel J12MS, $U_{jet} = 19.5m/s$, $Re_{gen,HBE} = 647$ (Ref. [13])

Moreover, the pattern named Stable Sheet with Ligaments is strictly similar to the atomization behavior manifested in Non-Newtonian fluids.In Figure 6.10 a comparison between Triethanolamine and Water +10 % Methocel it's showed . The sheet edge first breaks into ligaments, but in the Newtonian fluid further downstream these ligaments decay into filaments and then big droplets. In the gelled fluid, instead, the ligaments seems to destroy downstream only in filaments which dimension and characteristic are not comparable with the Newtonian droplets. Going in detail on the rupture mechanism of the sheet edge and rim, from Figure 6.11 it can be noted that, close to the most amplified aerodynamic waves, parts of the sheet and ligaments structure starts to detach by the stretching of holes previously cited.

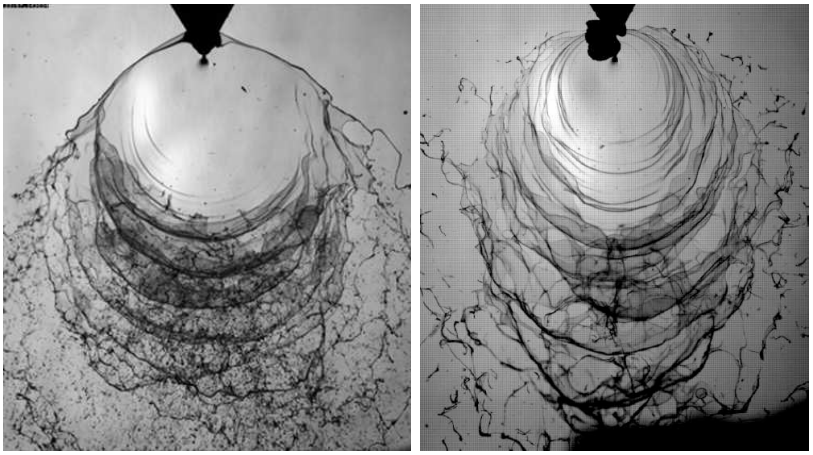

(a) Triethanolamine (b) Water + 10% Methocel

Figure 6.10: Stable sheet with ligaments: $U_{jet} = 40m/s$

For a better understanding on the causes of this breakup phenomena, further investigation are necessary.

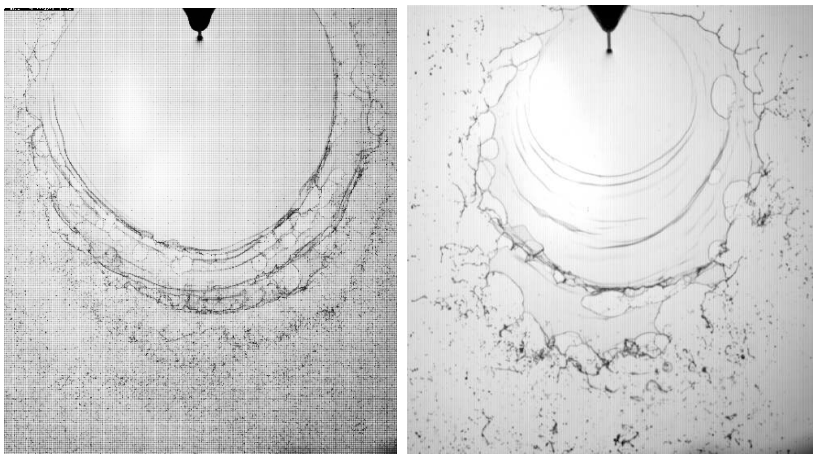

(a) Ethane 1,2 Diol (b) Water + 2% Methocel

Figure 6.11: Rupture mechanism of the stable sheet: $U_{jet} = 30m/s$

6.6 Sauter Mean Diameter Correlation

One of the parameters usually used to understand the goodness of an atomization process is the mean-drop diameter. As explained in Section 4.4, in the combustion science the Sauter Mean Diameter, or surface-volume mean diameter, is generally quoted. In this study a first attempt of droplets correlation between the D_{32} and the fluids properties has been done.

As can be seen from the upper part of Figure 6.12 the SMD vs Reynolds graph shows every single liquids per line, instead of the crossed lines present in the other two plots. This means that may be simple to correlate the drop size to a single fluids and then see if there are similarities or connection between the coefficients and some fluid property. Since on the semi-logarithmic plane the slope of the lines seems to be almost constant, it has been tried to find a linear correlation in the semi-logarithmic plane. To do this a simple coordinate change can be done:

$$X = Log(Re) \tag{6.3}$$

$$Y = \overline{D_{32}} \tag{6.4}$$

so that for the ith liquid considered:

$$Y_i = m_i \cdot X + q_i \tag{6.5}$$

In order to avoid loss in regression accuracy the upper part of the figure 4.21 has been cut dues to the strong slope change and the measurements under approx. $40\mu m$ haven't been considered as they manifest a Bi-modal particle size distribution. So the present analysis concerns a droplets diameter range of $40\mu m \leq D_{32} \geq 90\mu m$.

The resulting linear coefficients are listed below for each fluids. In table 6.2 is also reported the so called Correlation Coefficient (R^2), commonly used to identify the goodness of the regression made. This number varies between 0 and 1, in particular the closer the value is to 1, the better the regression will be. It can be noticed that an average $R^2 = 0.98$ could be obtained.

Nevertheless a useful correlation would be represented by only one equation that changes its coefficients in function of the desired variables. One of

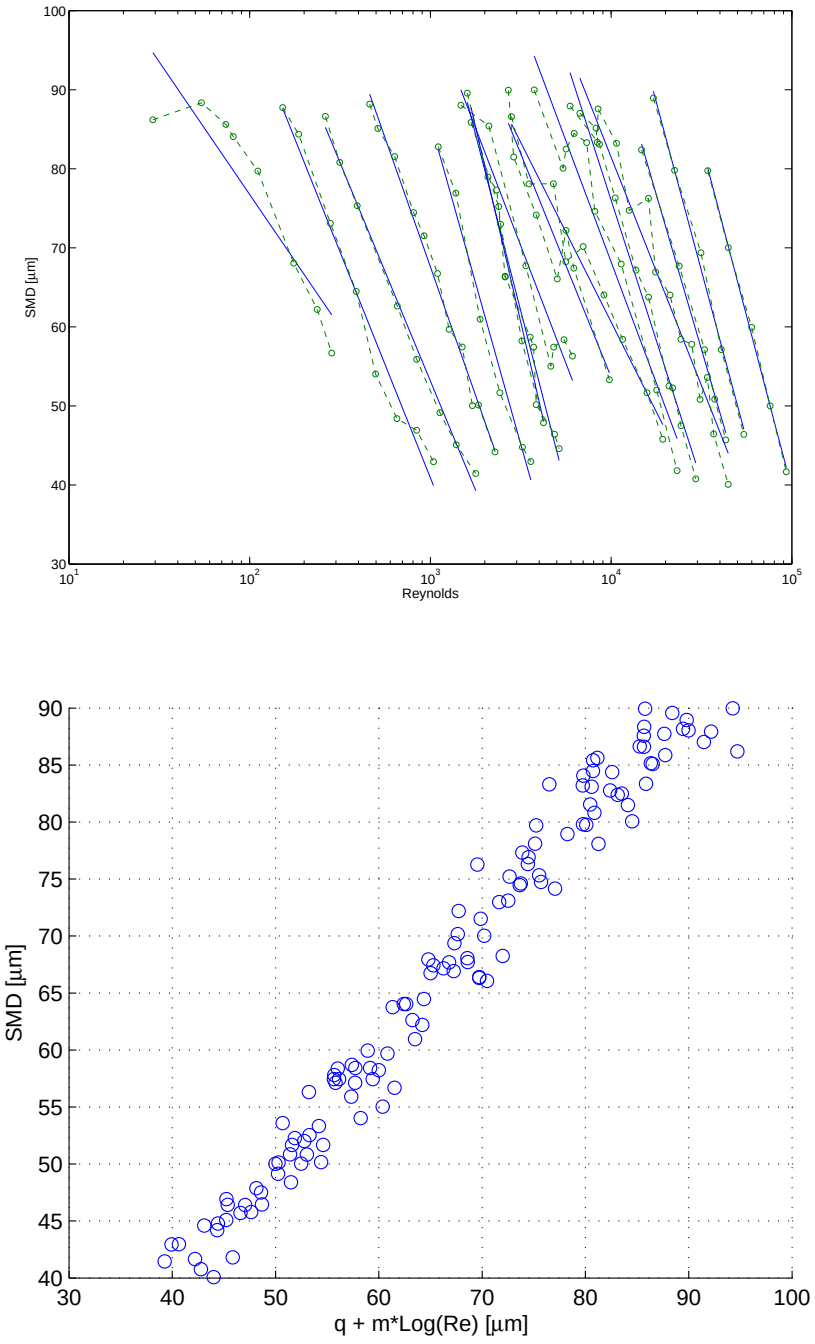

Figure 6.12: Reynolds correlation

Fluid	**m** [μm]	**q** [μm]	$\mathbf{R}^2$
Hexene	-37.833698	475.118792	0.998405
Heptane	-37.096720	451.445706	0.995114
Octane	-34.061134	410.062900	0.995062
Decane	-30.819974	359.885629	0.981487
Water5	-25.099140	312.635297	0.963591
Ethanol	-26.588669	313.103459	0.939654
Glyc30	-19.724908	242.291429	0.966828
Propanol	-24.541649	279.666316	0.905831
Butanol	-25.857640	278.645264	0.938903
Pentanol	-38.734884	374.191271	0.969040
Hexanol	-42.905155	406.364842	0.983240
Octanol	-35.430017	330.689548	0.980880
Ethigly	-28.249368	262.721724	0.991200
Glyc75	-23.998457	218.915754	0.994912
Glyc80	-24.821796	212.360793	0.979919
Glyc90	-14.561966	143.796668	0.843009

Table 6.2: $D_{32} = f(Re)$ correlation coefficients

the aim of this work is to characterize the results regarding the atomization dues to impinging injector by dimensionless numbers (see Section 4.1), so that:

$$\overline{D_{32}} = f(U_{jet}, \mu, \rho, \sigma, d_{inj}) = f(Re, Oh) \tag{6.6}$$

$$= m(Oh) \cdot Log(Re) + q(Oh). \tag{6.7}$$

Then it has been thought to observe if a relationship exists between the coefficients of the liquids and their physics properties through the Oh numbers. In fact plotting the q and m parameters on the Oh x axes can be noticed that they decrease for distinct fluid in distinct Oh regions. Hence performing a linear or logarithmic interpolations a relation between the examined parameters could be found.

The Figure 6.13 and 6.14 represents the description above while the Table

6.3 and 6.4 display the coefficients found. As can be seen for both alcan and alchool the linear correlation brings a reliable goodness factor. The glycerine mixtures instead show a bad correlation coefficient R^2, well marked for what regard the m results, so the correlation proposed is not accurate. A validation of this model is necessary and will be done in future.

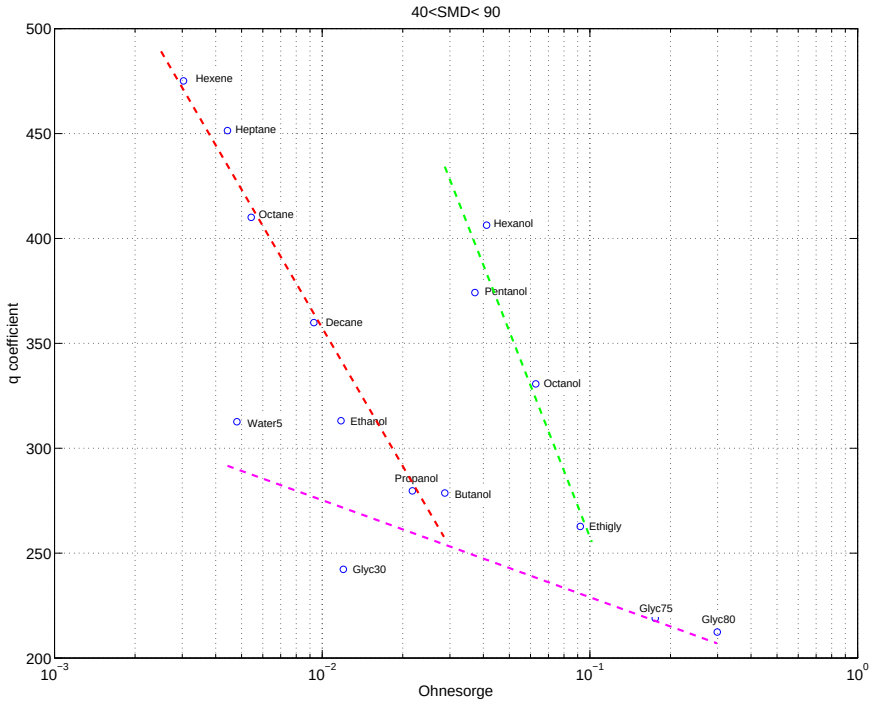

Figure 6.13: q-Oh correlation

Region	b_q $[\mu m]$	a_q $[\mu m]$	$\mathbf{R^2}$
$0.0027 \leq Oh \leq 0.029$	-72.5	5.1	0.984
$0.037 \leq Oh \leq 0.1$	-101.5	36.85	0.986
$30\% \leq Glycerine \leq 90\%$	-81.5	238.09	0.994

Table 6.3: $q = b \cdot f(Oh) + a$ correlation coefficients

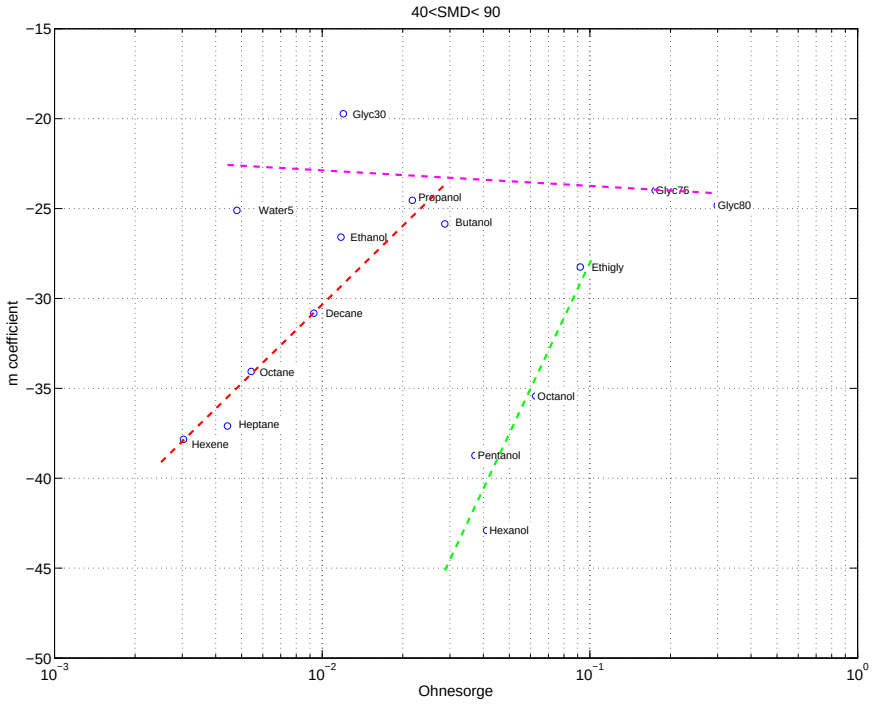

Figure 6.14: m-Oh correlation

Region	b_m $[\mu m]$	a_m $[\mu m]$	$\mathbf{R}^2$
$0.0027 \leq Oh \leq 0.029$	4.24	-9	0.984
$0.037 \leq Oh \leq 0.1$	9.53	-7.1	0.986
$30\% \leq Glycerine \leq 90\%$	6.576	-23.56	0.73

Table 6.4: $m = b \cdot f(Oh) + a$ correlation coefficients

6.7 Influence of Chamber Pressure

Going in detail with the observation made in section 5.3 several aspects of the atomization characteristics in pressurized condition can be analyzed. As could be seen from Figure 6.15, from the second row till the end, at the same velocity an increase in pressure causes a strong decrease of the sheet breakup

length (x_b). This effect becomes important the more the Ohnesorge of the fluid is higher. The biggest reduction of breakup length seems to happen always between 1 to 5 bars.

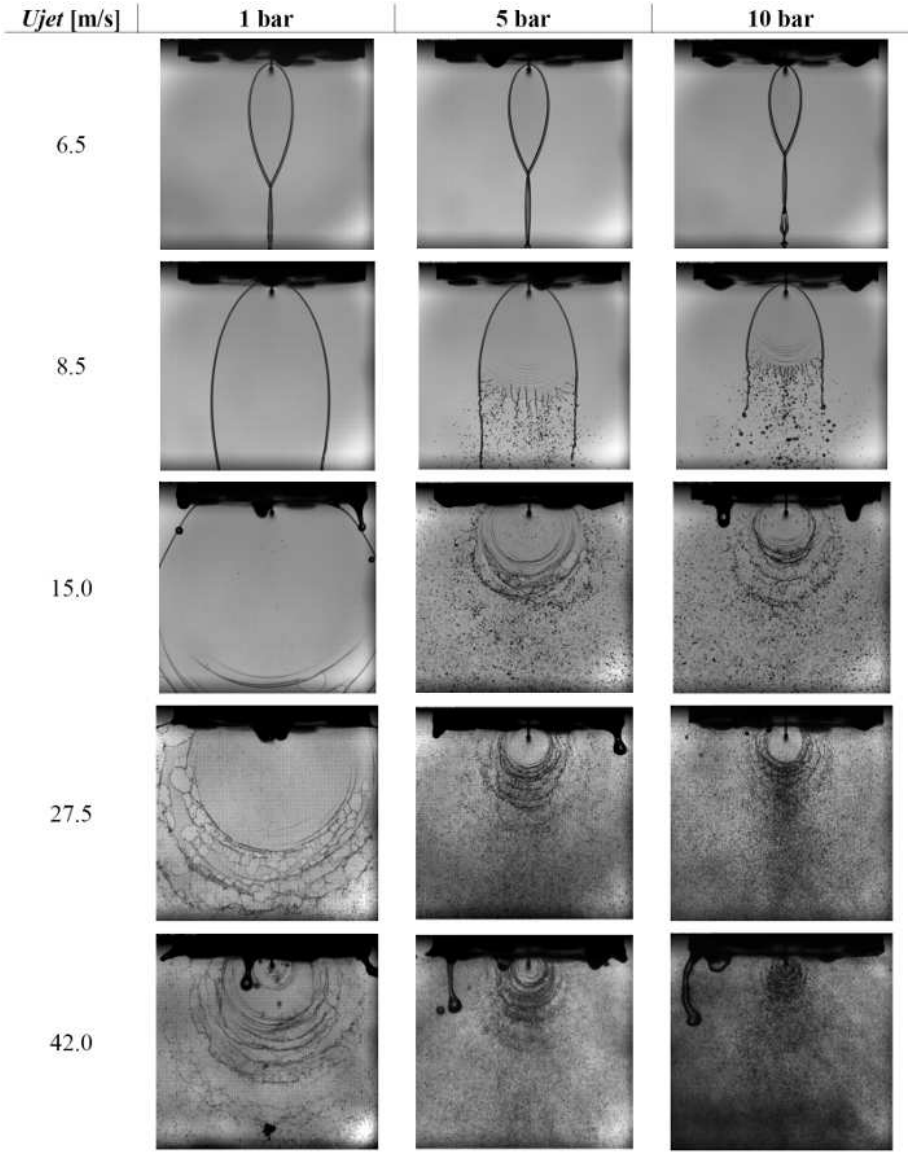

Figure 6.15: Pressure test: 1-Octanol

Considering the recent work of Jung et al [22], we may observe that the aerodynamic waves cause this behavior since they increase the amplitude rising the ambient density. The test series with 98% of Glycerine mixture

confirmed this statement as shown in Figure 6.16.

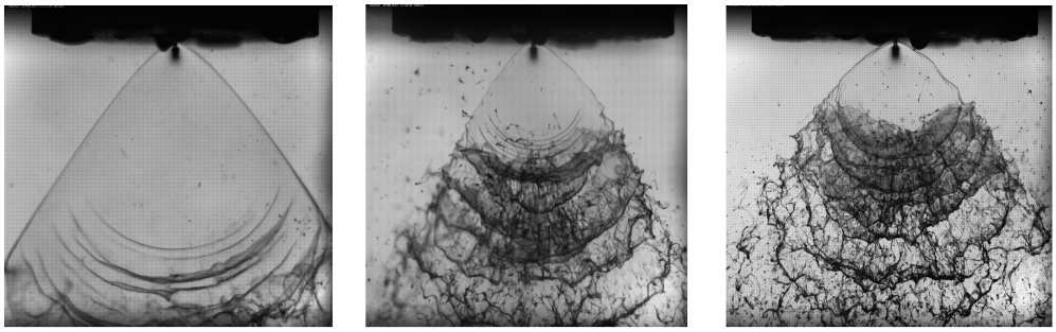

Figure 6.16: Strength of Aerodynamic Instability: 98% Glycerine, $U_{jet} = 100m/s$

Another important consideration it can be made observing the density of droplets spreading downstream the injection point. In fact, as can be clearly seen in the last rows of Figure 5.5, 6.15 and in picture 6.17, an increase of pressure cause a darker image that using the shadowgraph technique means an high density of materia in the region highlighted. This characteristic is very important concerning the propulsion and combustion sciences, and it has been previously observed only for water ([22]), water solutions and Ethyl Alchool (see Dombroski and Hooper [19]).

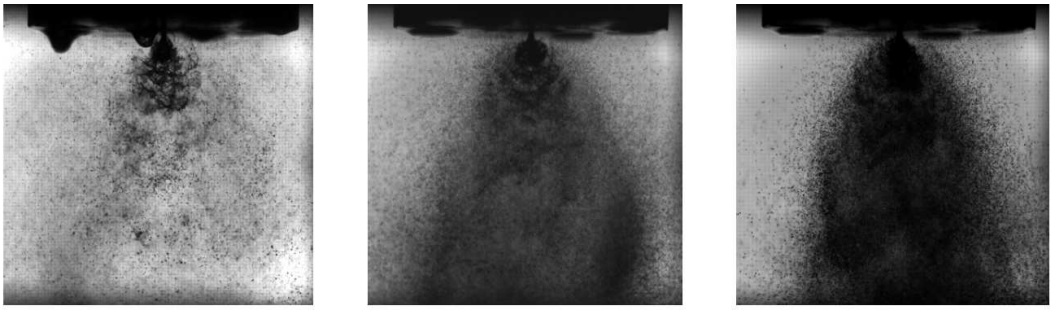

Figure 6.17: Increase of Droplet Density: Heptane, $U_{jet} = 50m/s$

Chapter 7

Conclusions and Future Developments

7.1 Conclusions

The injector system is comprised of injector elements that deliver propellant to the combustor and a manifold system that distributes the propellant to the injector elements. Because the design of the injector element, in conjunction with the injection pressure drop and the propellant properties, determines the propellant mass distribution and the spray drop size distribution, the injector determines the maximum achievable combustion efficiency, the heat transfer rates to the combustion chamber walls, and wether or not high frequency combustion instabilities will occur.

In rocket propulsion the impinging jet injectors are often used due to their simplicity of manufacturing, low costs and high efficiency of atomization. The ability to obtain a stability margin and high performance simultaneously may depend on the ability to understand and control the atomization process, which depends generally on the jet Weber number, the ambient density and whether the jet is laminar or turbulent.

In the present work a wide investigation on the atomization behavior of several Newtonian fluids is given. In particular the influence of fluids properties such as surface tension, viscosity and density, has been studied both

in ambient and pressurized conditions. For the ambient condition campaign the experimental setup developed at DLR for previous work has been used. This setup allows to acquire shadowgraph images, in the planes parallel and perpendicular to the fluid sheet, and the measurements of droplets diameter downstream the injection point. For the pressurized condition campaign a new experimental setup has been assembled combining an existent combustion chamber with the camera system of the previous experiment.

The selection of Newtonian fluids to investigate has been performed in according to their own safety and handling restrictions. The chosen substances has allowed to analyze the breakup behavior of liquids with a viscosity from 0.252 to 911 Pas, surface tension from 19 to 71.5 mN/m and density from 673 to 1256.4 kg/m^3, so that a large range of dimensionless numbers (Re, We, Oh) has been realized. To reduce the geometrical effect and regard this study exclusively on the liquid physic properties, a pre-impingement length of 5 mm has been chosen.

With the fluid candidates different Ohnesorge numbers have been realized and the breakup behavior within a broad range of Reynolds and Weber numbers have been shown in a regime diagram. First result on the atomization behaviors has shown how increasing the Ohnesorge number and jet velocity the wavy structures on the sheet disappear and it becomes more stable and smoother, the bounding rim is thicker and a peculiar change in the breakup in ligaments and then droplets at the downstream edge of the sheet occurs.

Although the spray behaviors are not identical for all fluids, similarities can be found and seven different main families of atomization patterns has been defined: Closed Rim, Open Rim, Rimless Separation, Smooth or Ruffled sheet with Ligaments, Fully Developed and a new Aerodynamic Instability Breakup mode. Hence, using as parameters the Reynolds and Weber dimensionless numbers, a regime diagram has been presented whereas the spray patterns identify breakup regions.

Through this diagram it can be seen that the Closed Rim mode occurs for all fluids below a constant Weber number of approximately $We < 300$, i.e.

where the surface tension forces act the major effect. The Rimless Separation mode represents the transition between the Open Rim and the two modes with ligaments structures. A transition between the Smooth and Ruffled mode can be observed around a $Re \simeq 4500$, probably related to the fact that the injector flow condition are laminar or not. Moreover it can be notices that the fully developed regime is located in the highest $Re - We$ region. Then it can be affirmed that at approximately $Re > 5103$ and $We > 1104$ a direct decay of droplets from the impingement point happens. This region is of particular interest since regards the typical values used in the rocket propulsion system.

The behavior of different Glycerine mixture used in this work has been investigated in detail since they manifest a singular type of fragmentation mechanism. The formation of holes and a partial rim rupture mechanism has been observed and a better understanding on the governing process is necessary. Nevertheless, a comparison between the spray behaviors of Ethanol and 30% Glycerine, which have the same Oh, at different Reynolds and Weber number shows agreement with the main families defined.

Perusal investigation has allowed to find similarities with gelled fluid. In fact, different polymeric solutions breakup their sheet according to the Smooth Sheet with Ligaments and Aerodynamic Instability Breakup mode. In the cases studied an almost general decaying in droplets, after a formation of filaments or ligaments from the rim, has been observed only for the Newtonian fluids.

The droplets diameter measurements show, as Sauter Mean Diameter, a general decrease increasing jet exit velocity to an asymptotic value of circa 35 μm. A correlation of the D_{32} in function of the fluid properties has been attempted using as variables the Reynold and the Ohnesorge number. Although a good regression correlation coefficient has been obtained further validation of the model is necessary.

The pressurized condition campaign has allowed to study the atomization behaviors of several Newtonian fluids in high air density environment. The injection internal geometry has been changed but the geometrical parameters used were the same of the ambient conditio tests. The seven main patterns are still recognizable. A general reduction of breakup length, an increase in droplets density and an anticipation of the spray pattern has been observed.

7.2 Future Developments

Up to now only for some of the observed breakup modes information about governing processes could partly be given or it could be referred to relevant literature. It is obvious that further investigations are necessary for a better understanding of the governing processes.

In particular a deeper investigation on the the fully developed regime may help to understand whether or not the spray of droplets spread in wavy clouds or marked streamlines. It should be mentioned that in this region the smallest droplets size has been measured. Also an analysis on the rupture mechanism of the sheet in the Smooth Sheet with Ligaments may be useful since has been observed both in Newtonian, Glycerine mixtures in particular, and non-Newtonian fluids. Moreover a validation of the SMD correlation proposed is necessary.

The influence of an higher pressure on droplets diameter should be studied in aim to confirm and enlarge the results obtained. In this case complete new experimental setup is needed with a direct implementation of the Malvern laser into the chamber.

The DLR M11.1 facility used in this work will be equipped for future studies on the atomization behavior of a triplets impinging jet injector.

Appendix A

Fluid Tests

In the current section all the fluid tests conducted in ambient condition are showed.

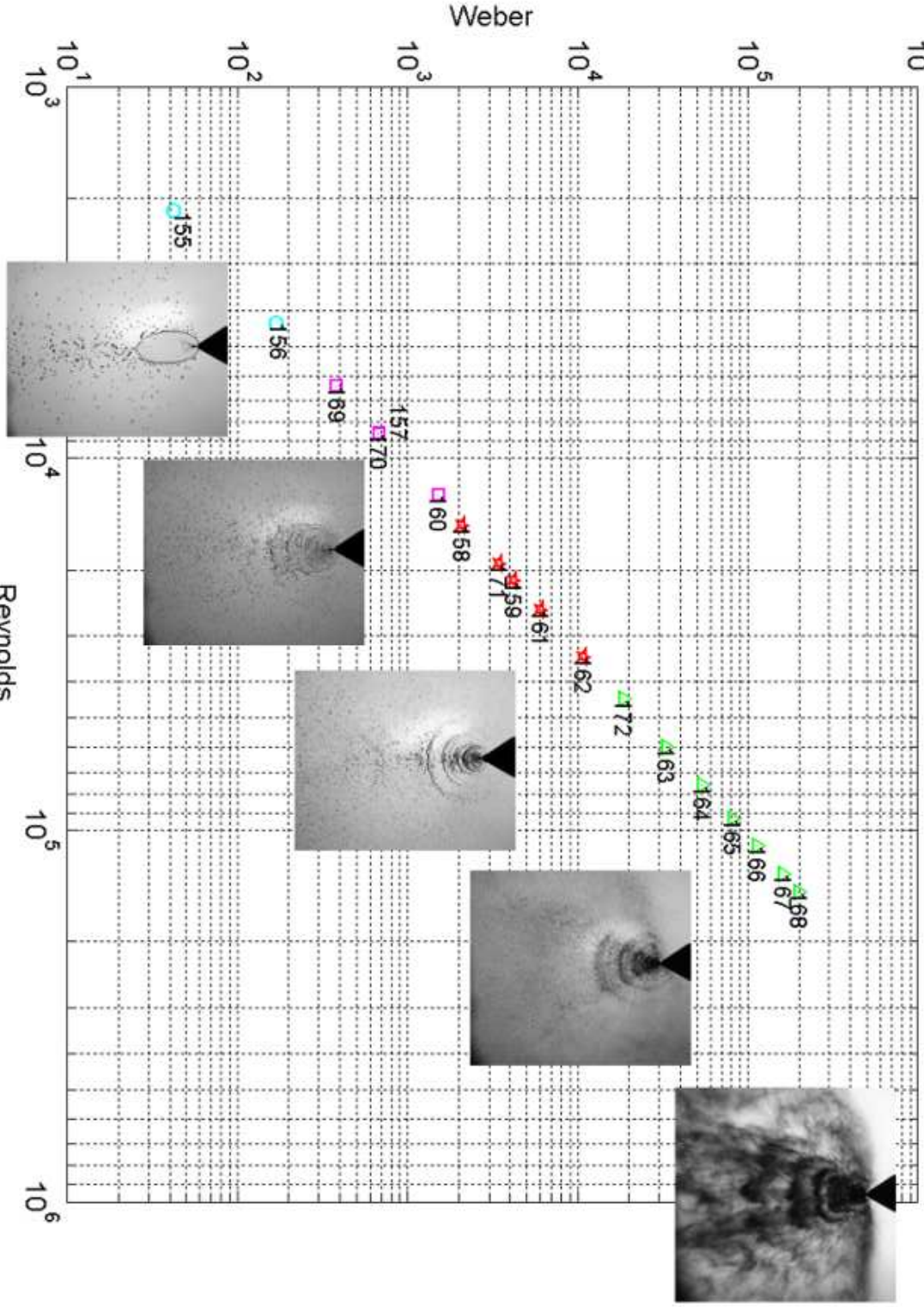

Figure A.1: 1-Hexene

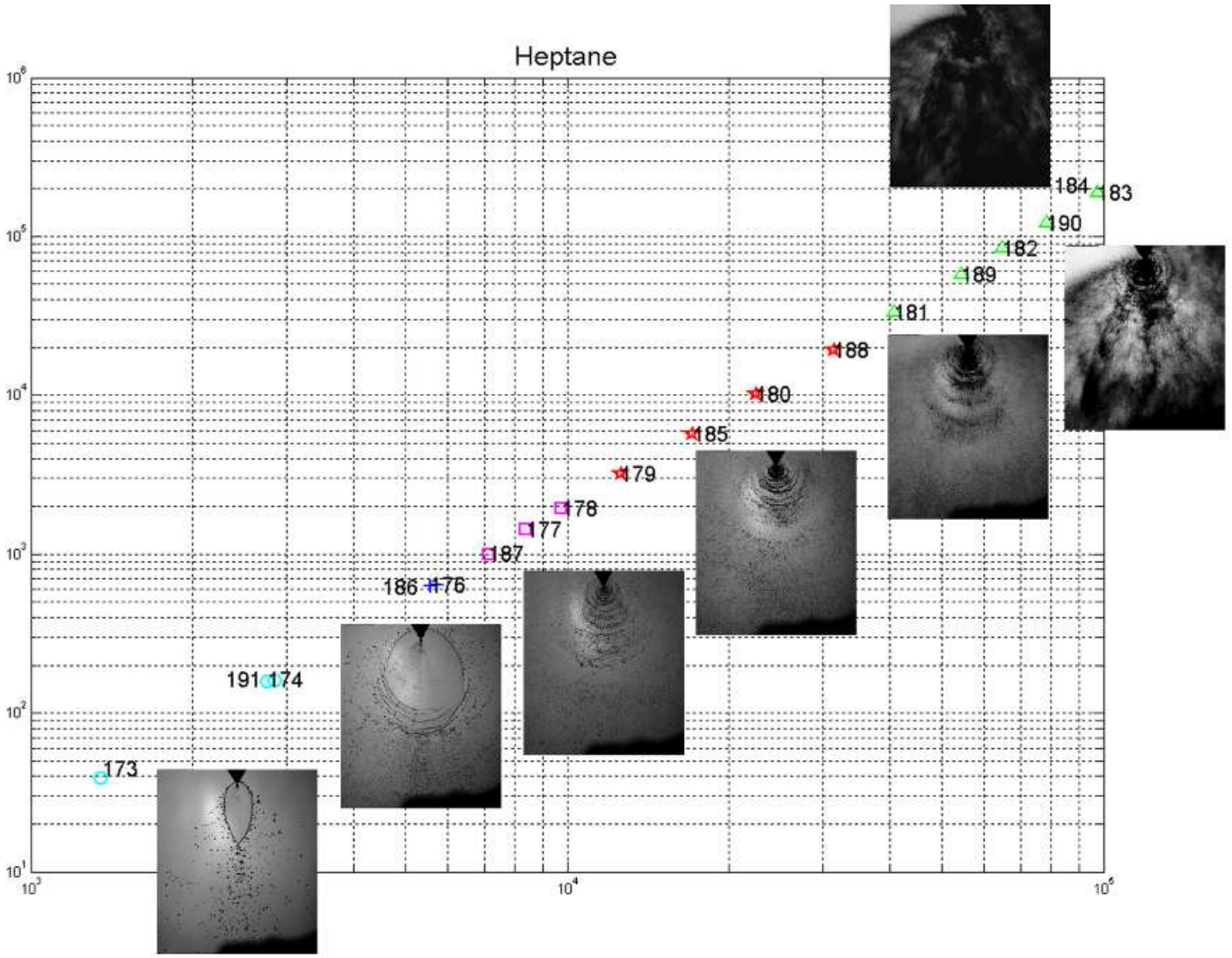

Figure A.2: n-Heptane

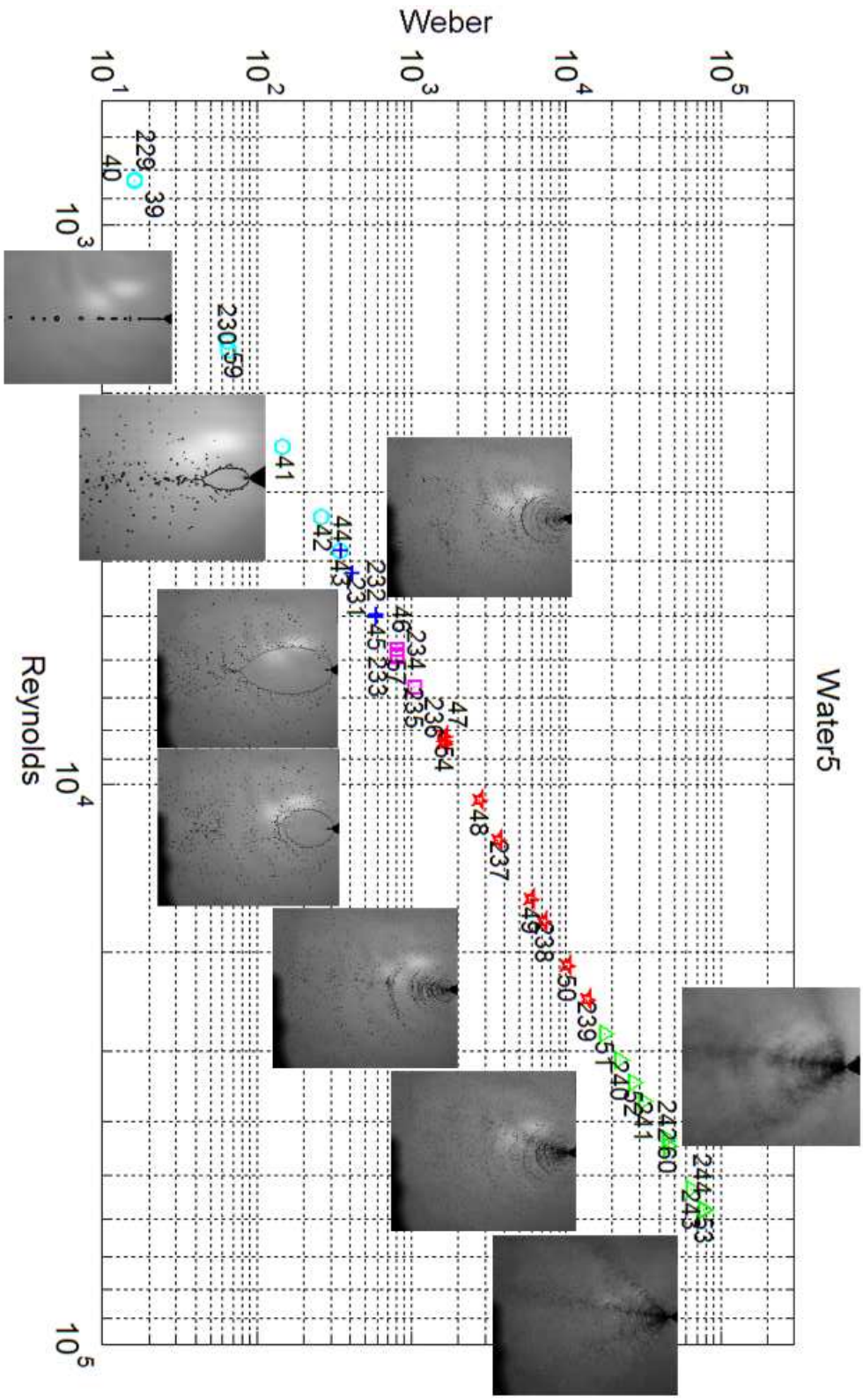

Figure A.3: Water

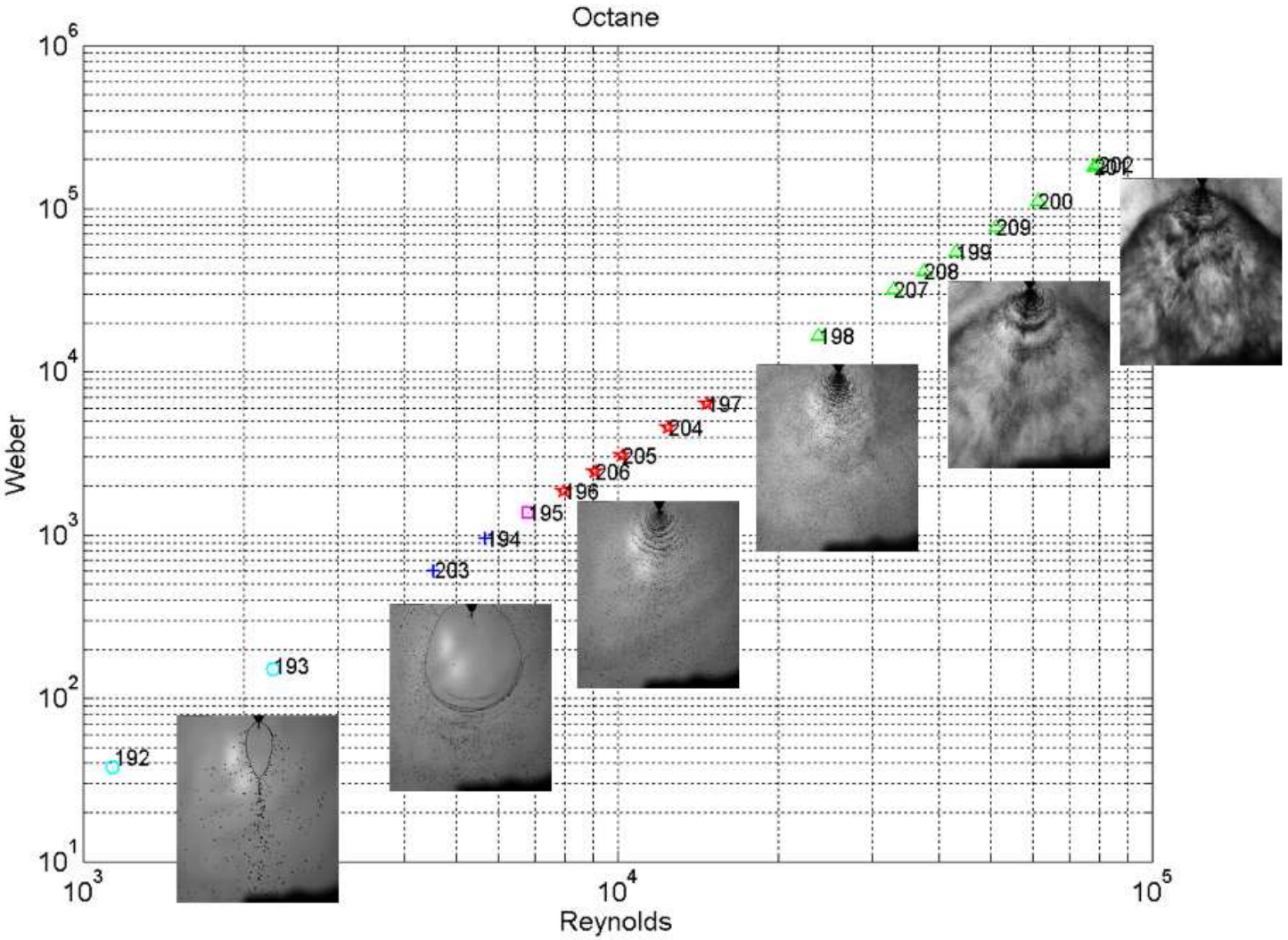

Figure A.4: n-Octane

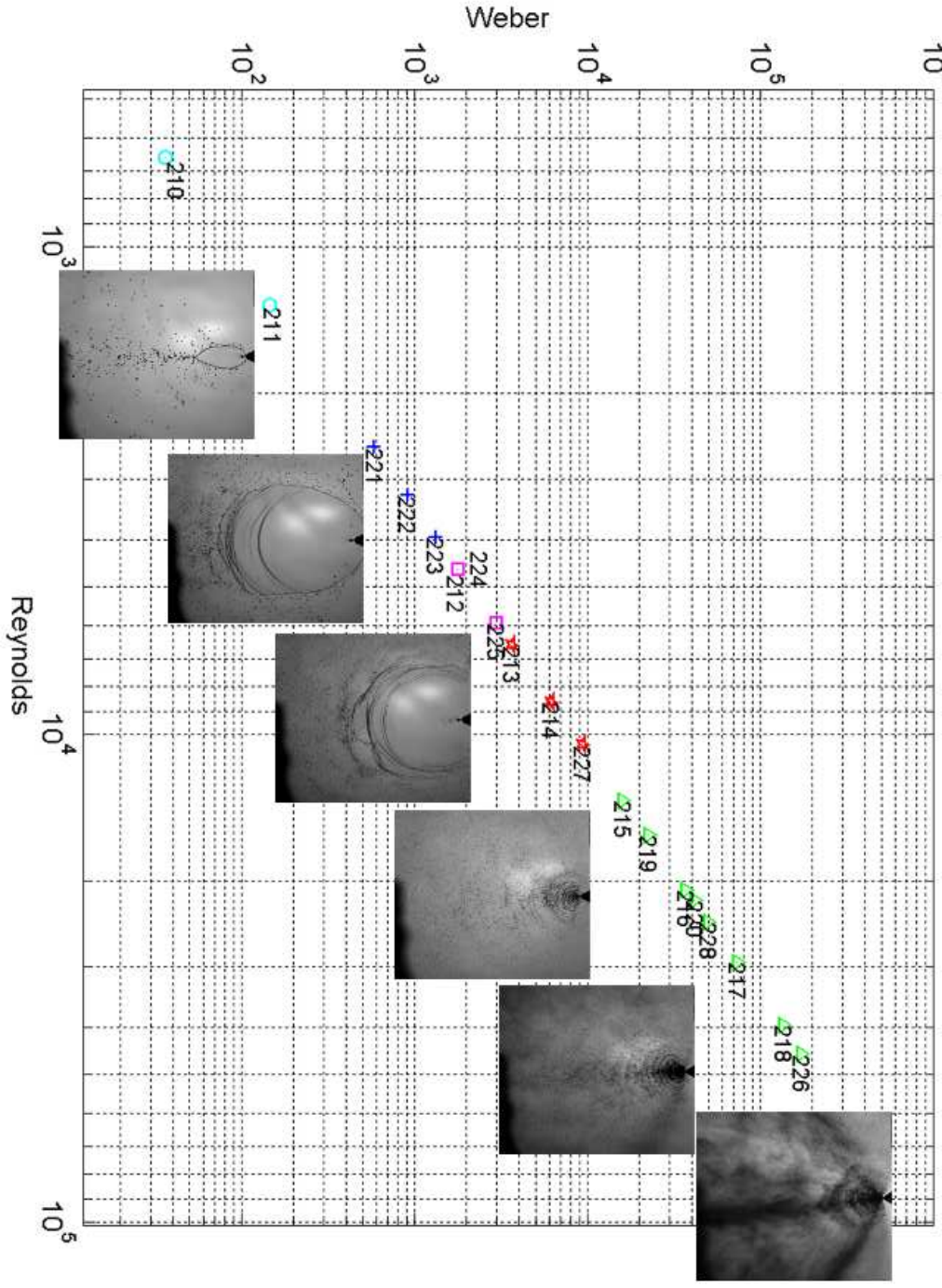

Figure A.5: n-Decane

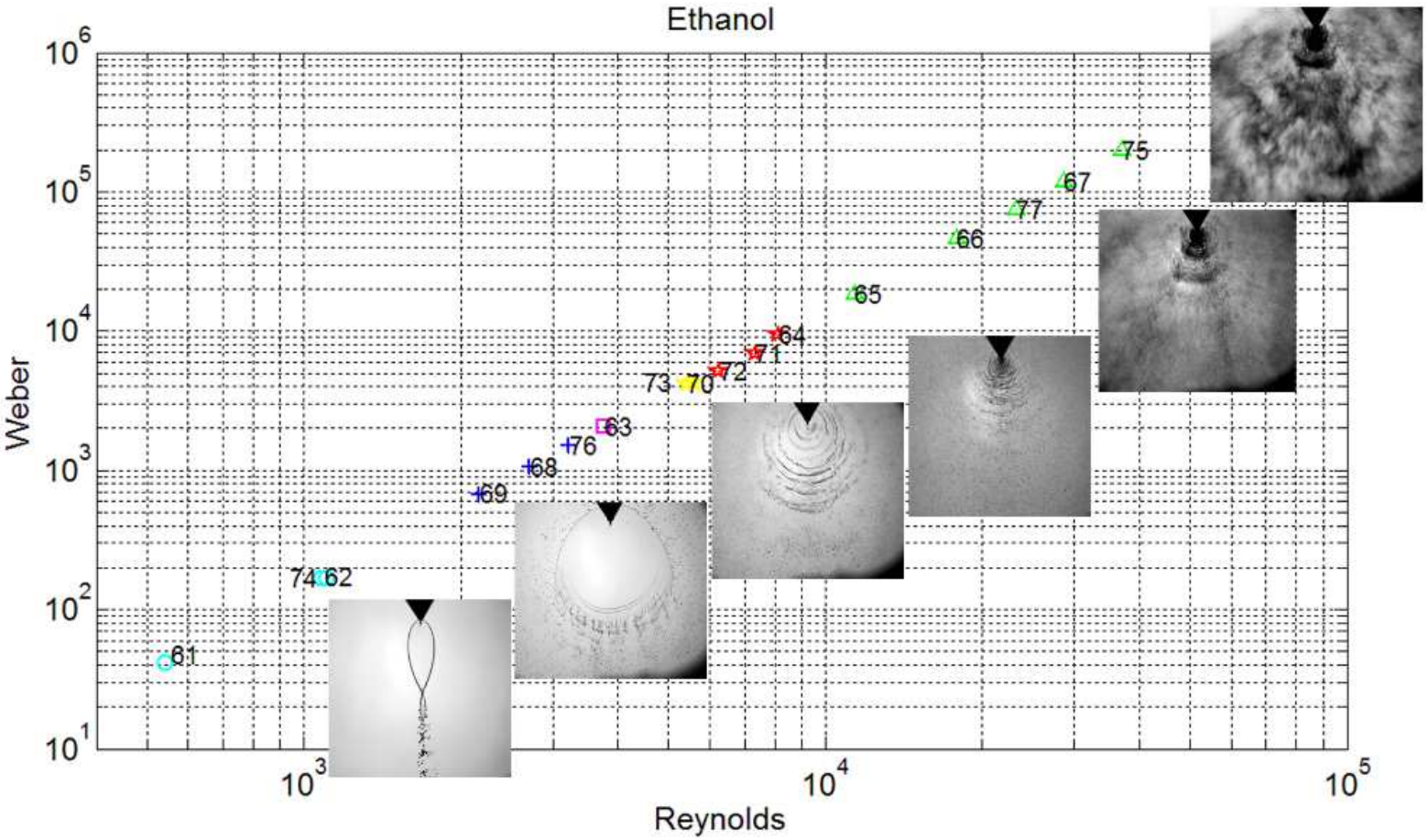

Figure A.6: Ethanol

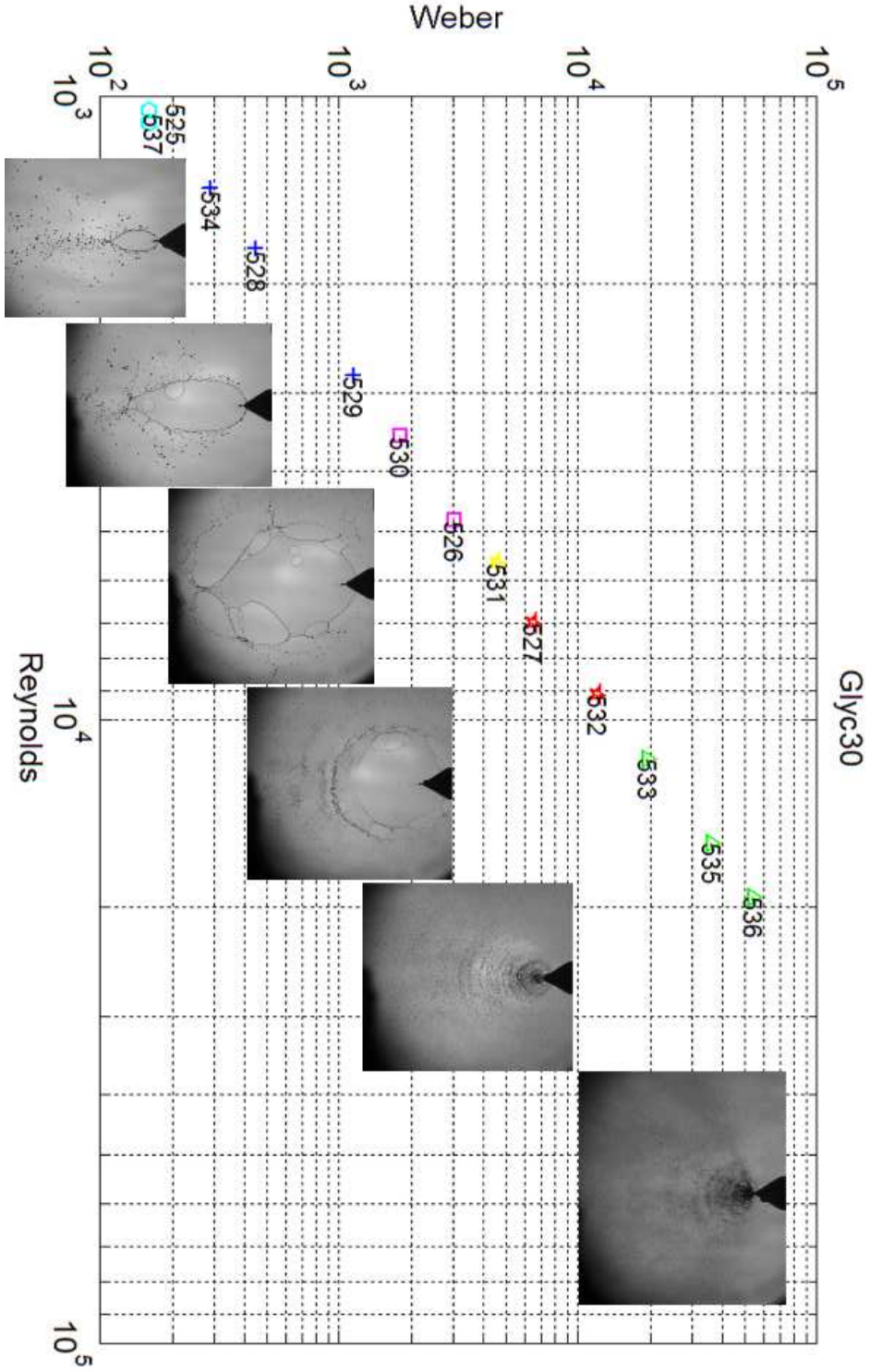

Figure A.7: 30% Glycerine

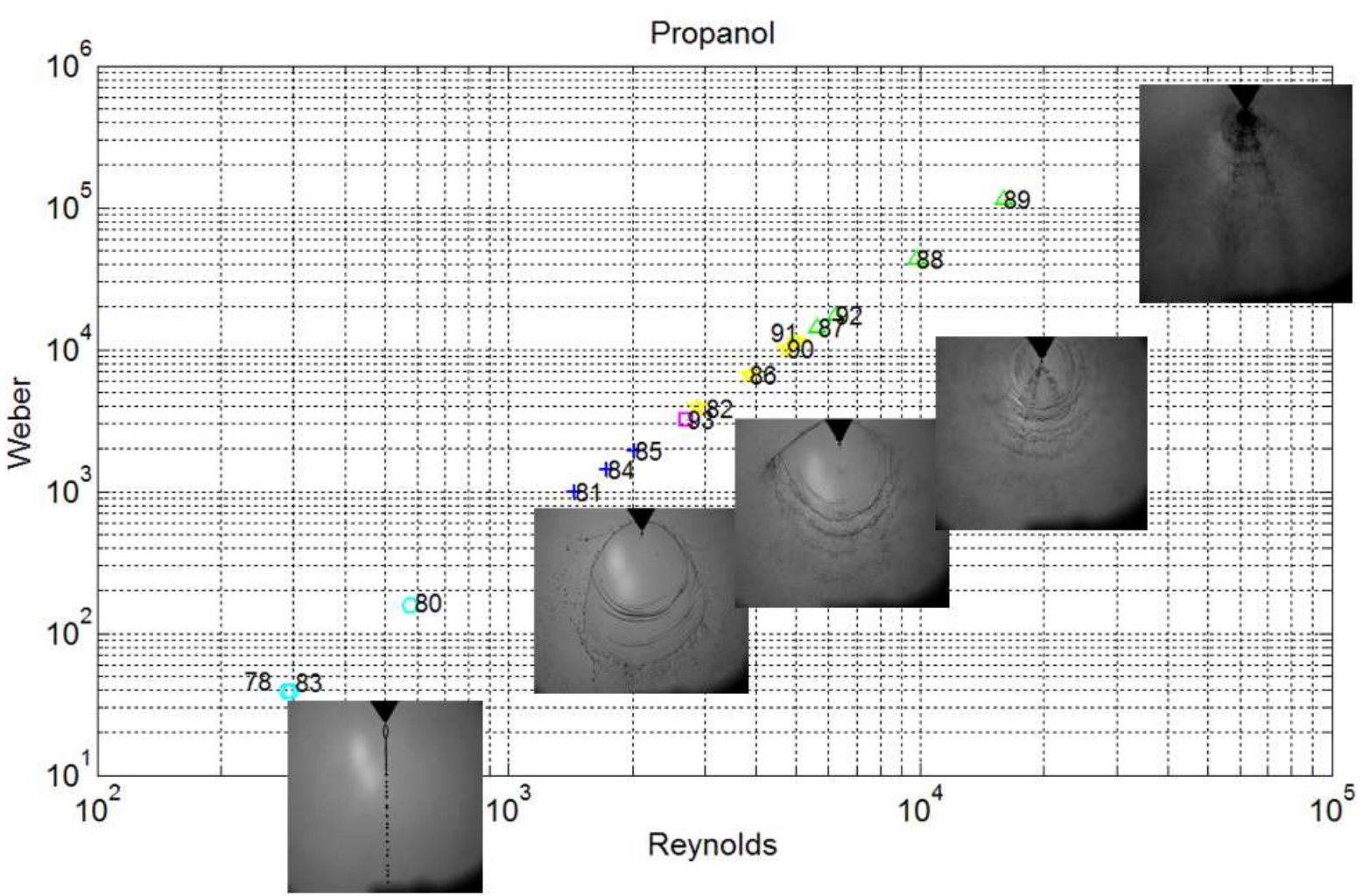

Figure A.8: 1-Popanol

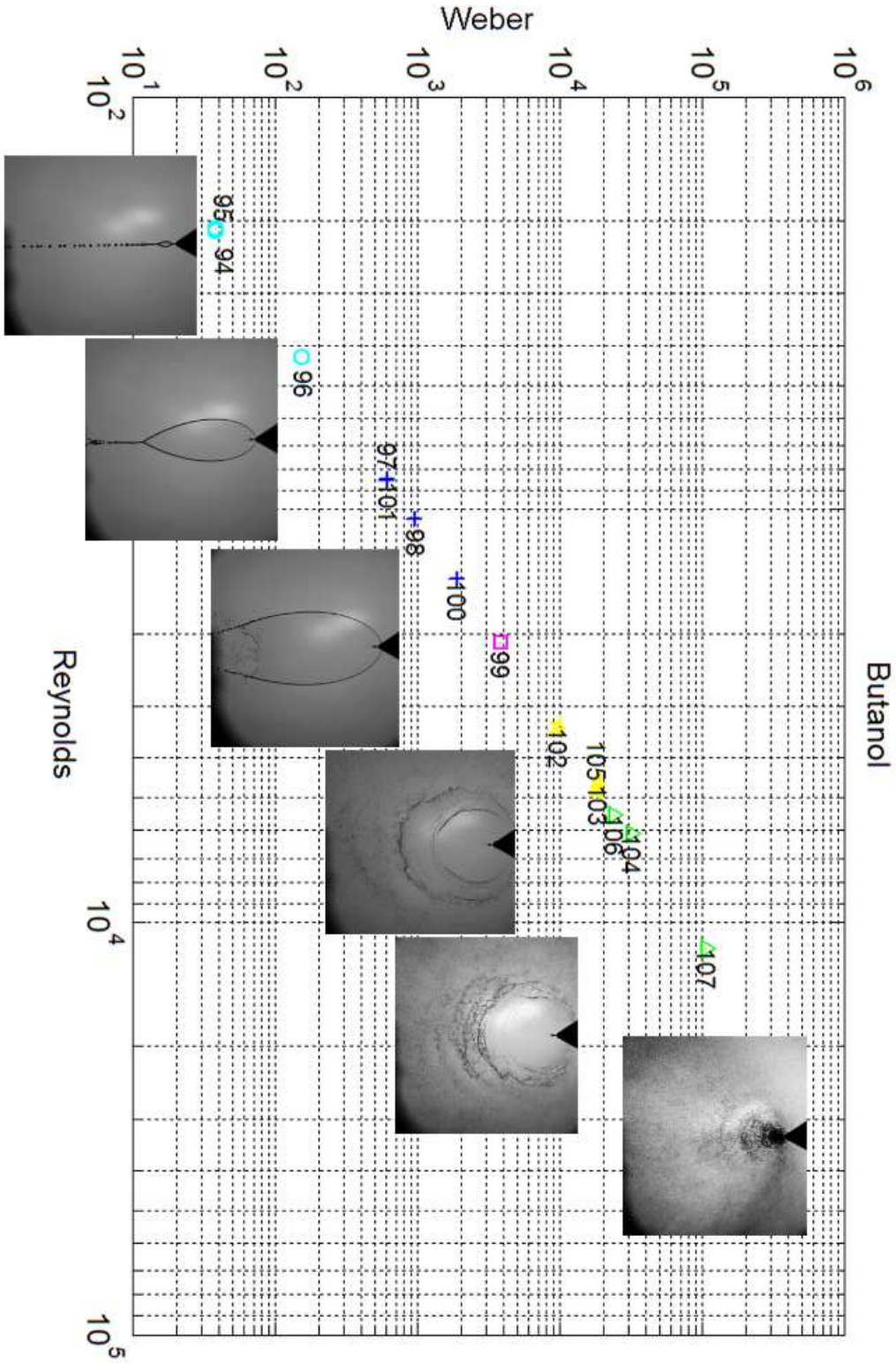

Figure A.9: 1-Butanol

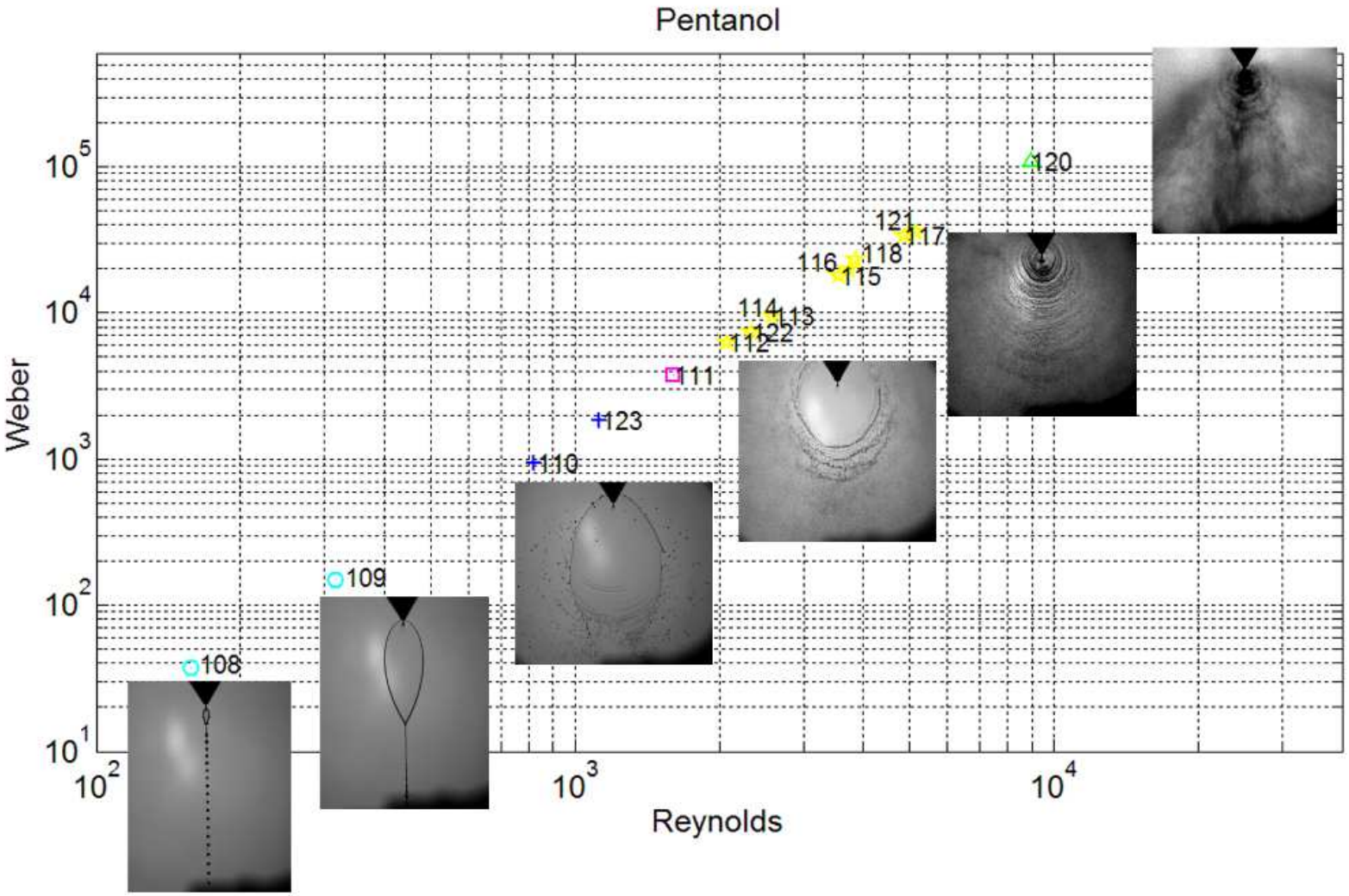

Figure A.10: 1-Pentanol

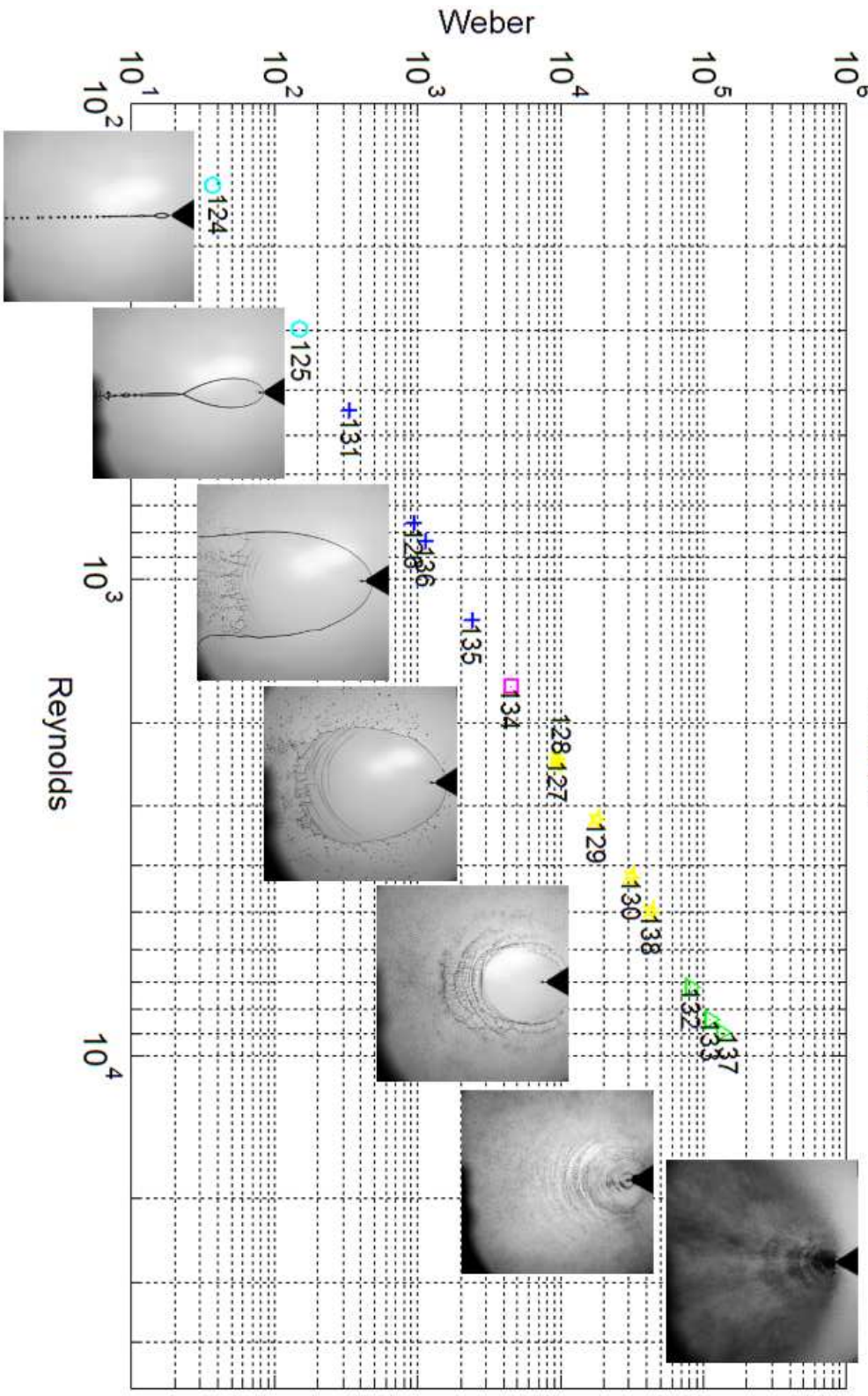

Figure A.11: 1-Hexanol

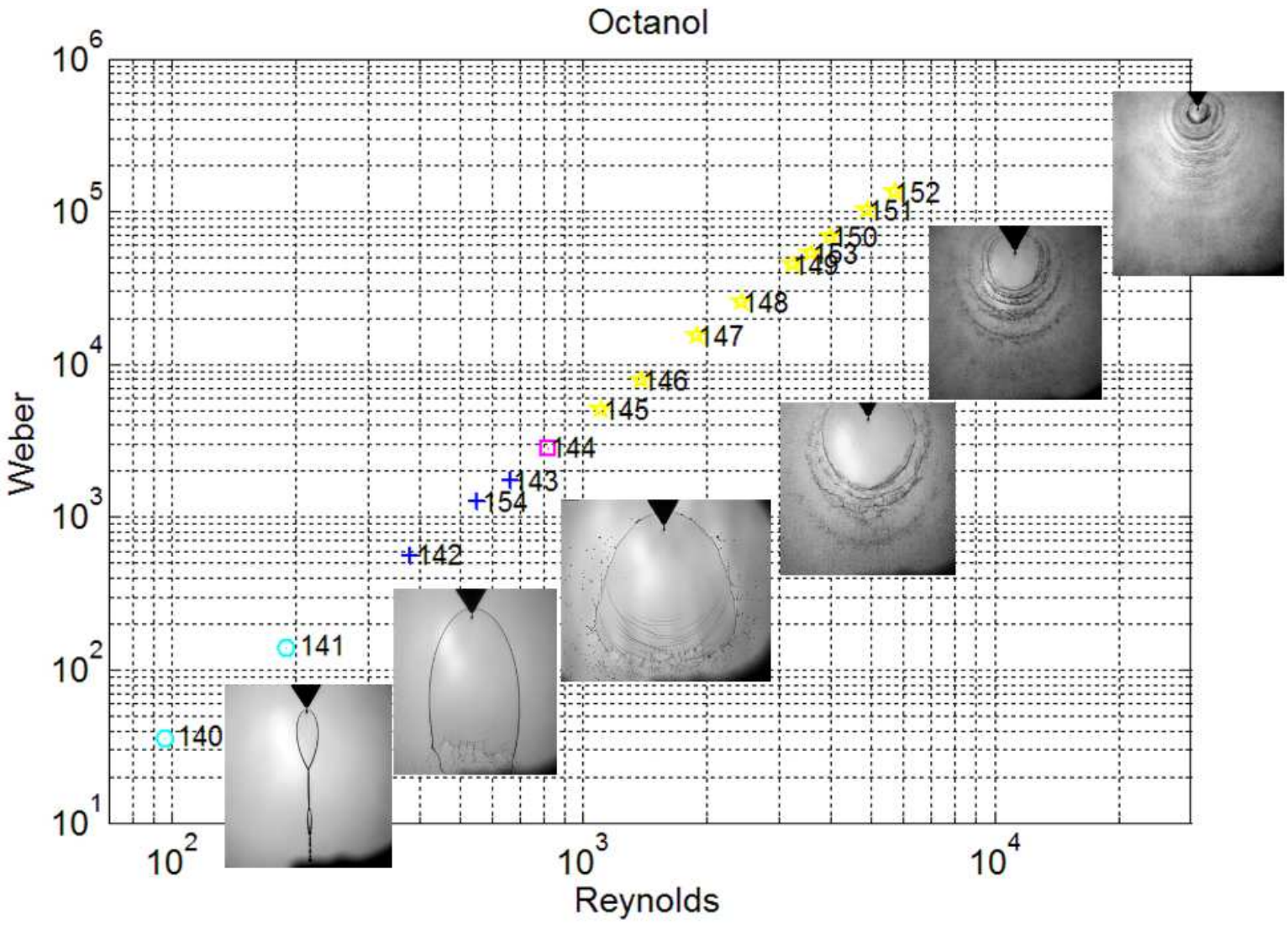

Figure A.12: 1-Octanol

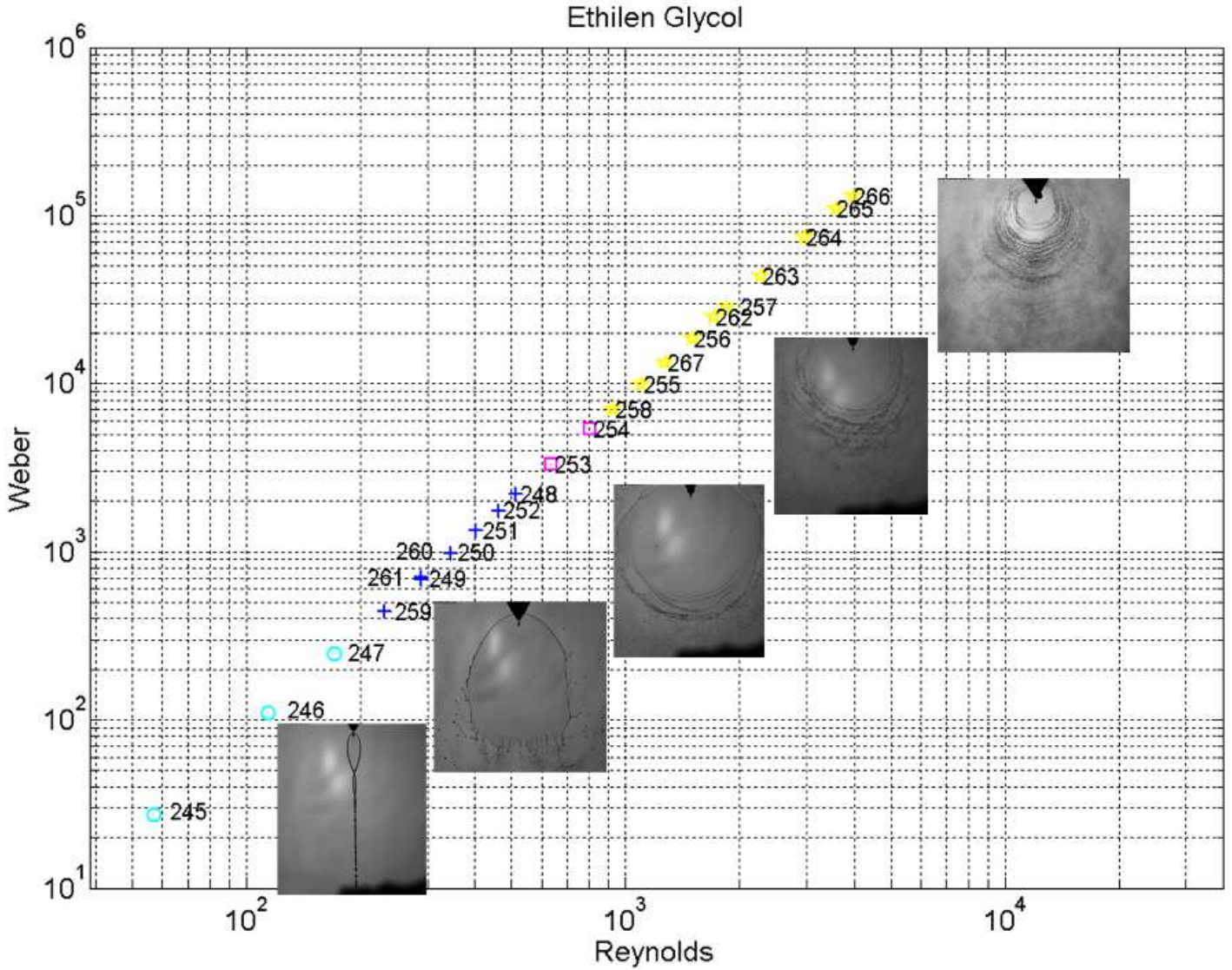

Figure A.13: Ethylene glycol

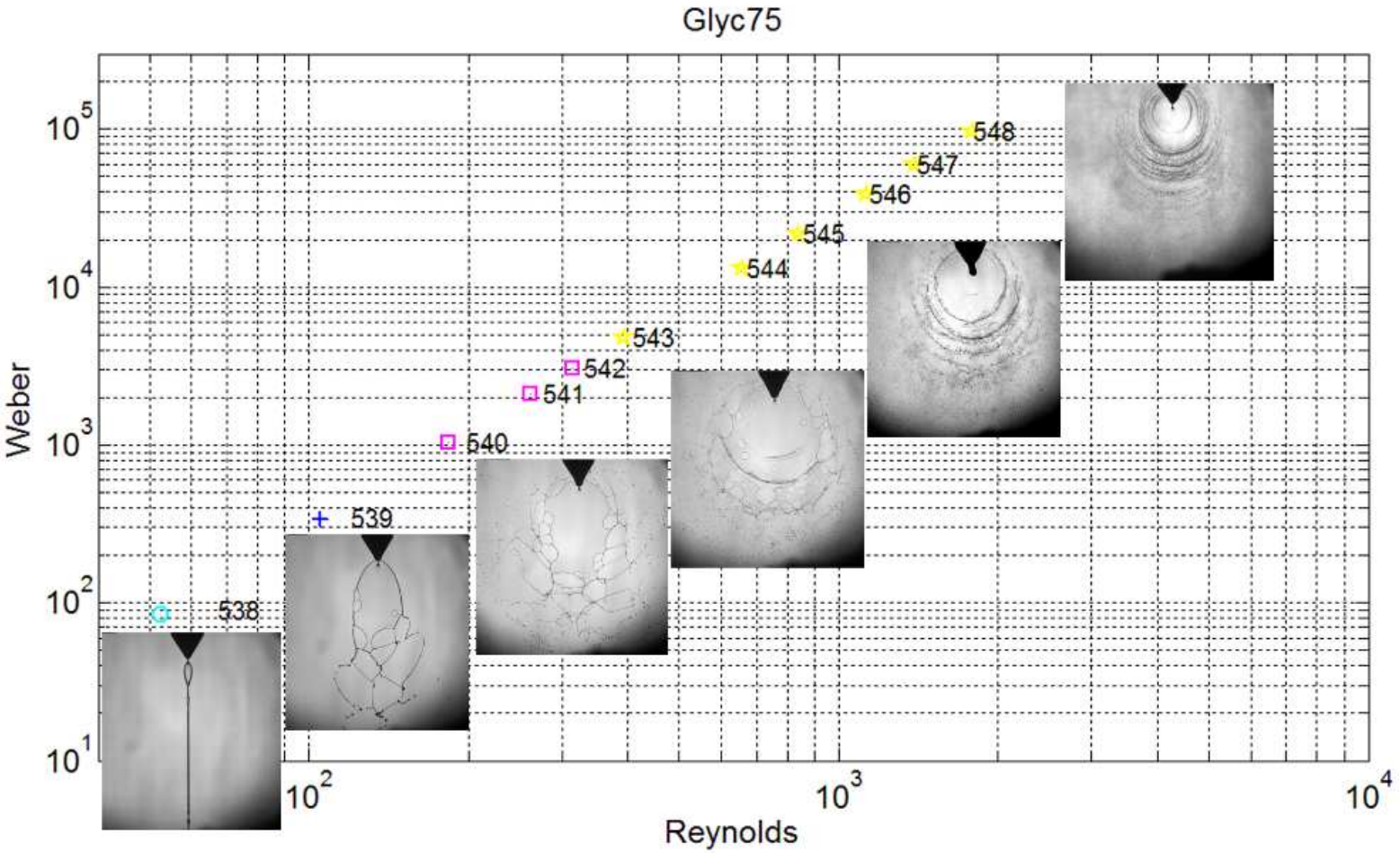

Figure A.14: 75% Glycerine

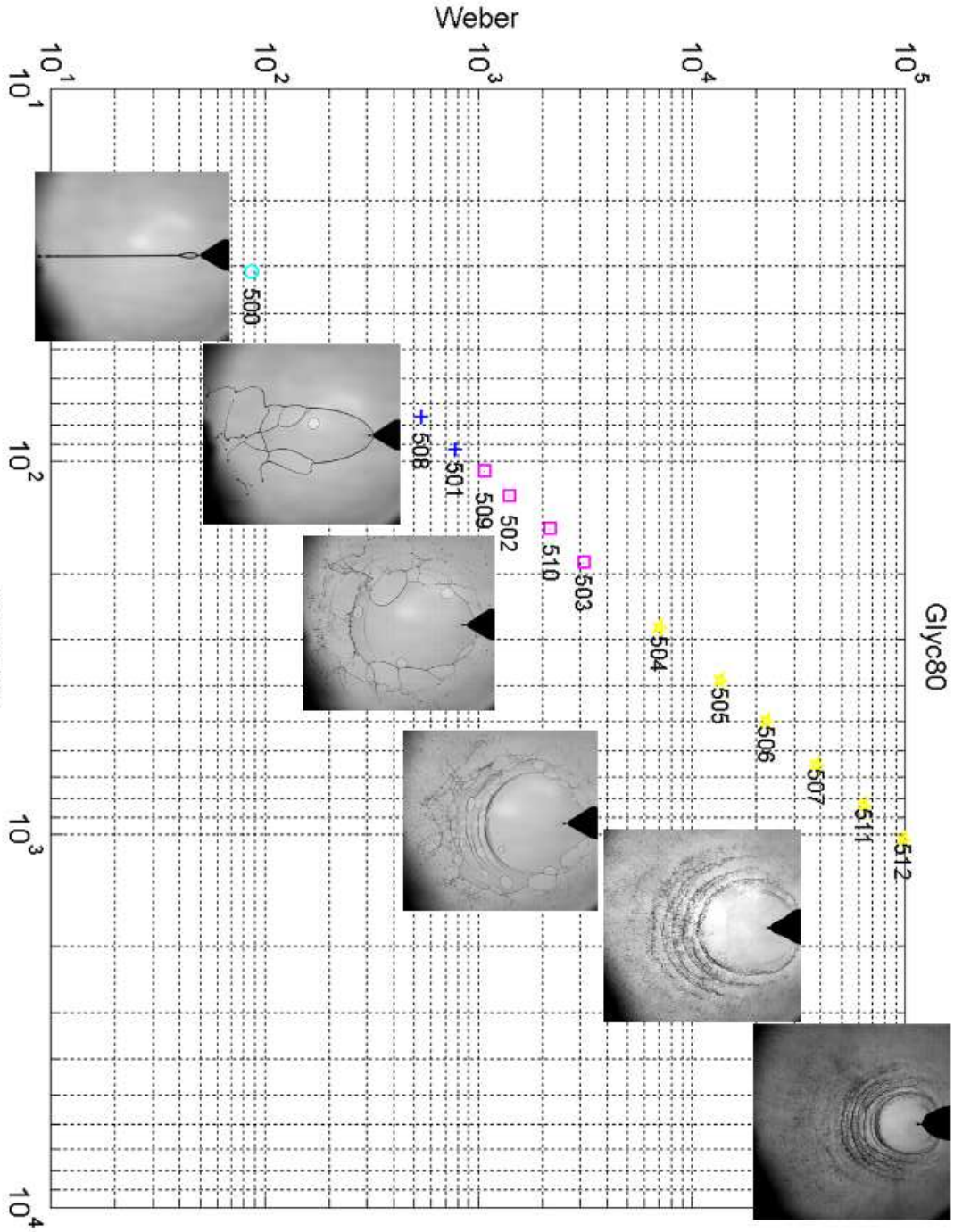

Figure A.15: 80% Glycerine

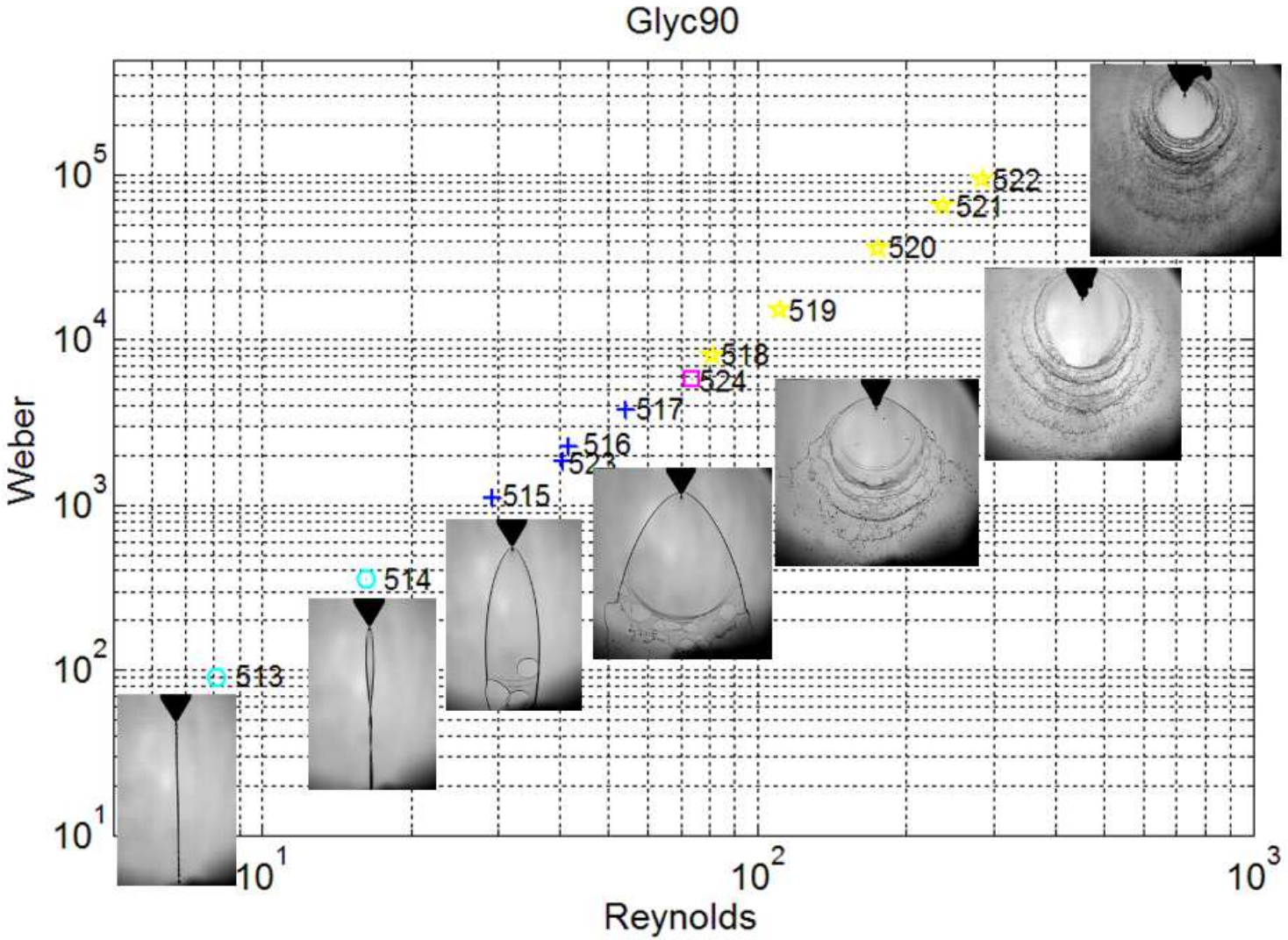

Figure A.16: 90% Glycerine

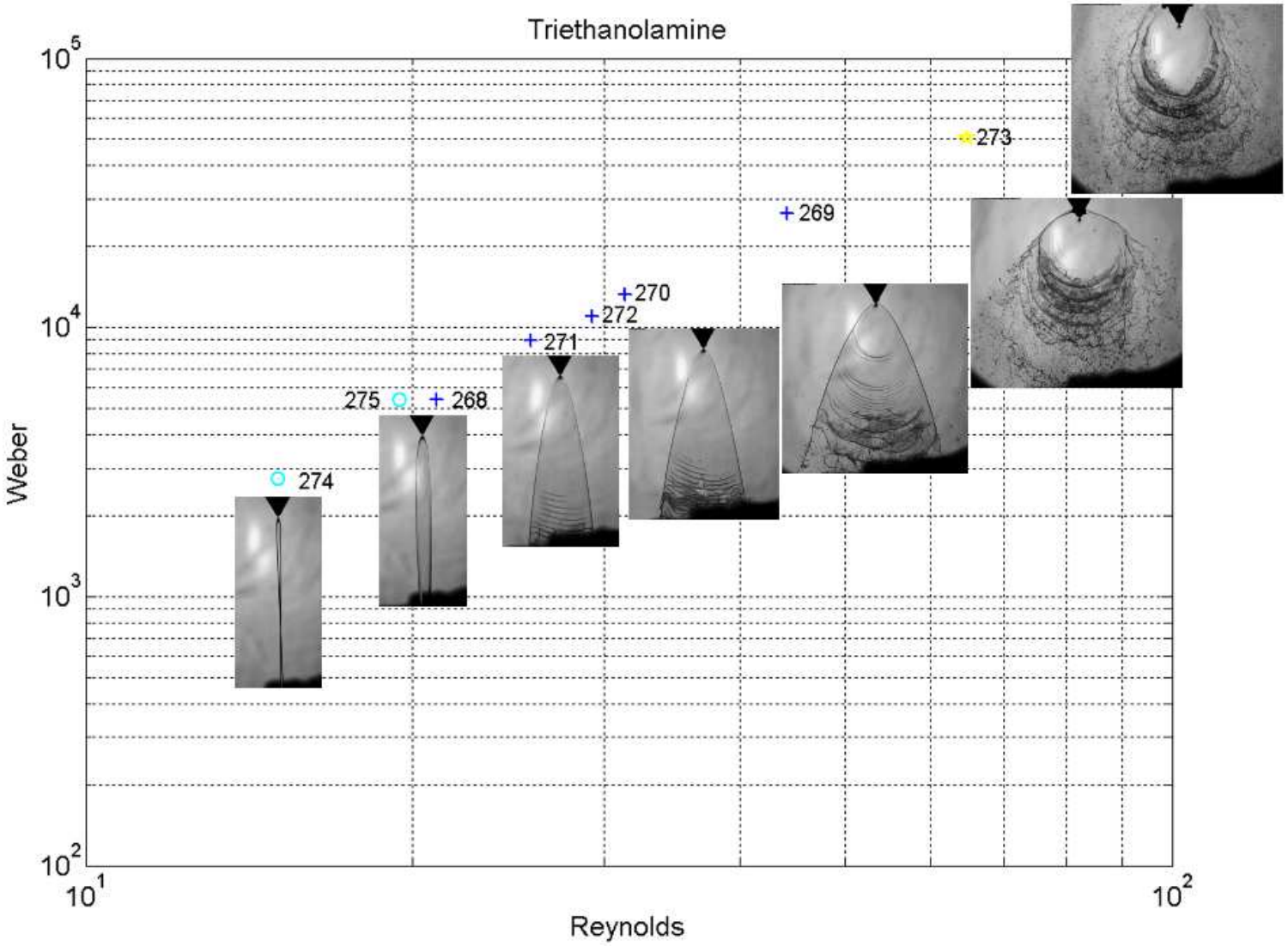

Figure A.17: Triethanolamine

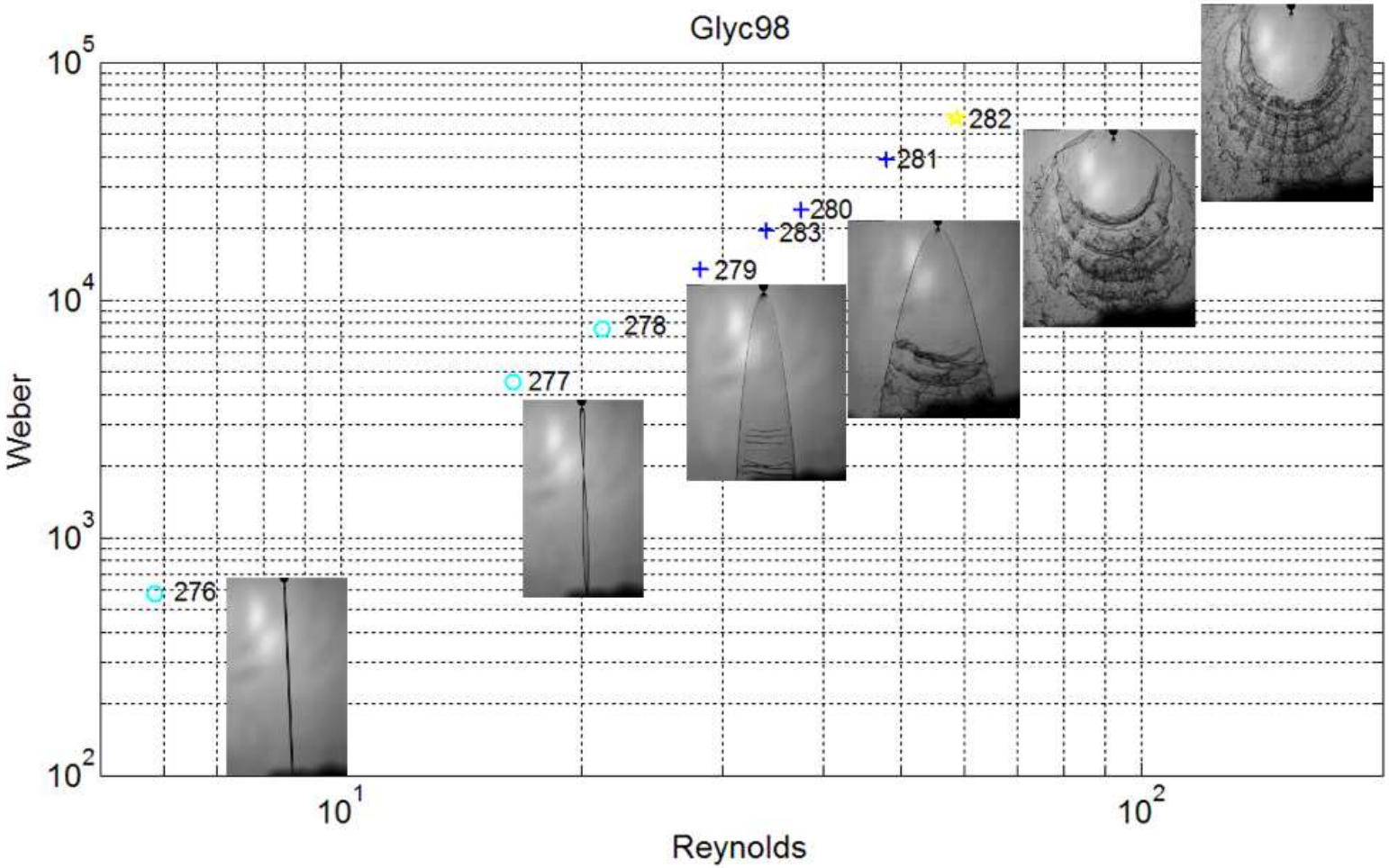

Figure A.18: 98% Glycerine

Appendix B

Fundamentals of Linear Stability Theory

As it's widely shown in this work, a sheet formed by two impinging jets under certain conditions becomes wavy and disintegrates into ligaments and droplets. Heislbetz and Ciezki ([27]) investigated the influence of fluid properties using the linear stability analysis of the temporal evolution of a high viscid liquid sheet. For the theoretical calculations a free, incompressible, two-dimensional and plane sheet with a constant density ρ_l, a constant kinematic viscosity μ and an undisturbed thickness $H = 2h$ is considered, which expands with a certain velocity U_0 through an also assumed incompressible but inviscid gaseous atmosphere with a given density ρ_l. The tension between the liquid sheet and the ambient gas is entitled as σ. Gravity effects are neglected due to the calculated capillary constant of the examined fluids under the used boundary conditions. Figure B.1 shows the two possible deformation modes of a liquid sheet expanding at a velocity U_0. For a detailed derivation of the dispersion relations for symmetric (varicose) and antisymmetric (sinuous) wave modes please see the detailed work of Squire [28], Dombrowski and Johns [29], Li and Tankin [30] and Lin [31]. These investigations showed that the antisymmetric mode grow on faster than the symmetrical mode. Further on, it was found as a mathematical fact that one can not differ between symmetric and antisymmetric modes in the limit of short wave modes. Based on the continuity and momentum equations

for both liquid and gaseous fluid, subject to the boundary conditions at the gas/liquid interfaces in first order, Li and Tankin have found that the general dispersion relation of infinitesimal surface disturbances of a liquid sheet according Eq. B.1

$$\eta_j(t) = \eta_{j,0} exp(\Omega t) j = 1, 2 \tag{B.1}$$

leads to antisymmetric interface deformations, given by

$$(\Omega + ikU_0 + 2k^2\mu)^2 \tanh(kh) + \rho\Omega^2 - 4k^3\mu^2 q \tanh(qh) + \frac{\sigma k^3}{\rho_l} = 0 \tag{B.2}$$

whereas $\rho = \rho_g/\rho_g$ and $q^2 = k^2 + (\Omega + ikU_0)/\mu$ are used as abbreviations. The complex growth rate is entitled as $\Omega = \Omega_r + i\Omega_i$ and $k = 2\pi/\lambda$ stands for the wave number of a given wave length λ . Since Eq. B.2 can not be solved analytically in general, its direct physical interpretation is difficult. Therefore Heislbetz and Ciezki have conducted approximations for significant limiting to improve the understanding of the influence of several parameters like fluid viscosity and sheet thickness to the possible instabilities and breakup characteristics.

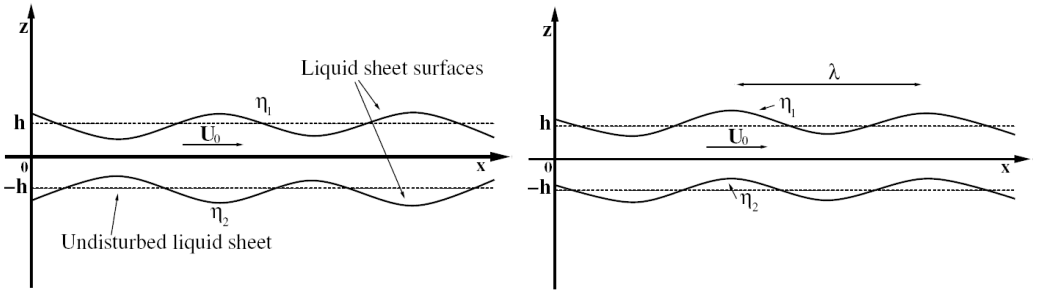

(a) symmetrical wave mode $\eta^s = \eta_1 + \eta_2$ (b) antisymmetrical wave mode $\eta^a = \eta_1 - \eta_2$

Figure B.1: Symmetrical/varicose and antysimmetrica/sinuous deformation modes of a liquid sheet (Ref. [27])

Appendix C

D.L.R.

The German aerospace center D.L.R., Deutcshes Zentrum für Luft und Raumfahrt, is a national research establishment with interests in the following fields: Aeronautics, Space flight, Energy and Transport. DLR comprises eight sites located in Köln-Porz, Berlin, Bonn, Braunschweig, Götingen, Lampoldhsuasen, Oberpfaffenhofen and Stuttgart, as well as offices in Paris and Washington. Five thousand employees are currently working in DLR. The central administration is located in Köln. The aim of DLR is to develop new technologies, in co-operation with industries and universities. Many of the innovations and researches concern environmental issues; this is for example the case in Aeronautics with effort to reduce the amount of polluted exhausts or the development of a new engines working with less dangerous and polluting propellants,in energy with the studies on regenerative energy sources. The Lampoldshausen research center has been founded in 1959 to test propellants and rocket engines,it is located in Baden- Württenberg,around 80 km north from Stuttgart. At the Lampoldshausen site operated ten different test facilities or test facility complex,respectively,for its own research and technology demands and both by contract of European space agencies (ESA, CNES) and in cooperation with the European space industries (NECMA, Austrium, EADS). These test facilities are used to test and qualify rocket engines fuelled with liquid propellants,cryogenic and storable, complete stages of rocket launchers,ramjets and propulsion system of satellites and orbital vehicles.For this purpose,the test site house an

Figure C.1: P5 test facility at DLR Lampolshausen

infra-structure enabling test both under sea-level and high-altitude condition. The main test facilities are, in detail:

- P1- High altitude test facility using a green propellant combination of alcohol and liquid hydrogen;
- P2- One of the first test facilities,used today by EADS to develop the upper stage of Ariane 5 and Aestus engine;
- P3- Used for the development of the combustion chamber of the Vulcain Engine;
- P4- For the rocket propulsion system or stages using storable propellants at trust levels up to 700 kN or up to 30 kN under vacuum conditions;
- P5- For the Vulcain Engine family for Ariane 5 rocket (Figure C.1) which as cryogenic propellants: liquid hydrogen as fuel and liquid oxygen as oxidizer;
- P8- For the investigation on the atomization,mixing and combustion of liquid oxygen at combustion pressure up to 300 bar in experimental

Figure C.2: M11-1 test facility

combustion chambers.

There are several others test facilities located in the site were study on specific topics are conducted. The tests presented in this work were realized at M 11 complex (Figure C.2)

The M11 complex is oriented on the development of different topics.In on hand is carried on the investigation of ramjets propulsion concepts.The studies are focused on two different propellants.Solid propellant for the ramjet development and gaseous hydrogen for the development of the so-called scramjet (ramjet with supersonic flow).In the order hand studies on gels kerosene-based propellants are conducted,particulary the are focused on atomization and impinging sheet break-up behavior. A combustion chamber was built to analyze gel propellant during real employment conditions.

Bibliography

[1] Sutton, G.P., *Rocket Propulsion Element: An Introduction to the Engineering of Rockets*, John Wiley, NY USA, 1992, pp.298-311.

[2] Heidmann, M.F. and Humphriey, J.C., *Fluctuation in a Spray Formed by Two Impinging Jets*, NACA TN 2349, 1951.

[3] Santoro, R.J., and Anderson, W.E., *Combustion Instability Phenomena of Importance to Liquid Propellant Engines*, AIAA 93-20214, 1993.

[4] Heidmann, M.F., Priem, R.J. and Humphriey, J.C.,*A Study of Sprays Formed by Two Impinging Jets*, NACA TN 3835, 1957.

[5] Taylor, G.I., *Formation of Thin Flat Sheets of Water*, Proc. Roy. Soc. A, 259, 1960, pp. 1-17.

[6] Ibrahim, E.A., and Przekwas, A.J., *Impinging Jet Atomization*, Phys. Fluids Vol. 3, No. 12, December 1991, pp. 2981-2987.

[7] Anderson, W.E, Ryan, H.M., Pal, S. and Santoro, R.J., *Fundamental Studies of Impinging Liquid Jets*, AIAA 92-0458, 1992.

[8] Anderson, W.E, Ryan, H.M., Pal, S. and Santoro, R.J., *Atomization Characteristics of Impinging Liquid Jets*, Journal of propulsion and Power, Vol.11 No.1, pp.135-145, Jan-Feb, 1994.

[9] Villermaux, E., and Clanet, C., *Life of a flapping liquid sheet*, J. Fluid Mech, vol. 462, pp.341-363, 2002.

[10] Lai, W.-H., Huang, T.-H., Jiang, T.-L. and Huang, W., *Effects of Fluid Properties on the Characteristics of Impinging-Jet Sprays*, Atomization and Sprays, vol.15, pp.457-468, 2005

[11] Li, R., and Ashgriz, N., *Characteristic of liquid sheets formed by two impinging jets*, Phys. Fluids 18, 087104, 2006.

[12] Ciezki, H.K., Tiedt, T., von Kampen, J. and Bartels,N., *Atomization Behavior of newtonian Fluids with an Impinging Jet Injector in Dependence upon Reynolds an Weber Numbers*, AIAA 2005-4467.

[13] Negri, M., Bailardi, G., and Ciezki,H.K., *Phenomena Associated with the Breakup of Sheets formed by Newtonian and non-Newtonian Fluids in an Impinging Injector*, Heidelberg, Germany, 3-5 May 2010.

[14] Settles, G.S., *Schlieren and Shadowgraph Techniques. Visualizin Phenomena in Transparent Media*, Springer-Verlag, 2001.

[15] *Handbook of Physic and Chemistry*, 3^{rd} Ed., 1984.

[16] Bremond, N., and Villermaux, E., *Atomization by jet impact*, J.FLuid Mech., vol.549,pp. 273-306, 2006.

[17] Bush, J.V.M., and Hasha, A.E., *On the collision of laminar jets: fliud chains and fishbones*, J.FLuid Mech., vol.511,pp. 585-310, 2004.

[18] Dombrowski, N., and Hooper, P.C., *A study of the Sprays Formed by Impinging Jets in Laminar and Turbulent Flow*, J. Fluid Mechanics, Vol.18, Part 3, pp. 392-400, 1963.

[19] Dombrowski, N., and Hooper, P.C., *The Effect of Ambient Density on Drop Formation in Sprays*, Chemical Engineering Science, Vol.17, pp. 291-305, 1961.

[20] Hasson, D. and Peck, R.E., *Thickness Distribution in a Sheet Formed by Impinging Jets*, AIChem Journal, September 1964, pp 752-754.

[21] Lai, W.-H. and Wang, H.-C., *Flow Patterns Generated by Like- and Unlike-Doublet Impinging jets*, AIAA 2002-3700, 7-10 July 2002, Indiana

[22] Jung, K., Lim, B., Khil, T., and Yoon, Y., *Breakup characteristics of laminar and turbulent liquid sheets formed by impinging jets in high pressure environments*, AIAA 2004-3526, 11-14 July 2004, Florida

[23] Ciezki, H. K., Bartels, N., von Kampen, J. and Madlener, K., *Properties of gelled propellants for throttleable propulsion systems*, Symposium on Energy Conversion Fundamental, Istanbul, Turkey, 21-23 June 2004

[24] Ciezki,H.K., von Kampen, J., Tiedt, T., and Madlener, K., *Some Aspects of the Atomization Behavior of Newtonian and of Shear-thinning Gelled non-Newtonian Fluids with an Impinging Jet Injector*, Workshop, Löwenstein, 29.-30.5.2006

[25] Madlener, K. and Ciezki, H.K., *Theoretical Investigation of the flow behavior of gelled fuels of the Extended Herschel-Bulkley type*, 1st European Conference for Aerospace Science (EUCASS), Moscow, Russia, July 4th-7th (2005)

[26] Rawle, A., *Basic principles of particle size analysis*, Malvern Instument Limited, Technical Paper.

[27] Heislbetz, B., Madlener, K. and Ciezki, H.K., *Breakup Characteristics of a Newtonian Liquid Sheet formed by a Doublet Impinging Jet Injector*, AIAA 2007-5694, 8-11 July 2007, Cincinnati, OH

[28] Squire, H.B., *Investigation of the instability of a moving liquid film*, Imperial College, Lonfon, Vol.4, June 1953

[29] Dombrowski, N., and Jhons, W.R., *The aerodynamic instability and disintegration of visocus liquid sheets*, Chemical Engineering Science, Vol.18, pp. 203-214, 1963.

[30] Li, X. and Tankin, R.S., *On the temporal Instability of a two-dimensional Viscous Liquid Sheet*, Journal of Fluid Mechanics, Vol. 226, 1991

[31] Lin, S.P., *Breakup of Liquid Sheets and Jets*, Cambridge University Press, 2003

[32] http://www.dguv.de

[33] http://srdata.nist.gov

[34] http://www.surface-tension.de

[35] http://www.alfa.com

[36] http://www.malvern.com

[37] http://www.scottecatalog.com/msds.nsf/